Supporting Information for:

Bis(catecholato)silanes: assessment, rationale and increase of silicon's Lewis superacidity

Deborah Hartmann, Marcel Schädler and Lutz Greb*

Content

1. Experimental Details

1.1. General considerations

Unless stated otherwise, all manipulations were carried out under a dry argon atmosphere by using standard Schlenk techniques to prevent oxidation and hydrolysis of the sensitive compounds. All solvents were rigorously dried by applying standard procedures, freshly degassed and stored over molecular sieves (3 Å resp. 4 Å) prior to use. All glassware, syringes, magnetic stirring bars and needles were thoroughly dried. The commercially available chemicals were used as received. All catechols were dissolved in Et_2O and stored over flame-dried molecular sieves (4 Å) to eliminate residual water traces. The solution was filtered under argon atmosphere and the solvent was removed *in vacuo* to yield the dry catechol compound. All other substances were prepared following either literature procedures or the methods described below. All air sensitive compounds were stored in a glove box (MBraun LABmaster dp, MB-20-G) under N_2-atmosphere. Purity and identity of the compounds were confirmed by high resolution multinuclear NMR-spectroscopy, mass spectrometry, elemental analysis and if possible, X-ray diffraction analysis. ^{1}H-, ^{13}C-, ^{19}F-, ^{31}P- and ^{29}Si-NMR spectra were recorded with a Bruker Advance II 400 or Bruker 2 Advance III 600 NMR spectrometer and referenced to the solvent in use. Chemical shifts are reported as dimensionless δ values in ppm, coupling constants J are given in hertz (Hz). Electrospray ionization mass spectra were obtained with a Bruker ApexQe FT-ICR instrument.

1.2. Syntheses

1.2.1. General Procedure: Preparation of Bis(catecholato)silanes – $Si(cat^X)_2(\cdot 2\ CH_3CN)$

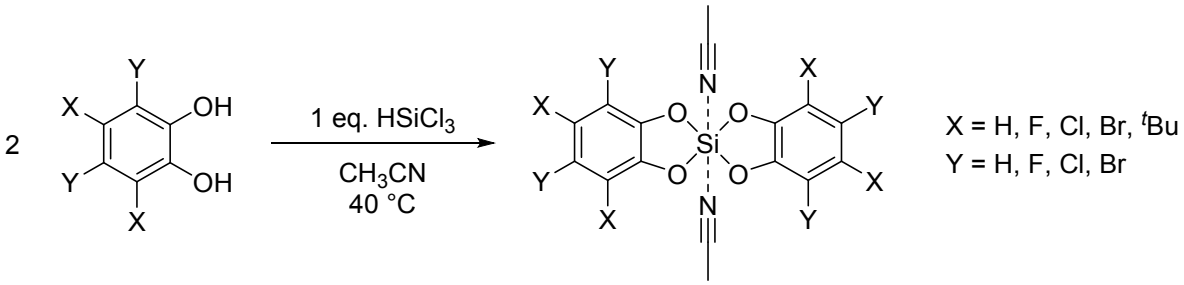

To a solution of 2 eq. catechol in acetonitrile, 1 eq. $HSiCl_3$ was added dropwise. The reaction was stirred for 1 h at room temperature until initial gas evolution was completed. During this period frequent exchange of the gaseous phase was performed. Afterwards the reaction was stirred at 40 °C for 12 h (24 h for X = ^{t}Bu). The precipitate was collected by filtration under argon atmosphere and washed 3 times with dichloromethane. The product was dried *in vacuo* for 8 h and stored under argon atmosphere. In the case of X = 3,5-^{t}Bu the crude product was purified by sublimation (200 °C, atm. pressure). Depending on the Lewis acidity of the product either the adduct-free acid (X = H, ^{t}Bu, F) or the bis-CH_3CN adduct (X = Cl, Br) was formed. The analytical data was in agreement with the literature data.[1]

Bis(catecholato)silane: Catechol (2 eq., 2.79 g, 25.3 mmol), $HSiCl_3$ (1 eq., 1.71 g, 12.7 mmol, 1.28 ml) and 8 ml CH_3CN were employed to yield **$Si(cat^H)_2$** as a colorless solid (2.76 g, 11.3 mmol, 89 %).

^{1}H-NMR (400 MHz, CD_2Cl_2): δ = 7.15–6.86 (m, 8H). **^{13}C-NMR** and **^{29}Si-NMR** spectra could not be obtained due to limited solubility, even in DMF. **EI-HRMS** (m/z): [M^+] calcd.: 244.01864 found: 244.01946.

Bis(3,5-di-*tert*-butyl-catecholato)silane: 3,5-Di-*tert*-butylcatechol (2 eq., 300 mg, 1.35 mmol), $HSiCl_3$ (1 eq., 91.4 mg, 0.675 mmol, 67.5 µl) and 3 ml CH_3CN were employed to yield **$Si(cat^{tBu})_2$** as a colorless solid (240 mg, 0.51 mmol, 76 %).

^{1}H-NMR (400 MHz, CD_2Cl_2): δ = 7.02 (d, 2H), 6.99 (d, 2H), 1.39 (s, 18H), 1.30 (s, 18H). **^{13}C-NMR** (100 MHz, DMF): δ = 149.7, 145.1, 139.3, 131.4, 111.4, 106.8, 34.3, 34.2, 31.8, 29.6. **^{29}Si-NMR** spectra could not be obtained due to limited solubility. **EI-HRMS** (m/z): [M^+] calcd.: 468.26904 found: 468.26670

Bis(perfluorocatecholato)silane: Tetrafluorocatechol (2 eq., 1.20 g, 6.59 mmol), $HSiCl_3$ (1 eq., 446 mg, 3.29 mmol, 333 µl) and 10 ml CH_3CN were employed to yield **$Si(cat^F)_2$** as a colorless solid (1.29 g, 2.73 mmol, 83 %).

^{19}F-NMR (376 MHz, CD_2Cl_2): δ = −158.1 (m, 4F), −162.6 (m, 4F). **^{13}C-NMR** and **^{29}Si-NMR** spectra could not be obtained due to limited solubility, even in DMF.

Bis(perchlorocatecholato)silane: Tetrachlorocatechol (2 eq., 3.43 g, 13.8 mmol), $HSiCl_3$ (1 eq., 930 mg, 6.87 mmol, 694 µl) and 20 ml CH_3CN were employed to yield **Si(cat^{Cl})$_2$·**2 CH_3CN as a colorless solid (3.54 g, 5.88 mmol, 85 %).

^{1}H-NMR (400 MHz, CD_2Cl_2): δ = 2.00 (bs, 6H). **^{13}C-NMR** (100 MHz, DMF): δ = 149.4, 117.3, 112.5. **^{29}Si-NMR** spectra could not be obtained due to limited solubility. **EI-HRMS** (m/z): [M^+ − 2 CH_3CN] calcd: 515.7069 found: 515.7075. **EA**: calcd. for $C_{16}H_6Cl_8N_2O_4Si$: C 31.93; H 1.00; N 4.65; found C 31.59; H 1.18; N 4.68.

Bis(perbromocatecholato)silane: Tetrabromocatechol (2 eq., 1.86 g, 4.37 mmol), $HSiCl_3$ (1 eq., 296 mg, 2.19 mmol, 221 µl) and 10 ml CH_3CN were employed to yield **Si(cat^{Br})$_2$·**2 CH_3CN as a colorless solid (1.62 g, 1.69 mmol, 77 %).

^{1}H-NMR (200 MHz, CD_2Cl_2): δ = 1.98 (s, 6H). **^{13}C-NMR** (100 MHz, DMF): δ = 151.0, 111.6, 105.4. **^{29}Si-NMR** spectra could not be obtained due to limited solubility. **ESI-HRMS** (negative, MeOH trace additive): $[Si(cat^{Br})_2(OMe)]^-$ m/z calcd. 906.3135, found: 906.3304. **EA**: calcd. for .$C_{16}H_6Br_8N_2O_4Si$: C 20.07; H 0.63; N 2.93; found: C 19.63; H 0.76; N 2.43.

1.2.2. General Procedure: Assessment of Lewis Acidity by the Gutmann-Beckett Method – Preparation of Et_3PO-Adducts

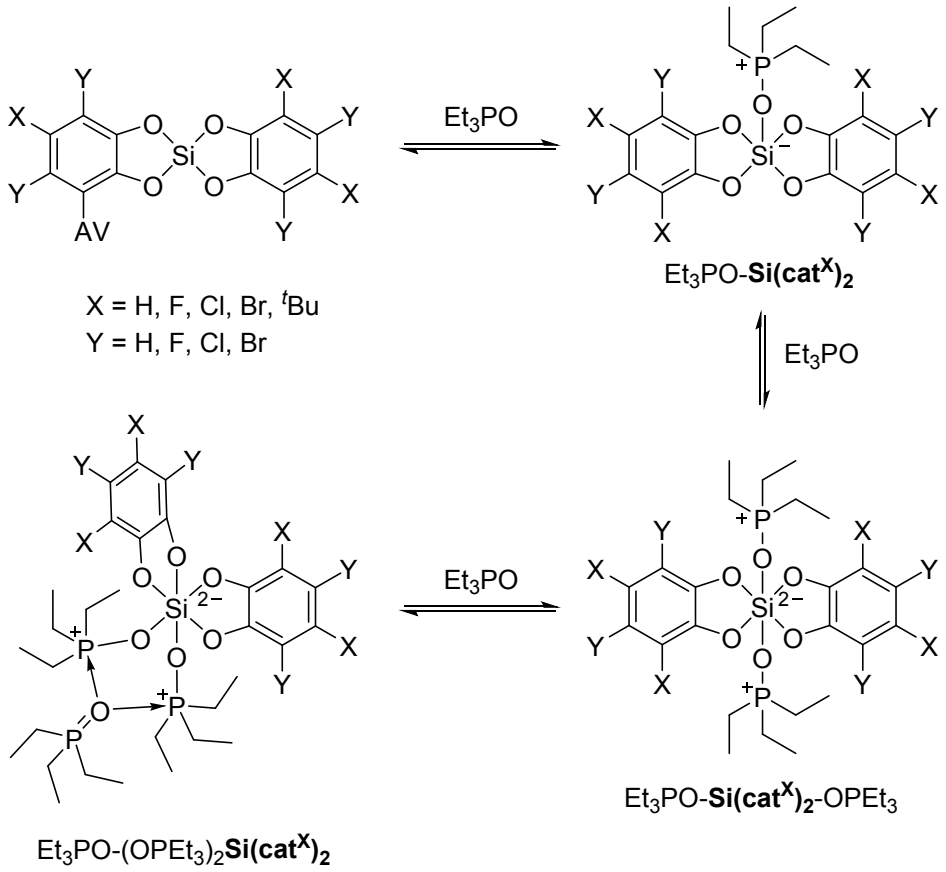

To a suspension of 0.25 µmol **$Si(cat^X)_2$** in 0.5 ml CD_2Cl_2, triethylphosphine oxide (Et_3PO) was successively added (0.5 eq., 1.0 eq., 2.0 eq. and 3.0 eq.) and monitored via $^1H/^{31}P$-NMR spectroscopy. The occurrence of a broad signal at around 70 ppm in ^{31}P-NMR was attributed to the coordination of a third Et_3PO in the coordination sphere of the bis-adducts (see scheme above), in analogy to a literature report.[2] Crystals suitable for X-ray diffraction were obtained by gaseous diffusion of either pentane or Et_2O into solutions of CD_2Cl_2.

$Si(cat^X)_2$	**δ ^{31}P-NMR [ppm] mono adduct**	**δ ^{31}P-NMR [ppm] bis adduct**
$Si(cat^{tBu})_2$	81.6	70.5
$Si(cat^H)_2$	83.2	67.7
$Si(cat^F)_2$	86.6	72.2
$Si(cat^{Cl})_2$	87.2	73.1
$Si(cat^{Br})_2$	87.3	73.1
blind sample of Et_3PO in CD_2Cl_2 (162 MHz): δ ^{31}P-NMR = 50.5 ppm		

Table S1: Comparison of ^{31}P-NMR shifts of different Et_3PO-adducts (162 MHz, CD_2Cl_2).

Et_3PO-Si(cat^H)$_2$: ^{1}H-NMR (400 MHz, CD_2Cl_2): δ = 6.84–6.80 (m, 4H), 6.72–6.68 (m, 4H), 1.98 (m, 6H), 1.03 (dt, $^2J_{H,P}$ = 18.6 Hz, $^3J_{H,H}$ = 7.7 Hz, 9H). **^{31}P-NMR:** (162 MHz, CD_2Cl_2): δ = 83.2.

Et_3PO-Si(cat^H)$_2$-$OPEt_3$: ^{1}H-NMR (400 MHz, CD_2Cl_2): δ = 6.83–6.77 (m, 4H), 6.71–6.66 (m, 4H), 1.82 (dq, $^2J_{H,P}$ = 12.0 Hz, $^3J_{H,H}$ = 7.7 Hz, 12H), 1.07 (dt, $^3J_{H,P}$ = 17.3 Hz, $^3J_{H,H}$ = 7.7 Hz, 18H). **^{31}P-NMR:** (162 MHz, CD_2Cl_2): δ = 67.7 (bs).

Et_3PO-Si(cat^{tBu})$_2$: ^{1}H-NMR (400 MHz, CD_2Cl_2): δ = 6.80 (d, $^3J_{H,H}$ = 2.2 Hz, 2H), 6.68 (d, $^3J_{H,H}$ = 2.2 Hz, 2H), 1.96 (dq, $^2J_{H,P}$ = 12.1 Hz, $^3J_{H,H}$ = 7.7 Hz, 6H), 1.41 (s, 18H), 1.28 (s, 18H), 1.04 (dt, $^3J_{H,P}$ = 18.4 Hz, $^3J_{H,H}$ = 7.7 Hz, 9H). **^{31}P-NMR:** (162 MHz, CD_2Cl_2): δ = 81.6.

Et_3PO-Si(cat^{tBu})$_2$-$OPEt_3$: ^{1}H-NMR (400 MHz, CD_2Cl_2): δ = 6.80 (d, $^3J_{H,H}$ = 2.2 Hz, 2H), 6.68 (d, $^3J_{H,H}$ = 2.2 Hz, 2H), 1.84 (dq, $^2J_{H,P}$ = 12.0 Hz, $^3J_{H,H}$ = 7.7 Hz, 12H), 1.41 (s, 18H), 1.28 (s, 18H), 1.07 (dt, $^3J_{H,P}$ = 17.7 Hz, $^3J_{H,H}$ = 7.7 Hz, 18H). **^{31}P-NMR:** (162 MHz, CD_2Cl_2): δ = 70.5.

Et_3PO-Si(cat^F)$_2$: ^{1}H-NMR (400 MHz, CD_2Cl_2): δ = 2.06 (dq, $^2J_{H,P}$ = 11.8 Hz, $^3J_{H,H}$ = 7.7 Hz, 6H) 1.11 (dt, $^3J_{H,P}$ = 19.2 Hz, $^3J_{H,H}$ = 7.7 Hz, 9H). **^{31}P-NMR:** (162 MHz, CD_2Cl_2): δ = 86.6.

Et_3PO-Si(cat^F)$_2$-$OPEt_3$: ^{1}H-NMR (400 MHz, CD_2Cl_2): δ = 1.89 (m, 12H), 1.06 (m, 18H). **^{31}P-NMR:** (162 MHz, CD_2Cl_2): δ = 72.2 (bs).

Et_3PO-Si(cat^{Cl})$_2$: ^{1}H-NMR (400 MHz, CD_2Cl_2): 2.04 (dq, $^2J_{H,P}$ = 12.4 Hz, $^3J_{H,H}$ = 7.6 Hz, 6H), 1.10 (dt, $^3J_{H,P}$ = 18.8 Hz, $^3J_{H,H}$ = 7.6 Hz, 9H). **^{31}P-NMR:** (162 MHz, CD_2Cl_2): δ = 87.2.

Et_3PO-Si(cat^{Cl})$_2$-$OPEt_3$: ^{1}H-NMR (400 MHz, CD_2Cl_2): δ = 1.99 (m, 12H) 1.03 (m, 18H). **^{31}P-NMR:** (162 MHz, CD_2Cl_2): δ = 73.1.

Et_3PO-Si(cat^{Br})$_2$: ^{1}H-NMR (400 MHz, CD_2Cl_2): 2.04 (dq, $^2J_{H,P}$ = 12.4 Hz, $^3J_{H,H}$ = 7.6 Hz, 6H), 1.10 (dt, $^3J_{H,P}$ = 18.8 Hz, $^3J_{H,H}$ = 7.6 Hz, 9H). **^{31}P-NMR:** (162 MHz, CD_2Cl_2): δ = 87.3.

Et_3PO-Si(cat^{Br})$_2$-$OPEt_3$: ^{1}H-NMR (400 MHz, CD_2Cl_2): δ = 2.00 (m, 12H) 1.01 (m, 18H). **^{31}P-NMR:** (162 MHz, CD_2Cl_2): δ = 73.1.

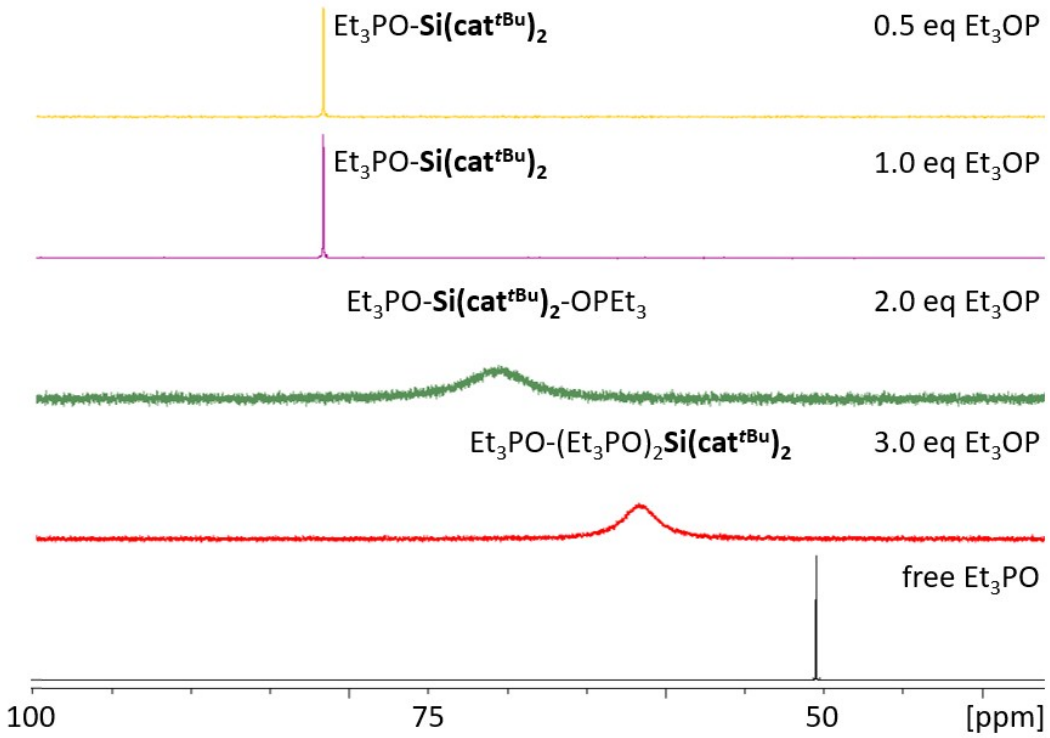

Figure S1: Changes in the ^{31}P-NMR spectra for samples of **Si(cat^{tBu})$_2$** and 0.5–3.0 eq. Et_3PO in CD_2Cl_2.

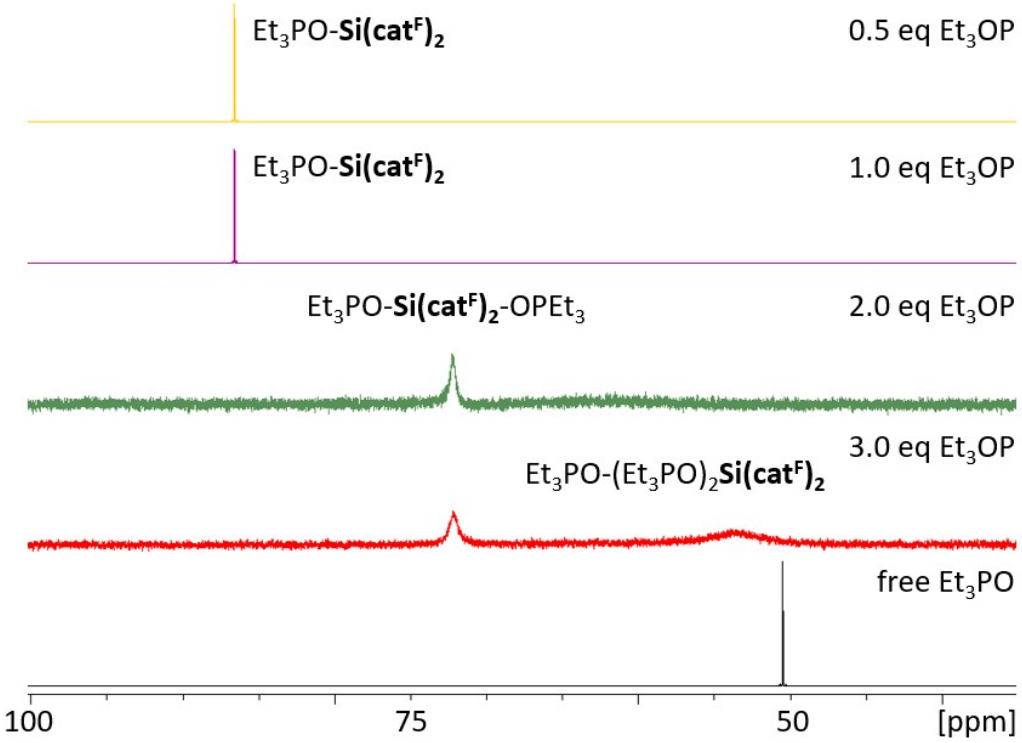

Figure S2: Changes in the ^{31}P-NMR spectra for samples of **Si(cat^{F})$_2$** and 0.5–3.0 eq. Et_3PO in CD_2Cl_2.

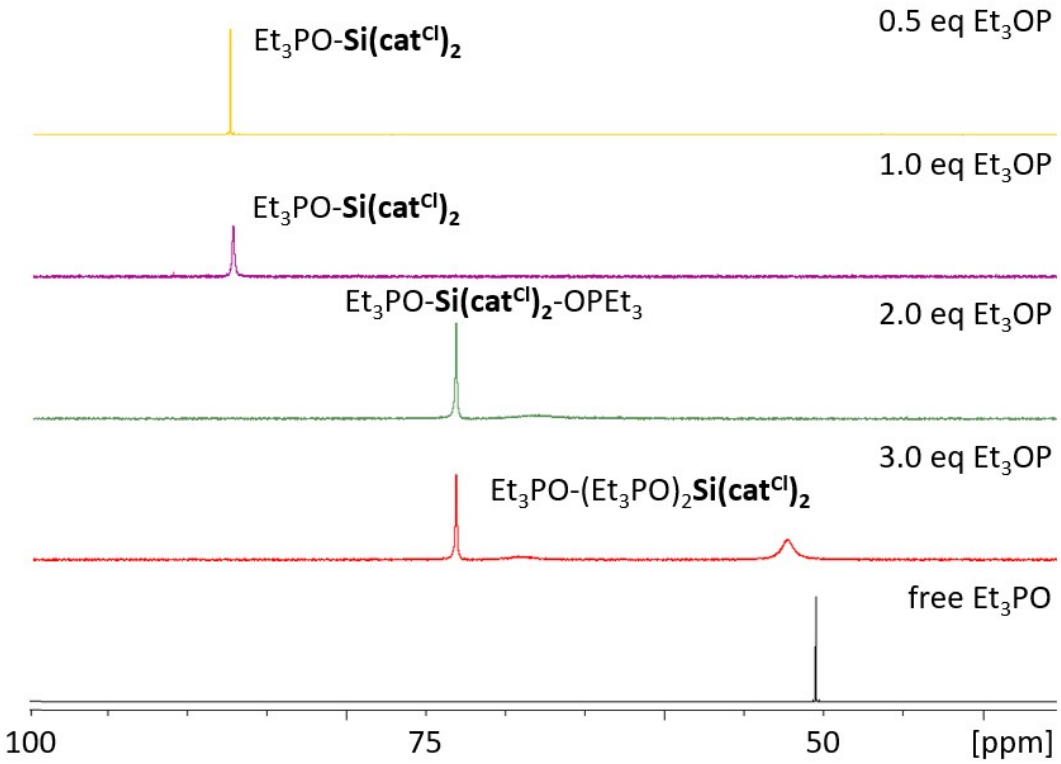

Figure S3: Changes in the ^{31}P-NMR spectra for samples of **Si(cat^{Cl})$_2$** and 0.5–3.0 eq. Et_3PO in CD_2Cl_2.

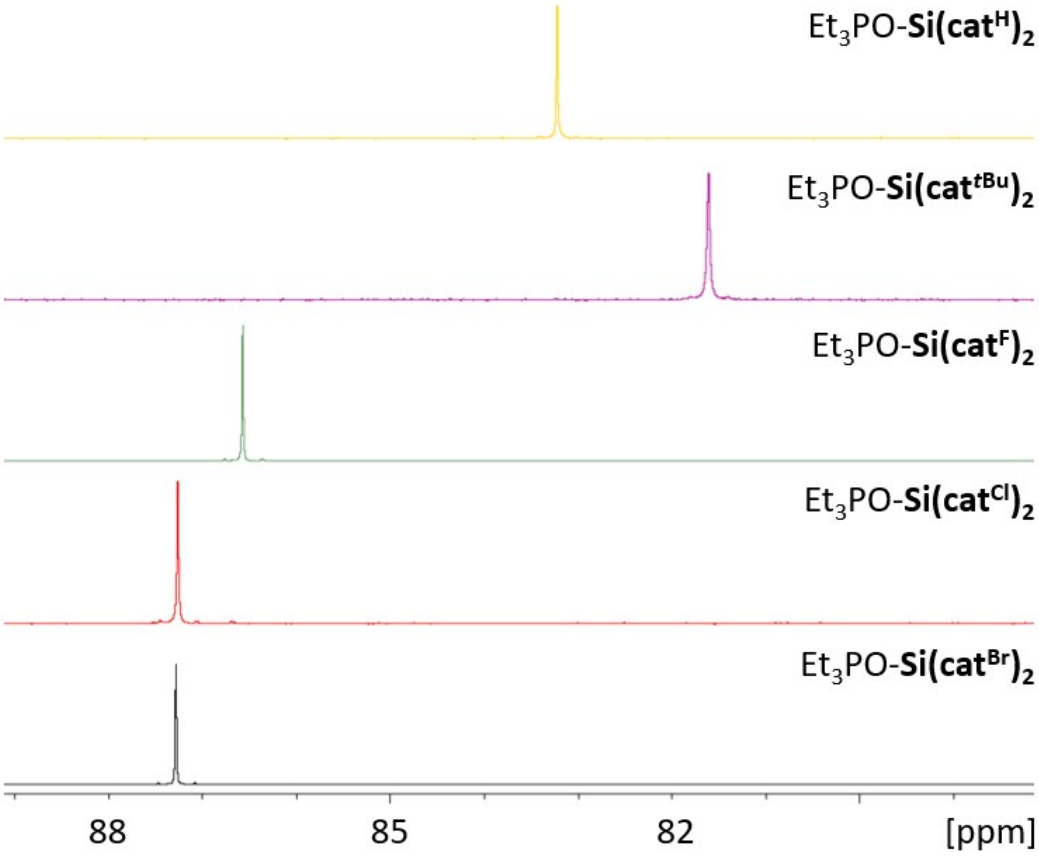

Figure S4: ^{31}P-NMR spectra of all Et_3PO mono adducts (Et_3PO-**Si(cat^{X})$_2$**, X = H, ^{t}Bu, F, Cl, Br).

1.2.3. General Procedure: Preparation of Monofluoride Adducts of Bis(catecholato)silanes

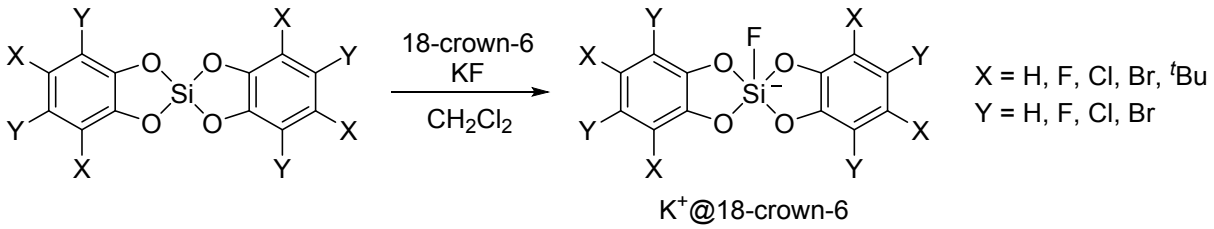

To a suspension of 1 eq. bis(catecholato)silane (**Si(cat^{X})$_2$**) in CH_2Cl_2, 1 eq. KF and 1 eq. 18-crown-6 were added. The reaction was stirred for 24 h at room temperature until all solids were dissolved to form the corresponding fluoride adduct. The solvent was removed *in vacuo* and the product was purified by recrystallization by gaseous diffusion of either pentane or Et_2O into a solution of CH_2Cl_2.

[K@18-crown-6][F-Si(cat^{H})$_2$]: Si(cat^{H})$_2$ (1 eq., 150.0 mg, 614.06 µmol), KF (1 eq., 35.7 mg, 614.06 µmol) and 18-crown-6 (1 eq., 162.3 mg, 614.06 µmol) in 5 ml CH_2Cl_2 were employed to yield the product as slightly grey crystals (278.1 mg, 490.78 µmol, 80 %).

^{1}H-NMR (400 MHz, CD_2Cl_2): δ = 6.77 (dd, $^{3}J_{H,H}$ = 5.6 Hz, $^{5}J_{H,H}$ = 3.5 Hz, 4H), 6.62 (dd, $^{3}J_{H,H}$ = 5.6 Hz, $^{5}J_{H,H}$ = 3.5 Hz, 4H), 3.56 (s, 24H). **^{13}C-NMR** (100 MHz, CD_2Cl_2): δ = 149.8, 118.6, 110.9, 70.4. **^{19}F-NMR:** (376 MHz, CD_2Cl_2): δ = −133.1 (s, 1F, ^{29}Si-satellites 191.2 Hz). **^{29}Si-NMR** (79 MHz, CD_2Cl_2): δ = −104.8 (d, $^{1}J_{Si,F}$ = 191.2 Hz). **ESI-HRMS** (negative): [F-Si(cat^{H})$_2$]$^-$ m/z calcd. 263.0181, found: 263.0180.

[K@18-crown-6][F-Si(cat^{tBu})$_2$]: Si(cat^{tBu})$_2$ (1 eq., 100.0 mg, 213.35 µmol), KF (1 eq., 12.4 mg, 213.35 µmol) and 18-crown-6 (1 eq., 56.4 mg, 213.35 µmol) in 2 ml CH_2Cl_2 were employed to yield the product as a colorless solid (163.1 mg, 206.16 µmol, 97 %).

^{1}H-NMR (400 MHz, CD_2Cl_2): δ = 6.78 (d, $^{3}J_{H,H}$ = 2.2 Hz, 2H), 6.62 (bs, 2H), 3.55 (s, 24H), 1.42 (s, 18H), 1.27 (s, 18H). **^{19}F-NMR:** (376 MHz, CD_2Cl_2): δ = −131.6 (bs), −133.7 (s), −134.0 (bs). **^{29}Si-NMR** (79 MHz, CD_2Cl_2): δ = −104.8 (d, $^{1}J_{Si,F}$ = 188.9 Hz).

Due to different stereoisomers of the preferred tbp-confirmation (see Figure S5), three ^{19}F-NMR resonances are observed. A dynamic equilibrium between the two *trans*-diastereomeres via Berry-pseudorotation causes signal broadening. The sharp mid signal should stem from the *cis*-tbp stereoisomer, which is separated from the trans isomers through a larger energetic barrier. The same dynamic effects caused severe signal broadening in the **^{13}C-NMR** spectra, hampering peak identification.

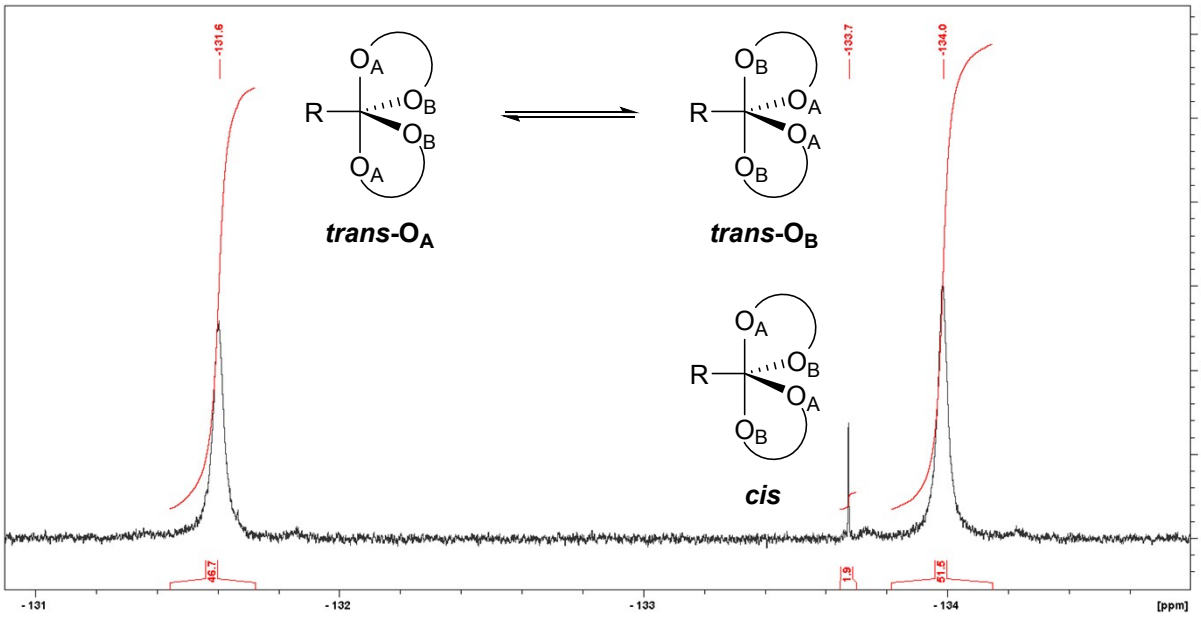

Figure S5: ^{19}F-NMR spectrum of [K@18-crown-6][F-Si(cat^{tBu})$_2$]. Formation of *trans*-diastereomers [K@18-crown-6][F-Si(cat^{tBu})$_2$]-A and [K@18-crown-6][F-Si(cat^{tBu})$_2$]-B, as well as 1.9 % of a *cis*-tbp isomer (δ = −133.7 ppm).

[K@18-crown-6][F-Si(cat^{F})$_2$]: Si(cat^{F})$_2$ (1 eq., 300 mg, 638 µmol), KF (1 eq., 44.9 mg, 638 µmol) and 18-crown-6 (1 eq., 204 mg, 638 µmol) in 5 ml CH_2Cl_2 were employed to yield the product as slightly grey crystals (411 mg, 579 µmol, 75 %).

^{1}H-NMR (400 MHz, CD_2Cl_2): δ = 3.58 (s, 24H). **^{13}C-NMR** spectra unsuitable due to the higher order multiplets of carbon caused by fluorine coupling. **^{19}F-NMR:** (376 MHz, CD_2Cl_2): δ = −133.5 (s, 1F, ^{29}Si-satellites 194.8 Hz), −168.4 (m, 4F), −175.5 (m, 4F). **^{29}Si-NMR** (79 MHz, CD_2Cl_2): δ = −101.6 (d, $^{1}J_{Si,F}$ = 194.8 Hz). **ESI-HRMS** (negative): [F-Si(cat^{F})$_2$]$^-$ m/z calcd. 487.2685, found: 487.2683.

[K@18-crown-6][F-Si(cat^{Cl})$_2$]: Si(cat^{Cl})$_2$·2 CH_3CN (1 eq., 200 mg, 332 µmol), KF (1 eq., 19.3 mg, 332 µmol) and 18-crown-6 (1 eq., 87.8 mg, 332 µmol) in 5 ml CH_2Cl_2 were employed to yield the product as slightly grey crystals (224 mg, 266 µmol, 80 %).

^{1}H-NMR (400 MHz, CD_2Cl_2): δ = 3.54 (s, 24H). **^{13}C-NMR** (100 MHz, CD_2Cl_2): δ = 145.9, 121.5, 114.8, 70.4. **^{19}F-NMR:** (376 MHz, CD_2Cl_2): δ = −132.6 (s, 1F, ^{29}Si-satellites 195.2 Hz). **^{29}Si-NMR** (79 MHz, CD_2Cl_2): δ = −105.1 (d, $^{1}J_{Si,F}$ = 195.2 Hz). **ESI-HRMS** (negative): [F-Si(cat^{Cl})$_2$]$^-$ m/z calcd. 534.7064, found: 534.7073.

[K@18-crown-6][F-Si(cat^{Br})$_2$]: Si(cat^{Br})$_2$·2 CH_3CN (1 eq., 214 mg, 224 µmol), KF (1 eq., 13.0 mg, 224 µmol) and 18-crown-6 (1 eq., 59.2 mg, 224 µmol) in 6 ml CH_2Cl_2 were employed to yield the product as slightly grey crystals (231 mg, 193 µmol, 86 %).

^{1}H-NMR (400 MHz, CD_2Cl_2): δ = 3.55 (s, 24H). **^{13}C-NMR** (100 MHz, CD_2Cl_2): δ = 147.6, 116.1, 107.1, 70.5. **^{19}F-NMR:** (376 MHz, CD_2Cl_2): δ = −132.3 (s, 1F, ^{29}Si-satellites 195.2 Hz). **^{29}Si-NMR** (79 MHz, CD_2Cl_2): δ = −107.0 (d, $^{1}J_{Si,F}$ = 195.2 Hz). **ESI-HRMS** (negative): $[F\text{-}Si(cat^{Br})_2]^-$ m/z calcd. 886.3022, found: 886.3034.

1.2.4. General Procedure: Preparation of Monochloride Adducts of Bis(catecholato)silanes

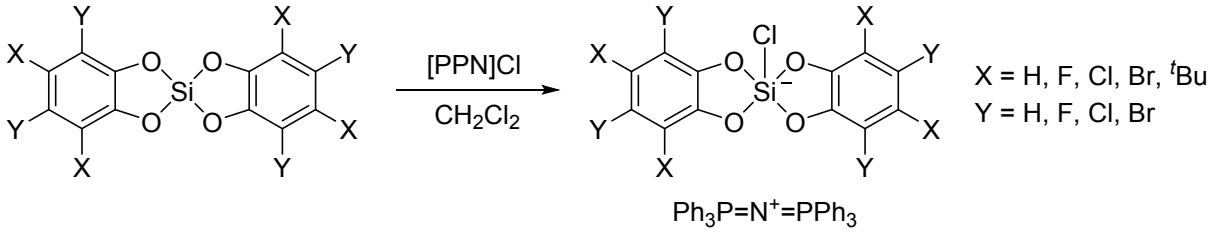

To a suspension of 1 eq. $Si(cat^{X})_2$ in CH_2Cl_2, 1 eq. bis(triphenylphosphine)iminiumchloride ([PPN]Cl) was added. The reaction was stirred at room temperature for 24 h until all solids were dissolved to form the corresponding chloride adduct. The product was purified by precipitation with pentane into a solution of CH_2Cl_2.

[PPN][Cl-Si(cat^{H})$_2$]: $Si(cat^{H})_2$ (1 eq., 250 mg, 1.02 mmol) and [PPN]Cl (1 eq., 588 mg, 1.02 mmol) in 3 ml CH_2Cl_2 were employed to yield the product as slightly grey solid (703 mg, 860 µmol, 84 %). Crystals suitable for X-ray crystallography were obtained by slow diffusion of pentane in a solution of CH_2Cl_2.

^{1}H-NMR (400 MHz, CD_2Cl_2): δ = 7.67–7.63 (m, 6H), 7.50–7.45 (m, 24H), 6.78–6.75 (m, 4H), 6.62–6.59 (m, 4H). **^{13}C-NMR** (100 MHz, CD_2Cl_2): δ = 149.4, 134.1, 132.5 (m), 129.8 (m), 127.4 (d, $^{1}J_{C,P}$ = 107.8 Hz), 118.7, 111.0. **^{29}Si-NMR** (79 MHz, CD_2Cl_2): δ = −91.6. **^{31}P-NMR:** (162 MHz, CD_2Cl_2): δ = 21.1.

[PPN][Cl-Si(cat^{tBu})$_2$]: $Si(cat^{tBu})_2$ (1 eq., 280 mg, 597 µmol) and [PPN]Cl (1 eq., 343 mg, 597 µmol) in 3 ml CH_2Cl_2 were employed to yield the product as a colorless solid (565 mg, 542 µmol, 91 %).

^{1}H-NMR (400 MHz, CD_2Cl_2): δ = 7.64–7.63 (m, 6H), 7.50–7.44 (m, 24H), 6.83 (bs, 2H), 6.67 (d, $^{3}J_{H,H}$ = 2.2 Hz, 2H), 1.41 (s, 18H), 1.28 (s, 18H). **^{13}C-NMR** (100 MHz, CD_2Cl_2): δ = 148.9, 144.9, 140.1, 134.1, 132.5 (m), 132.1, 129.8 (m), 129.9, 127.4 (d, $^{1}J_{C,P}$ = 108.0 Hz), 112.3, 107.1, 34.7, 34.5, 32.1, 29.8. **^{29}Si-NMR** (79 MHz, CD_2Cl_2): δ = −91.8. **^{31}P-NMR:** (162 MHz, CD_2Cl_2): δ = 21.1.

[PPN][Cl-Si(cat^{F})$_2$]: Si(cat^{F})$_2$ (1 eq., 200 mg, 425 µmol) and [PPN]Cl (1 eq., 244 mg, 425 µmol) in 2.5 ml CH_2Cl_2 were employed to yield the product as a colorless solid (354 mg, 368 µmol, 71 %).

^{1}H-NMR (400 MHz, CD_2Cl_2): δ = 7.51–7.44 (m, 30H). **^{13}C-NMR** spectra unsuitable due to the higher order multiplets of carbon caused by fluorine coupling. **^{19}F-NMR:** (376 MHz, CD_2Cl_2): δ = −167.8 (m, 4F), −174.9 (m, 4F). **^{29}Si-NMR** (79 MHz, CD_2Cl_2): δ = −87.1. **^{31}P-NMR:** (162 MHz, CD_2Cl_2): δ = 21.1.

[PPN][Cl-Si(cat^{Cl})$_2$]: Si(cat^{Cl})$_2$•2 CH_3CN (1 eq., 300 mg, 499 µmol) and [PPN]Cl (1 eq., 286 mg, 498 µmol) in 3 ml CH_2Cl_2 were employed to yield the product as a colorless solid (538 mg, 491 µmol, 99 %).

^{1}H-NMR (400 MHz, CD_2Cl_2): δ = 7.62–7.58 (m, 6H), 7.49–7.40 (m, 24H). **^{13}C-NMR** (100 MHz, CD_2Cl_2): δ = 145.5, 134.1, 132.5 (m), 129.8 (m), 127.4 (d, $^{1}J_{C,P}$ = 108.0 Hz), 121.8, 115.1. **^{29}Si-NMR** (79 MHz, CD_2Cl_2): δ = −90.4. **^{31}P-NMR** (162 MHz, CD_2Cl_2): δ = 21.0.

[PPN][Cl-Si(cat^{Br})$_2$]: Si(cat^{Br})$_2$•2 CH_3CN (1 eq., 300 mg, 313 µmol) and [PPN]Cl (1 eq., 180 mg, 313 µmol) in 6 ml CH_2Cl_2 were employed to yield the product as slightly grey solid (214 mg, 148 µmol, 47 %).

^{1}H-NMR (400 MHz, CD_2Cl_2): δ = 7.65–7.61 (m, 6H), 7.50–7.43 (m, 24H). **^{13}C-NMR** (100 MHz, CD_2Cl_2): δ = 147.2, 134.1, 132.5 (m), 129.8 (m), 127.4 (d, $^{1}J_{C,P}$ = 108.0 Hz), 116.4, 107.3. **^{29}Si-NMR** (79 MHz, CD_2Cl_2): δ = −92.5. **^{31}P-NMR:** (162 MHz, CD_2Cl_2): δ = 21.0.

1.2.5. General Procedure: Catalytic Hydrodefluorination Reaction of 1-Adamantylfluoride

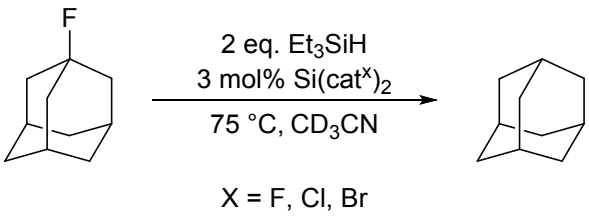

1-Adamantylfluoride (1 eq., 20.0 mg, 130 µmol), Et_3SiH (2 eq., 30.2 mg, 260 µmol) and 3 mol% of $Si(cat^X)_2$ were mixed in 0.5 ml CD_3CN. The sample was inserted in the preheated NMR machine at 75 °C and NMR spectra were recorded at fixed time intervals. The conversion was determined by ^{19}F-NMR integration against C_6F_6 (43 mM) as internal standard (see Figure S6).

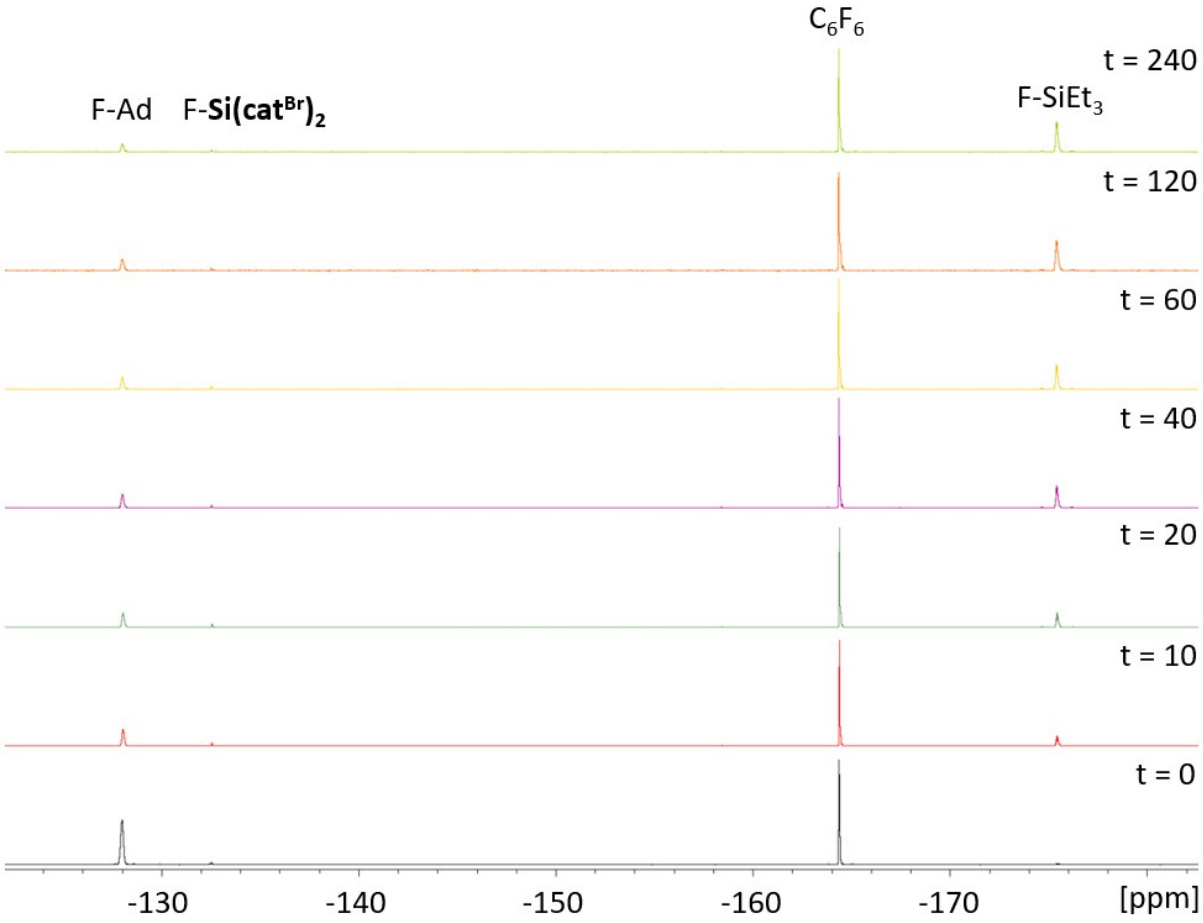

Figure S6: ^{19}F-NMR spectra of **Si(cat^{Br})$_2$** catalyzed hydrodefluorination of 1-adamantylfluoride recorded between t = 0 and t = 240 min. F-Ad (δ ^{19}F = –128.0 ppm) depicts the resonance of the decreasing educt while the peak at –175.4 ppm corresponds to the increasing side product F-$SiEt_3$.

1.2.6. General Procedure: Assessment of Relative Solution Phase Fluoride and Chloride Ion Affinities (FIA_{sol} and ClA_{sol}) – Fluoride- and Chloride-Exchange Reactions

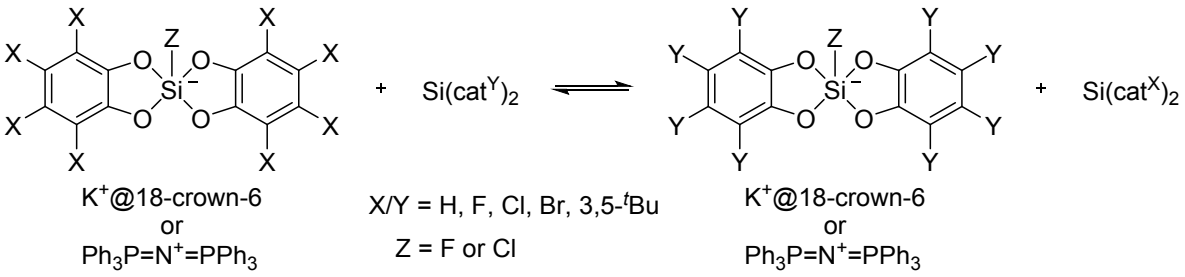

[K@18-crown-6]**[F-Si(cat^{X})$_2$]** or [PPN]**[Cl-Si(cat^{X})$_2$]** (1 eq., 25.0 µmol) was dissolved in 0.5 ml CD_2Cl_2 and **Si(cat^{Y})$_2$** (1 eq., 25.0 µmol) was added. The formed suspension was mixed until equilibrium was reached (min 36 h, up to 5d at 40°C). The reaction was monitored by $^{1}H/^{13}C/^{19}F/^{29}Si$-NMR spectroscopy. Table for FIA_{sol}: see main text.

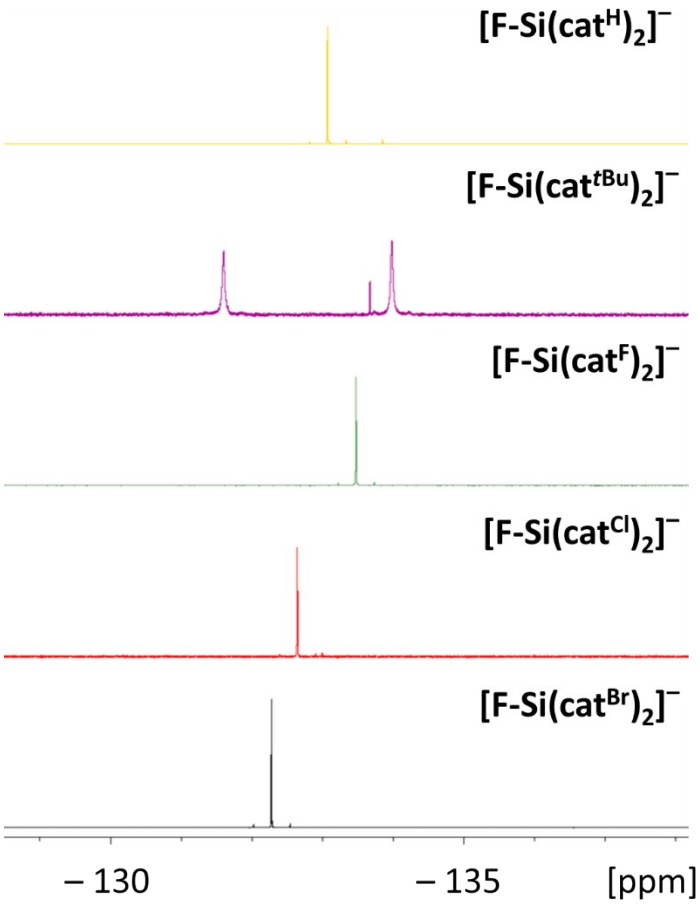

Figure S7a: ^{19}F NMR spectra of all **[F-Si(cat^{X})$_2$]$^-$** species (X = H, 3,5-^{t}Bu, F, Cl, Br) at room temp. in CD_2Cl_2.

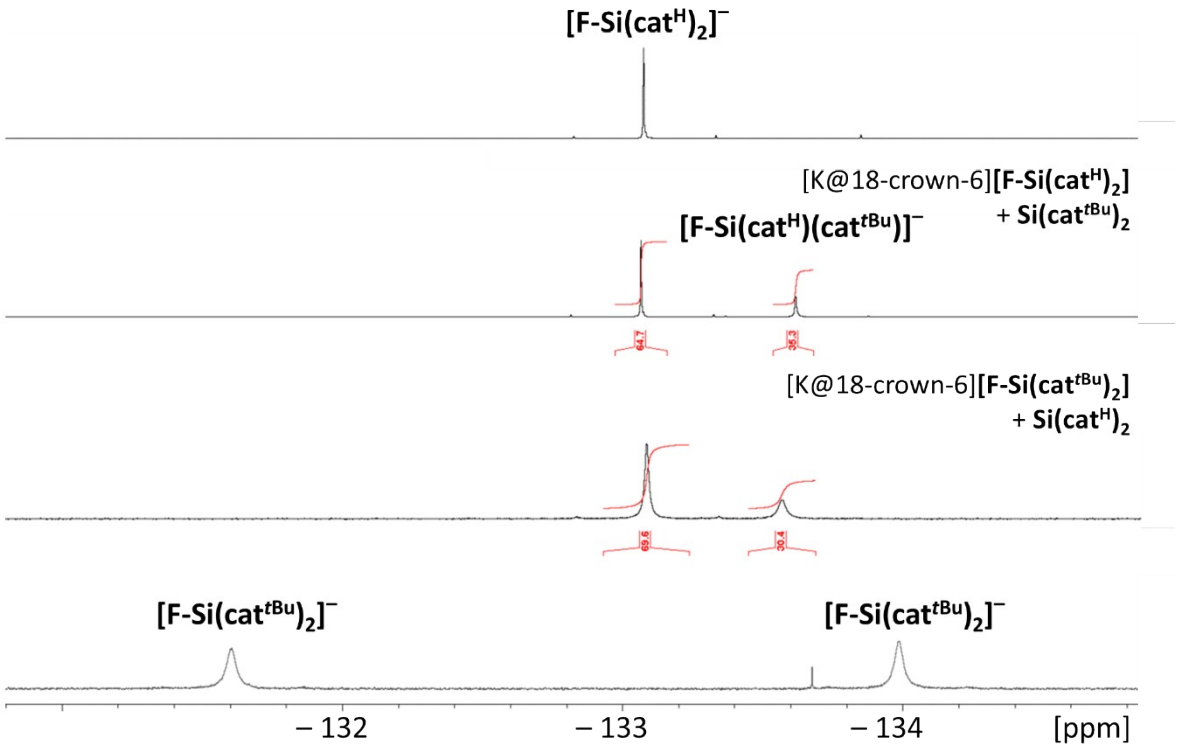

Figure S7b: ^{19}F NMR spectra of **[F-Si(cat^{X})$_2$]$^-$** + **Si(cat^{Y})$_2$** for X/Y = H, ^{t}Bu (0.05 M, CD_2Cl_2, room temp.), calibrated on the **[F-Si(cat^{X})$_2$]$^-$** signals (top and bottom).

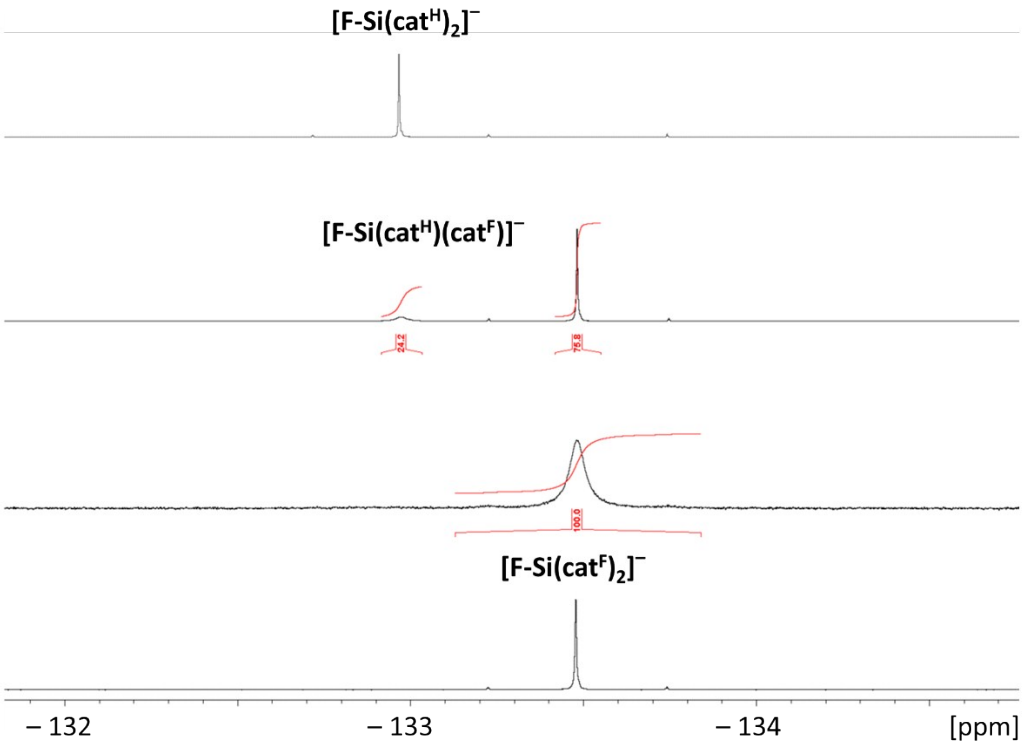

Figure S7c: ^{19}F NMR spectra of **[F-Si(cat^{X})$_2$]$^-$** + **Si(cat^{Y})$_2$** for X/Y = H, F (0.05 M, CD_2Cl_2, room temp.), calibrated on the **[F-Si(cat^{X})$_2$]$^-$** signals (top and bottom).

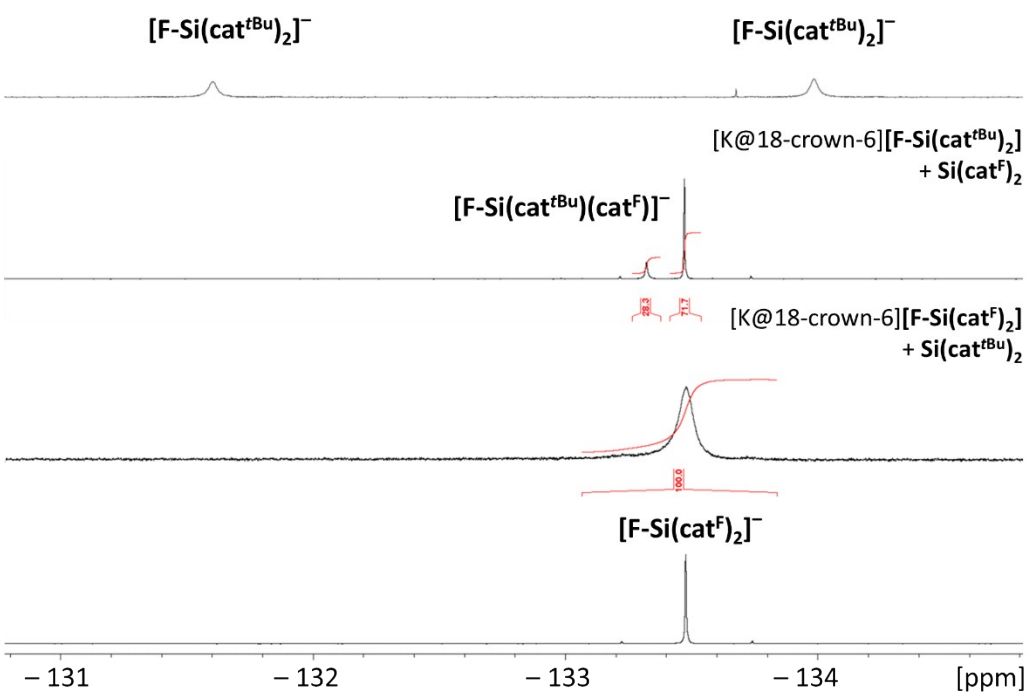

Figure S7d: ^{19}F NMR spectra of **[F-Si(cat^X)$_2$]$^-$** + **Si(cat^Y)$_2$** for X/Y = ^{t}Bu, F (0.05 M, CD_2Cl_2, room temp.), calibrated on the **[F-Si(cat^X)$_2$]$^-$** signals (top and bottom).

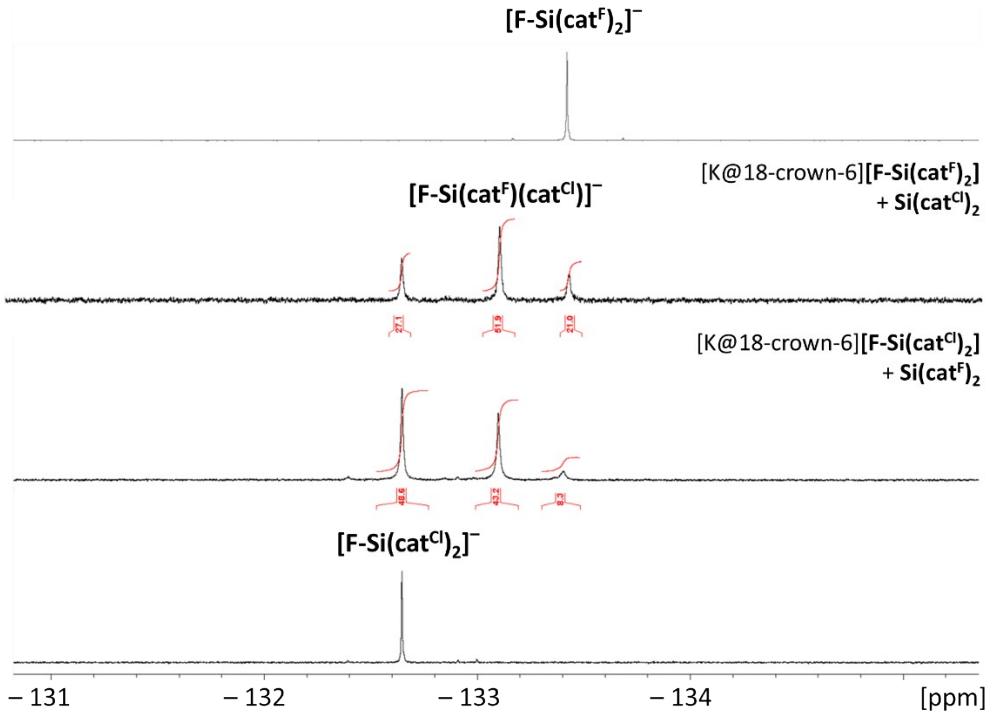

Figure S7e: ^{19}F NMR spectra of **[F-Si(cat^X)$_2$]$^-$** + **Si(cat^Y)$_2$** for X/Y = F, Cl (0.05 M, CD_2Cl_2, room temp.), calibrated on the **[F-Si(cat^X)$_2$]$^-$** signals (top and bottom).

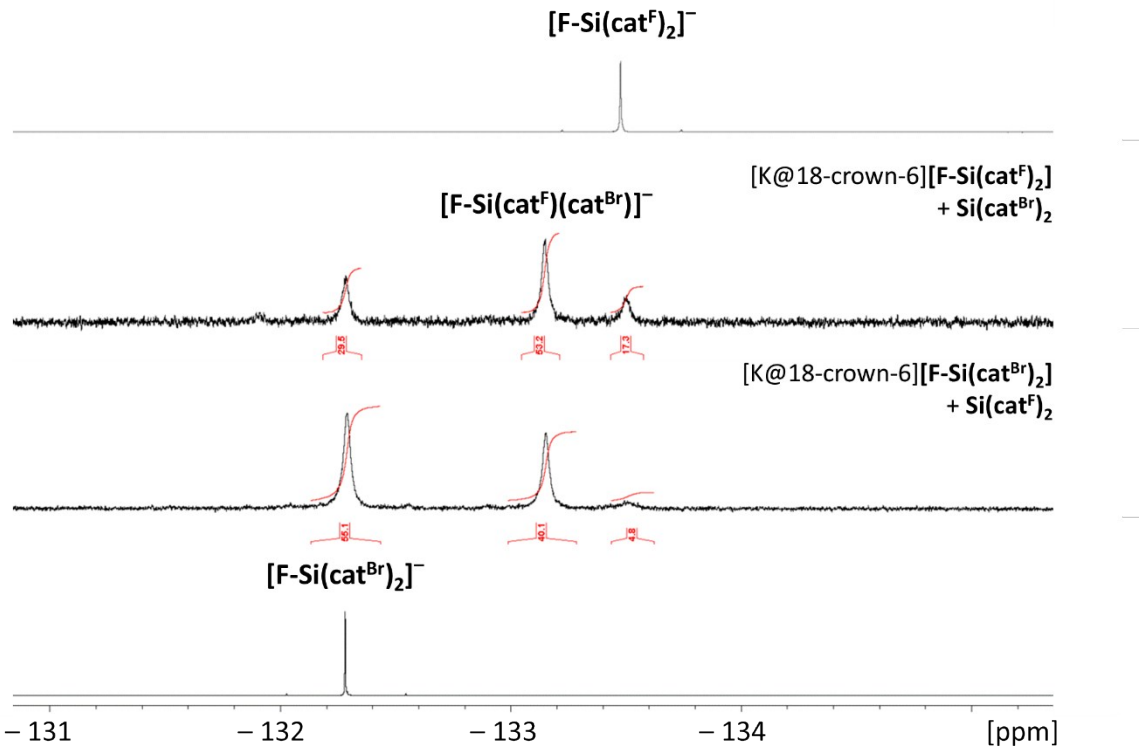

Figure S7f: ^{19}F NMR spectra of **[F-Si(cat^{X})$_2$]$^-$** + **Si(cat^{Y})$_2$** for X/Y = F, Br (0.05 M, CD_2Cl_2, room temp.), calibrated on the **[F-Si(cat^{X})$_2$]$^-$** signals (top and bottom).

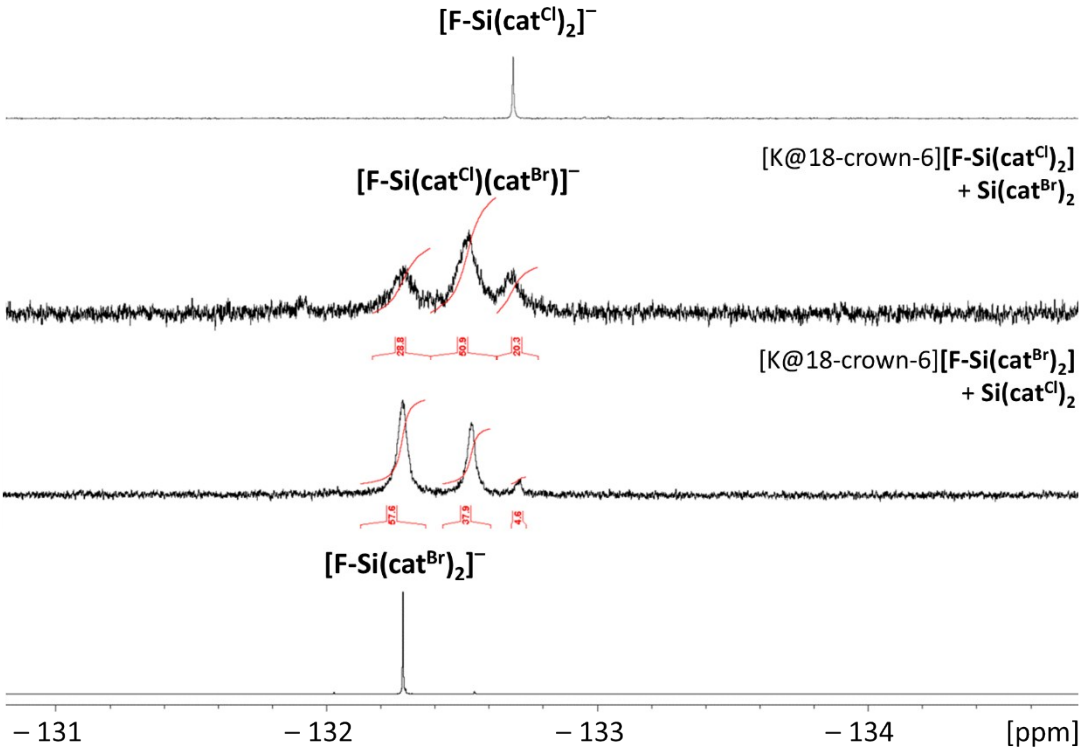

Figure S7g: ^{19}F NMR spectra of **[F-Si(cat^{X})$_2$]$^-$** + **Si(cat^{Y})$_2$** for X/Y = Cl, Br (0.05 M, CD_2Cl_2, room temp.), calibrated on the **[F-Si(cat^{X})$_2$]$^-$** signals (top and bottom).

$[Cl\text{-}Si(cat^X)_2]^- + Si(cat^Y)_2$	Chloride abstraction observed?	Monitored by	*rel. CIA_{sol}*
X = H, Y = ^{t}Bu	no	^{1}H/^{13}C-NMR	H > ^{t}Bu
X = ^{t}Bu, Y = H	yes	^{1}H/^{13}C/^{29}Si-NMR	
X = H, Y = F	yes	^{19}F/^{29}Si-NMR	F > H
X = F, Y = H	no	^{19}F/^{29}Si-NMR	
X = ^{t}Bu, Y = F	yes	^{19}F/^{29}Si-NMR	F > ^{t}Bu
X = F, Y = ^{t}Bu	no	^{19}F/^{29}Si-NMR	
X = F, Y = Cl	yes	^{1}H/^{13}C/^{29}Si-NMR	Cl > F
X = Cl, Y = F	no	^{13}C-NMR	
X = F, Y = Br	yes	^{13}C/^{29}Si-NMR	Br > F
X = Br, Y = F	no	^{13}C/^{29}Si-NMR	
X = Br, Y = Cl	no	^{13}C/^{29}Si-NMR	Br > Cl
X = H, Y = Cl	yes	^{13}C/^{29}Si-NMR	Cl > H
X = ^{t}Bu, Y = Cl	yes	^{13}C/^{29}Si-NMR	Cl > ^{t}Bu
0.05 M of [PPN][Cl-Si(cat^X)$_2$] and 0.05 M Si(cat^Y)$_2$ in CD_2Cl_2, room temp., min. 36 h equilibration time, for Y = Cl and Br, the CH_3CN adducts were used.			

Table S2: Relative solution phase chloride ion affinity: Overview of performed chloride abstraction experiments and used detection methods, the last column gives the relative solution phase chloride ion affinities.

1.2.7. Scrambling Experiments between two Fluoride Adducts

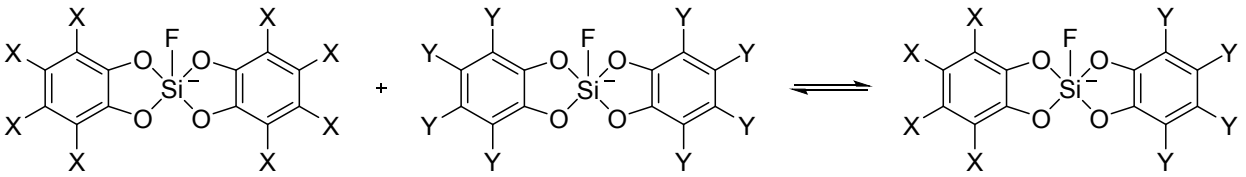

X/Y = H, F, Cl, Br, 3,5-^{t}Bu

Equimolar amounts of two different [K@18-crown-6][F-Si(cat$^{X/Y}$)$_2$] were dissolved in 0.5 ml CD_2Cl_2. Formation of new heteroleptic species was monitored by ^{19}F and ^{29}Si-NMR spectroscopy as well as X-ray diffraction (for X = F, Y = Br) and ESI-HRMS (for X = H, Y = F; X = F, Y = Cl; and X = Cl, Y = Br).

[K@18-crown-6][Si(cat^{H})(cat^{tBu})$_2$]: ^{19}F-NMR: (376 MHz, CD_2Cl_2): δ = −133.7 (s, 1F), −133.8 (s, 1F). **^{29}Si-NMR** (79 MHz, CD_2Cl_2): δ = −104.8 (d, $^1J_{Si,F}$ = 190.8 Hz). No additional signal could be observed in the ^{29}Si-NMR spectrum because both educts have the same shift and coupling constant.

Si(cat^{H})(cat^{F})$_2$: ^{19}F-NMR: (376 MHz, CD_2Cl_2): *δ* = –133.1 (s, 1F, ^{29}Si-satellites 193.0 Hz), –169.1 (m, 2F), –176.4 (m, 2F). **^{29}Si-NMR** (79 MHz, CD_2Cl_2): –103.0 (d, $^1J_{Si,F}$ = 193.0 Hz). **ESI-HRMS** (negative): [F-Si(cat^{H})(cat^{F})]$^-$ m/z calcd. 334.9804, found: 334.9806.

Si(cat^{tBu})(cat^{F})$_2$: ^{19}F-NMR: (376 MHz, CD_2Cl_2): *δ* = –133.3 (s, 1F, ^{29}Si-satellites 192.6 Hz), –169.2 (m, 2F), –176.8 (m, 2F). **^{29}Si-NMR** (79 MHz, CD_2Cl_2): –102.9 (d, $^1J_{Si,F}$ = 192.6 Hz).

Si(cat^{F})(cat^{Cl})$_2$: ^{19}F-NMR: (376 MHz, CD_2Cl_2): *δ* = –133.2 (s, 1F), –168.2 (m, 2F), –175.3 (m, 2F). **^{29}Si-NMR** (79 MHz, CD_2Cl_2): *δ* = –103.3 (d, $^1J_{Si,F}$ = 194.3 Hz). **ESI-HRMS** (negative): [F-Si(cat^{F})(cat^{Cl})]$^-$ m/z calcd. 472.8216, found: 472.8217.

Si(cat^{F})(cat^{Br})$_2$: ^{19}F-NMR: (376 MHz, CD_2Cl_2): *δ* = –133.1 (bs, 1F), –168.1 (m, 2F), –175.3 (m, 2F). **^{29}Si-NMR** (79 MHz, CD_2Cl_2): *δ* = -104.3 (d, $^1J_{Si,F}$ = 194.2 Hz)

Si(cat^{Cl})(cat^{Br})$_2$: ^{19}F-NMR: (376 MHz, CD_2Cl_2): *δ* = –132.5 (s, 1F). **^{29}Si-NMR** (79 MHz, CD_2Cl_2): *δ* = –106.0 (d, $^1J_{Si,F}$ = 195.4 Hz). **ESI-HRMS** (negative): [F-Si(cat^{Cl})(cat^{Br})]$^-$ m/z calcd. 716.4973, found: 716.4977.

1.2.8. General Procedure: Chloride-Abstraction from Trityl Chloride

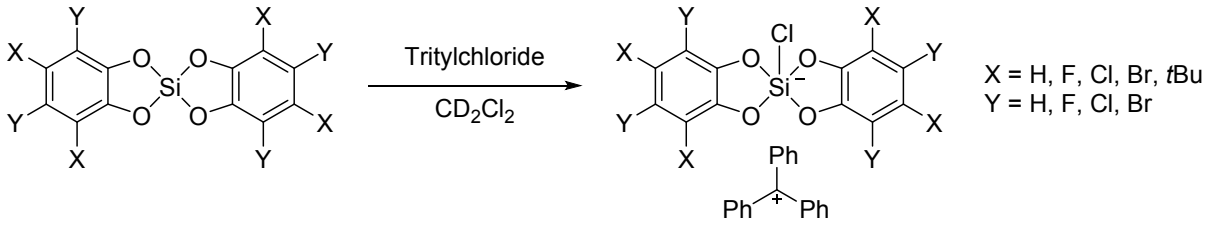

To a solution of trityl chloride (1 eq., 2.90 mg, 10.4 µmol) in 0.5 ml CD_2Cl_2 1 eq. $Si(cat^X)_2$ was added. For X = H, ^{t}Bu no considerable reaction took place, for X = F, Cl, Br the solution turned yellow, indicating the formation of the tritylium cation along with the corresponding chloridosilicate $[CPh_3][$**Cl-Si(cat^X)$_2$**$]$ in a ratio given in table 5 in the main part. Conversion was monitored by integration of ^{1}H-NMR spectra (see Figure S8). Signs of degradation of the trityl cations were observable after heating the mixtures for > 24 at 50 °C. The obtained equilibrium data was obtained after only 2 h, wherein this decomposition was negligible/invisible.

NMR data for the chlorosilicates are given in chapter 1.2.5.

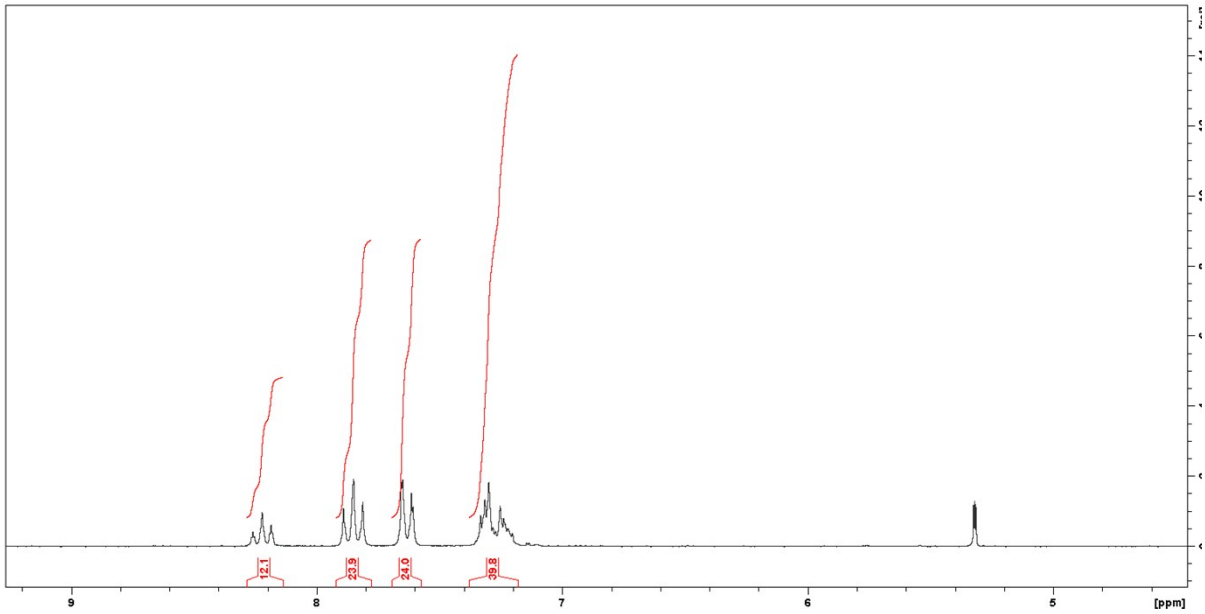

Figure S8: ^{1}H-NMR spectrum of the mixture of $Si(cat^{Cl})_2$•2 CH_3CN and tritylchloride after 1.5 h at 50 °C. The three left signals correspond to the tritylium cation whilst the multiplett on the right belongs to unreacted tritylchloride.

2. Definition of Berry coordinate and Topography Parameter (TP)

Considering the geometry of pentavalent compounds, there are two main coordination forms: the more common trigonal-bipyramidal (tbp) and less common square planar (sp) form. There is a change with only a small energy barrier from tbp to a sp geometry.

The distortion takes place along the Berry coordinate (see Figure S9). Couzijn et. al gives a simple quantitative description of this effect by using a topology parameter (TP).[3] The obtained value allows a rough estimation of the distortion along the Berry coordinate. The TP ranges from 1 = ideal tbp to 0 = ideal sp. The largest angle is defined as Θ_{ax}. The three remaining atoms lie in the plane of the trigonal pyramid, the largest angle therein is defined as Θ_{eq}. The Berry coordinate is defined by the axis of the remaining atom and the center.

$$TP = \frac{\theta_{ax} - \theta_{eq}}{60°}$$

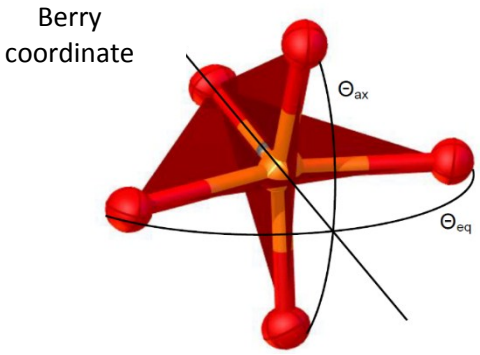

Figure S9: Formula and schematic depiction for the computation of the topology parameter.

3. Computational Details

3.1. Geometry optimization and single point energies for FIA/CIA computations

Geometry optimizations and single point energy calculations have been performed with ORCA 4.0.1.[4] The RI approximation[5] for the Coulomb integrals was used in all cases (RIJCOSX), with application of corresponding auxiliary basis sets.[6] Previous benchmark studies on the ideal method for geometry optimization revealed the PW6B95[7] including Grimme's semi-empirical dispersion correction[8] with Becke-Johnson damping function[9] (D3(BJ) and the def2-TZVPP[10] basis set as ideal to reproduce the experimental solid-state structural parameters. All calculated geometries have been confirmed as energetic minima on the potential energy surface by analytical calculation of harmonic frequencies at the BP86-D3(BJ)/def2-SVP level. Enthalpies at 298 K have been calculated with the same level of theory by using the rigid-rotor harmonic oscillator (RRHO) approximation,[11] as implemented in ORCA. The final single point electronic energies for the evaluation of FIA/CIA were calculated with the highly accurate and linear scaling version of domain based localized pair natural orbitals based coupled cluster theory (DLPNO-CCSD(T)), as implemented in ORCA 4.0.[12] It has been shown that the DLPNO-CCSD(T) method reproduces experimentally obtained bond energies within an accuracy of < 1 kcal mol^{-1}.[13] Benchmark calculations with TightPNO vs NormalPNO settings revealed a change of energies by < 1 kcal/mol^{-1}, thus NormalPNO settings and the default thresholds were used throughout these studies. Dunning's augmented correlation consistent aug-cc-pVQZ basis set and matching auxiliary basis sets were used for all DLPNO-CCSD(T) single point energies. As it can be expected with this basis set size, no extrapolation techniques or BSSE corrections are required for an accurate description.[14]

The final FIA/CIA reaction enthalpies were calculated according to the scheme proposed by Krossing,[15] using the therein given G3 anchor points and isodesmic reactions. Due to heavy linear dependencies in the FIA calculation for $Si(OPh)_4$ with DLPNO-CCSD(T)/aug-cc-pVQZ, the smaller cc-pVQZ basis set (without augmented functions) had to be used exclusively in this case. Based on comparative computations of the FIA with cc-pVQZ vs. aug-cc-pVQZ (SiH_4, $Si(OMe)_4$, $Si(cat)_2$), an amount of 6 kJ mol^{-1} was added to the cc-pVQZ value of $Si(OPh)_4$. Table S3 lists all relevant data for the FIA and CIA calculation. The FIA of other Lewis acids in Figure 5 in the main text have been computed at the same level of theory and details will be reported as part of a larger FIA collection in close future.

The corresponding solvation free enthalpies were obtained from COSMO-RS[16] calculations as implemented in the ADF program package,[17] based on BP86-D3/TZP[18] single point energy calculations for the solute-solvent interaction (Table S3d). The final solvation corrected enthalpies were obtained by combining the solvation energies for X^-, the respective Lewis acid and the fluoride adduct with the DLPNO-CCSD(T)/aug-cc-pVQZ vacuum enthalpies.

	E [Hartree] BP86 D3/def2-SVP	in kJ	thermal correction [kJ]	electronic + thermal [kJ]	LA + Me_3SiY (A)	Me_3Si^+ + LA-Y^- (B)	(B)-(A)	CIA/ FIA
$Si(cat^H)_2$	-1052.0841	-2762246.7	492.6	-2761754.1				
$[Cl\text{-}Si(cat^H)_2]^-$	-1512.3298	-3970622.0	497.8	-3970124.2	-5043746.4	-5043219.9	526.6	232.8
$[F\text{-}Si(cat^H)_2]^-$	-1152.0016	-3024580.3	499.9	-3024080.4	-4097693.6	-4097176.0	517.5	440.9
$Si(cat^F)_2$	-1845.3213	-4844890.9	346.0	-4844545.0				
$[Cl\text{-}Si(cat^F)_2]^-$	-2305.5963	-6053343.1	350.3	-6052992.8	-7126537.3	-7126088.5	448.8	310.6
$[F\text{-}Si(cat^F)_2]^-$	-1945.2687	-5107303.0	352.5	-5106950.5	-6180484.4	-6180046.2	438.2	520.2
$Si(cat^{Cl})_2$	-4728.0889	-12413597.3	322.5	-12413274.8				
$[Cl\text{-}Si(cat^{Cl})_2]^-$	-5188.3693	-13622063.5	329.7	-13621733.9	-14695267.1	-14694829.5	437.6	321.8
$[F\text{-}Si(cat^{Cl})_2]^-$	-4828.0419	-12676024.1	331.9	-12675692.3	-13749214.2	-13748787.9	426.3	532.2
$Si(cat^{Br})_2$	-21640.2511	-56816479.3	315.8	-56816163.5				
$[Cl\text{-}Si(cat^{Br})_2]^-$	-22100.5343	-58024952.7	323.4	-58024629.3	-59098155.9	-59097725.0	430.9	328.5
$[F\text{-}Si(cat^{Br})_2]^-$	-21740.2070	-57078913.4	325.6	-57078587.8	-58152103.0	-58151683.5	419.5	538.9
SiH_4	-291.8148	-766159.7	89.7	-766070.0				
$[F\text{-}SiH_4]^-$	-391.6250	-1028211.4	93.5	-1028117.9	-2102009.4	-2101213.6	795.8	162.6
$Si(OMe)_4$	-749.7882	-1968569.0	474.6	-1968094.4				
$[F\text{-}Si(OMe)_4]^-$	-849.6302	-2230704.0	475.8	-2230228.2	-3304033.8	-3303323.9	709.9	248.5
$SiOPh_4$	-1516.3184	-3981094.1	1045.5	-3980048.6				
$[F\text{-}Si(OPh)_4]^-$	-1616.2079	-4243353.9	1050.6	-4242303.3	-5315988.0	-5315398.9	589.0	369.4

Table S3a: Computation of FIAs at the BP86-D3/SVP level of theory (including thermal and ZPE correction).

Compound	E [Hartree] PW6B95-D3/def2-TZVPP	electronic + thermal (from BP86) [kJ]	LA + Me_3SiY (A)	Me_3Si^+ + LA-Y^- (B)	(B)-(A)	CIA/ FIA
$Si(cat^H)_2$	-1054.1986	-2767305.8				
$[Cl\text{-}Si(cat^H)_2]^-$	-1514.8998	-3976871.7	-5052158.2	-5051590.4	567.8	191.6
$[F\text{-}Si(cat^H)_2]^-$	-1154.3367	-3030211.0	-4105488.8	-4104929.7	559.1	399.3
$Si(cat^F)_2$	-1849.2085	-4854750.9				
$[Cl\text{-}Si(cat^F)_2]^-$	-2309.9442	-6064408.2	-7139603.4	-7139126.8	476.5	282.9
$[F\text{-}Si(cat^F)_2]^-$	-1949.3825	-5117751.3	-6192933.9	-6192469.9	464.0	494.4
$Si(cat^{Cl})_2$	-4733.9182	-12428579.7				
$[Cl\text{-}Si(cat^{Cl})_2]^-$	-5194.6564	-13638240.8	-14713432.1	-14712959.5	472.6	286.8
$[F\text{-}Si(cat^{Cl})_2]^-$	-4834.0950	-12691584.5	-13766762.7	-13766303.2	459.5	498.9
$Si(cat^{Br})_2$	-21651.6529	-56846098.9				
$[Cl\text{-}Si(cat^{Br})_2]^-$	-22112.3929	-58055764.1	-59130951.4	-59130482.8	468.6	290.8
$[F\text{-}Si(cat^{Br})_2]^-$	-21751.8314	-57109107.7	-58184281.9	-58183826.4	455.5	502.9
SiH_4	-292.1502	-766950.6				
$[F\text{-}SiH_4]^-$	-392.2063	-1029644.1	-2105133.6	-2104362.8	770.8	187.6
$Si(OMe)_4$	-751.2037	-1971810.7				
$[F\text{-}Si(OMe)_4]^-$	-851.2727	-2234540.7	-3309993.7	-3309259.4	734.3	224.1
$SiOPh_4$	-1519.5217	-3988458.7				
$[F\text{-}Si(OPh)_4]^-$	-1619.6275	-4251281.4	-5326641.8	-5326000.1	641.6	316.8

Table S3b: Computation of FIAs at the PW6B95/TZVPP-D3 level of theory (including thermal and ZPE correction from BP86).

Compound	E [Hartree] DLPNO-CCSD(T)/aug-cc-pVQZ	electronic + thermal (from BP86) [kJ]	LA + Me_3SiY (A)	Me_3Si^+ + LA-Y^- (B)	(B)-(A)	CIA/ FIA
$Si(cat^H)_2$	-1051.2148	-2759471.8				
$[Cl\text{-}Si(cat^H)_2]^-$	-1511.1069	-3966913.3	-5039355.6	-5038776.7	579.0	180.4
$[F\text{-}Si(cat^H)_2]^-$	-1151.1379	-3021812.7	-4094243.6	-4093676.1	567.6	390.9
$Si(cat^F)_2$	-1844.4684	-4842305.9				
$[Cl\text{-}Si(cat^F)_2]^-$	-2304.3979	-6049846.3	-7122189.7	-7121709.7	480.0	279.4
$[F\text{-}Si(cat^F)_2]^-$	-1944.4288	-5104745.4	-6177077.7	-6176608.7	468.9	489.5
$Si(cat^{Cl})_2$	-4724.4524	-12403727.3				
$[Cl\text{-}Si(cat^{Cl})_2]^-$	-5184.3884	-13611282.2	-14683611.1	-14683145.6	465.6	293.8
$[F\text{-}Si(cat^{Cl})_2]^-$	-4824.4206	-12666184.4	-13738499.1	-13738047.7	451.4	507.1
$Si(cat^{Br})_2$	-21628.6525	-56785711.3				
$[Cl\text{-}Si(cat^{Br})_2]^-$	-22088.5950	-57993282.6	-59065595.1	-59065146.0	449.1	310.3
$[F\text{-}Si(cat^{Br})_2]^-$	-21728.6327	-57048199.5	-58120483.1	-58120062.9	420.2	538.3
SiH_4	-291.4516	-765116.6				
$[F\text{-}SiH_4]^-$	-391.2920	-1027243.6	-2099888.4	-2099107.0	781.4	177.0
$Si(OMe)_4$	-749.2606	-1966709.2				
$[F\text{-}Si(OMe)_4]^-$	-849.1134	-2228871.4	-3301481.0	-3300734.8	746.2	212.2
$SiOPh_4$	-1514.9741	-3977564.4				
$[F\text{-}Si(OPh)_4]^-$	-1614.8561	-63337960.4	-5311271.4	-5310609.4	662.0	296.4

Table S3c: Computation of FIAs at the DLPNO-CCSD(T)/aug-cc-pVQZ level of theory (including thermal and ZPE correction from BP86). [a]the cc-pVQZ basis set was used and extrapolated to aug-cc-pVQZ energy (+6 kJ mol, see text above)

Compound	free Energy of solvation (COSMO-RS, kJ/mol)	solvation correction term: E_{solv}(LA-F) - E_{solv}(X^-) - E_{solv}(LA)	solvation corrected CIA/ FIA			
$Si(cat^H)_2$	-38.7					
$[Cl\text{-}Si(cat^H)_2]^-$	-205.4	103.3	77.2			
$[F\text{-}Si(cat^H)_2]^-$	-204.4	150.2	240.7			
$Si(cat^F)_2$	-40.2					
$[Cl\text{-}Si(cat^F)_2]^-$	-170.1	140.1	139.2			
$[F\text{-}Si(cat^F)_2]^-$	-168.3	187.7	301.8			
$Si(cat^{Cl})_2$	-69.8					
$[Cl\text{-}Si(cat^{Cl})_2]^-$	-195.3	144.5	149.3			
$[F\text{-}Si(cat^{Cl})_2]^-$	-193.2	192.5	314.5			
$Si(cat^{Br})_2$	-87.4					
$[Cl\text{-}Si(cat^{Br})_2]^-$	-214.0	143.4	166.9			
$[F\text{-}Si(cat^{Br})_2]^-$	-211.5	191.7	346.5			
SiH_4	-4.3	-765116.6				
$[F\text{-}SiH_4]^-$	-220.8	-1027243.6	77.7			
$Si(OMe)_4$	-31.8	-1966709.2				
$[F\text{-}Si(OMe)_4]^-$	-223.2	-2228871.4	87.8			
					halide	E_{solv} [kJ mol^{-1}]
$SiOPh_4$	-67.8	-3977564.4			F^-	-315.8
$[F\text{-}Si(OPh)_4]^-$	-213.9	-63337960.4	126.7		Cl^-	-270.0

Table S3d: Combination of energies of solvation (COSMO-RS, in CH_2Cl_2) with FIA and CIA at the DLPNO-CCSD(T)/aug-cc-pVQZ level of theory.

3.2. Discussion of the influence of CH_3CN for $Si(cat^{Cl})_2$

The association equilibria of CH_3CN with **$Si(cat^{Cl})_2$** were computed at the PW6B95-D3(BJ)/def2-TZVPP level of theory. Enthalpies and entropies at 298 K have been calculated at the BP86-D3(BJ)/def2-SVP level by using the rigid-rotor harmonic oscillator (RRHO) approximation,[11] as implemented in ORCA.

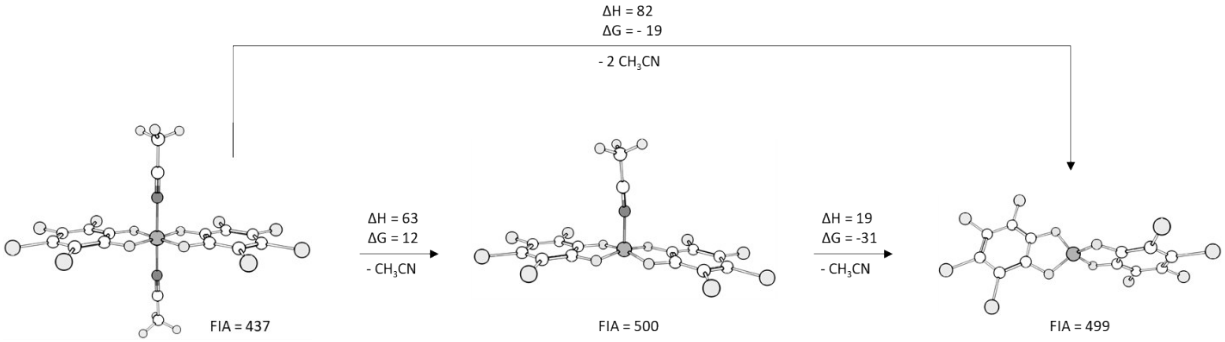

Figure S10: Thermodynamics of the dissociation of CH_3CN from $Si(cat^{Cl})_2 \cdot 2\ CH_3CN$ computed at PW6B95-D3(BJ)/def2-TZVPP, all values in kJ mol^{-1}.

It can be seen, that the spontaneous dissociation of two units of CH_3CN from $Si(cat^{Cl})_2 \cdot 2\ CH_3CN$ is indeed favorable, due to entropy gain (endothermic but exergonic). This makes the overall discussion based on the free acids as plausible. The FIA (enthalpy!) of the CH_3CN bis-adduct is attenuated by the loss of bond energy of Si-$NCCH_3$, but the FIA of the mono-adduct is actually even larger as the FIA for the free Lewis acid.

3.3. ^{29}Si-NMR shift calculation

^{29}Si-NMR chemical shifts of the chlorosilicates **$[Cl\text{-}Si(cat^{X})_2]^-$** were calculated based on the PW6B95-D3(BJ)/def2-TZVPP structures using the respective modules[19] in the ADF program package, with the PBE0 hybrid functional[20] and a triple-ζ Slater type basis set (TZ2P)[18], in which relativistic spin orbit contributions to the magnetic shielding constants were treated by the two-component zero order regular approximation (SO-ZORA).[21] Solvation (CH_2Cl_2) was modeled with COSMO[22] as implemented in ADF.[23] NMR chemical shifts are given relative to TMS (0 ppm), calculated at the same level of theory.

Compound	^{29}Si-NMR calc. [ppm][a]	^{29}Si-NMR exp. [ppm][b]
$[Cl\text{-}Sicat^{H}_2]^-$	–91.8	–91.6
$[Cl\text{-}Si(cat^{tBu})_2]^-$	–91.6	–91.8
$[Cl\text{-}Si(cat^{F})_2]^-$	–88.7	–87.1
$[Cl\text{-}Si(cat^{Cl})_2]^-$	–91.7	–90.4
$[Cl\text{-}Si(cat^{Br})_2]^-$	–94.1	–92.5
[a]SO-ZORA-PBE0/TZ2P(COSMO, CH_2Cl_2)//PW6B95/def2-TZVPP, [b]in CD_2Cl_2 at rt		

Table S4: computed ^{29}Si-NMR shifts for chlorosilicates.

3.4. Energy decomposition analysis (EDA) of the fluoride adducts

The EDA scheme (based on BP86-D3/TZ2P, ADF) arbitrarily decomposes the interaction energies (ΔE_{int}) between the *prepared* monomers into contributions of Pauli repulsion (ΔE_{Pauli}), electrostatic interaction (ΔE_{elstat}), orbital interaction (ΔE_{orb}) and dispersion (ΔE_{disp}). To obtain the final association energies (D_e) between the *relaxed* fragments, the preparation energies (ΔE_{prep}) have to be added to the interaction energies. The intuitive fragmentation into two closed shell monomeric species (fluoride + neutral Lewis acid) was chosen, and the corresponding EDA values can be found in the main text.

3.5. NBO analysis of fluoride adducts

Natural localized molecular orbitals (NLMO) and second order perturbation energies were obtained by NBO analysis with NBO 7.0,[24] based on PBE0-D3/def2-TZVPP densities obtained from ORCA. The values can be found in the main text.

3.6. QTAIM analysis of the Si-F bonds in the fluoride adducts

QTAIM analyses were performed on the PBE0-D3/def2-TZVPP electron densities, using the AIMAll software with default integration.[25] To describe and compare the nature of chemical bonds, a variety of descriptors have been developed in the context of Bader's theory of AIM, specifically at the so-called bond critical points (BCP).[26] The components considered in the QTAIM analysis are the electron density, $\rho(\mathbf{r}_{BCP})$, and the Laplacian of the density, $\nabla^2\rho(\mathbf{r}_{BCP})$ and the delocalization index (DI). Low electron densities and positive Laplacians are an indication for closed shell (ionic) interactions whereas the opposite is found for shared (covalent) bonds. The respective values can be found in the main text.

3.7. Global electrophilicity index (GEI)

The global electrophilicity index (GEI) was calculated according the recently published procedure on the HOMO/LUMO energies of the PW6B95/def2-TZVPP calculations and plotted against the FIA obtained by DLPNO-CCSD(T)/aug-cc-pVQZ.[27] A clear correlation can be found within the class of $Si(cat^X)_2$ Lewis acids (blue dots) which, however, breaks down for the structurally differing Lewis acids (orange dots) (figure S10).

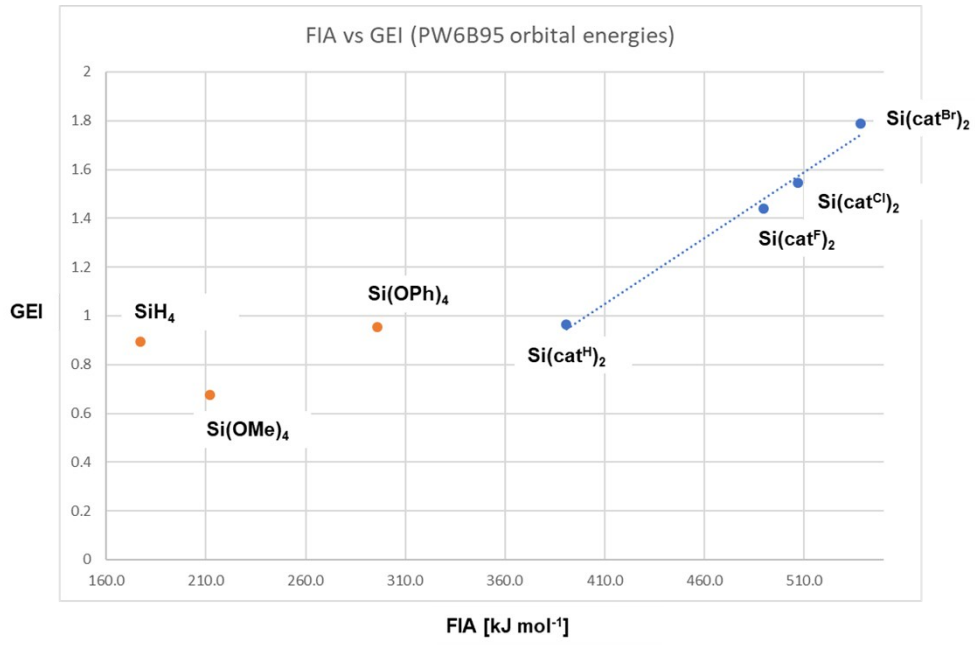

Figure S11: FIA vs GEI plot of the investigated Lewis acids in this study.

4. X-Ray diffraction

General

Suitable crystals of the compounds were taken directly out of the mother liquor, immersed in perfluorinated polyether oil, and fixed on top of a glass capillary. Measurements were made on a Nonius-Kappa charge-coupled device diffractometer with a low-temperature unit using graphite-monochromated Mo-K_α radiation. The temperature was set at 120 K. The data collected were processed using standard Nonius software (https://www.nonius.nl/KappaCCD/manuals/denzo-smn/). Structures were solved by direct methods using the SHELXS (http://shelx.uni-ac.gwdg.de/SHELX/shelxs_keywords.php) or by intrinsic phasing using the SHELXT (http://shelx.uni-ac.gwdg.de/SHELX/shelxt_keywords.php) program and refined with the SHELXL program (http://shelx.uni-ac.gwdg.de/SHELX/shelxl_user_guide.pdf). Graphical handling of the structural data during solution and refinement was performed with Olex2.[28] Atomic coordinates and anisotropic thermal parameters of non-hydrogen atoms were refined by full-matrix least-squares calculations. Hydrogen atoms were included using a riding model or rigid methyl groups. For absorption and scaling of intensity data the SADABS program was used, if suitable.[29] Crystallographic data (including structure factors) for the structure reported in this Article are deposited with the Cambridge Crystallographic Data Centre as supplementary publication no. CCDC 1905749-1905760, and can be obtained free of charge. Crystal data and structures for the compounds are summarized in the following tables.

Et_3PO-**Si(cat^H)$_2$**

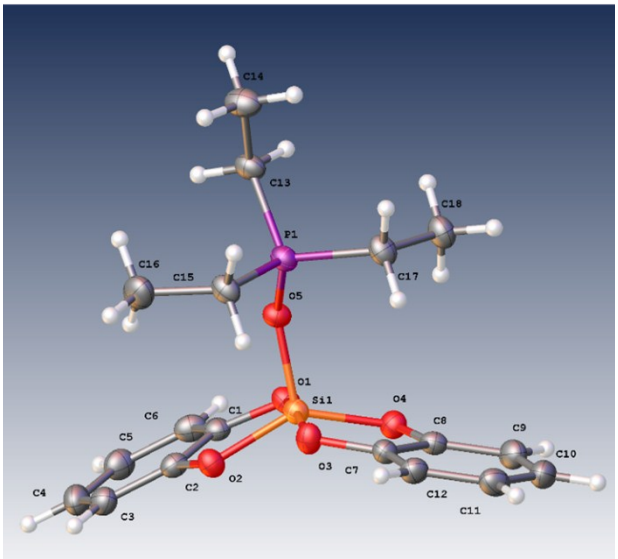

Identification code	ms24b_P2
Empirical formula	$C_{18}H_{23}O_5PSi$
Formula weight	378.42
Temperature/K	120
Crystal system	monoclinic
Space group	$P2_1/c$
a/Å	10.012(2)
b/Å	15.717(3)
c/Å	12.437(3)
α/°	90
β/°	109.77(3)
γ/°	90
Volume/Å^3	1841.7(7)
Z	4
ρ_{calc} g/cm^3	1.365
μ/mm^{-1}	0.240
F(000)	800.0
Crystal size/mm^3	0.6 × 0.5 × 0.5
Radiation	MoK_α (λ = 0.71073)
2Θ range for data collection/°	5.04 to 60.044
Index ranges	-14 ≤ h ≤ 14, -22 ≤ k ≤ 22, -17 ≤ l ≤ 17
Reflections collected	10498
Independent reflections	5371 [R_{int} = 0.0710, R_{sigma} = 0.1013]
Data/restraints/parameters	5371/0/229
Goodness-of-fit on F^2	0.996
Final R indexes [I>=2σ (I)]	R_1 = 0.0536, wR_2 = 0.1152
Final R indexes [all data]	R_1 = 0.1292, wR_2 = 0.1439

Largest diff. peak/hole / e $Å^{-3}$	0.40/-0.42

Et_3PO-**Si(cat^{Br})$_2$**

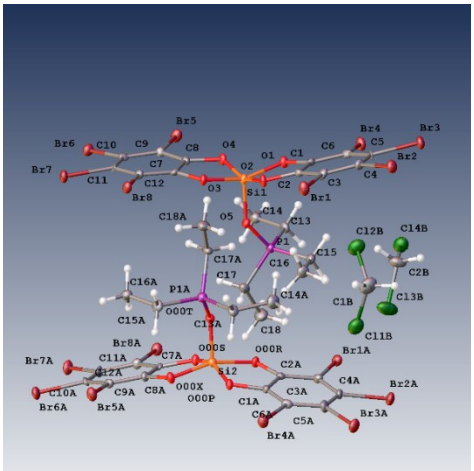

Identification code	ms19f
Empirical formula	$C_{19}H_{17}Br_8Cl_2O_5PSi$
Formula weight	1094.56
Temperature/K	120
Crystal system	triclinic
Space group	P-1
a/Å	11.061(2)
b/Å	12.978(3)
c/Å	22.591(5)
α/°	86.42(3)
β/°	79.44(3)
γ/°	67.26(3)
Volume/Å^3	2940.2(12)
Z	4
ρ_{calc} g/cm^3	2.473
μ/mm^{-1}	11.219
F(000)	2056.0
Crystal size/mm^3	0.5 × 0.4 × 0.35
Radiation	MoK_α (λ = 0.71073)
2Θ range for data collection/°	3.402 to 57.998
Index ranges	-14 ≤ h ≤ 15, -17 ≤ k ≤ 17, -30 ≤ l ≤ 30
Reflections collected	29045
Independent reflections	15632 [R_{int} = 0.0630, R_{sigma} = 0.1036]
Data/restraints/parameters	15632/0/655
Goodness-of-fit on F^2	0.958
Final R indexes [I>=2σ (I)]	R_1 = 0.0437, wR_2 = 0.0672
Final R indexes [all data]	R_1 = 0.1004, wR_2 = 0.0784
Largest diff. peak/hole / e Å^{-3}	0.93/-1.09

Multi-scan absorption correction (Bruker Sadabs) was used. The unordinary displacement parameter of C11 could not be resolved, and might stem from phase transition upon cooling of the crystal.

Et_3PO-**Si(cat^F)$_2$**

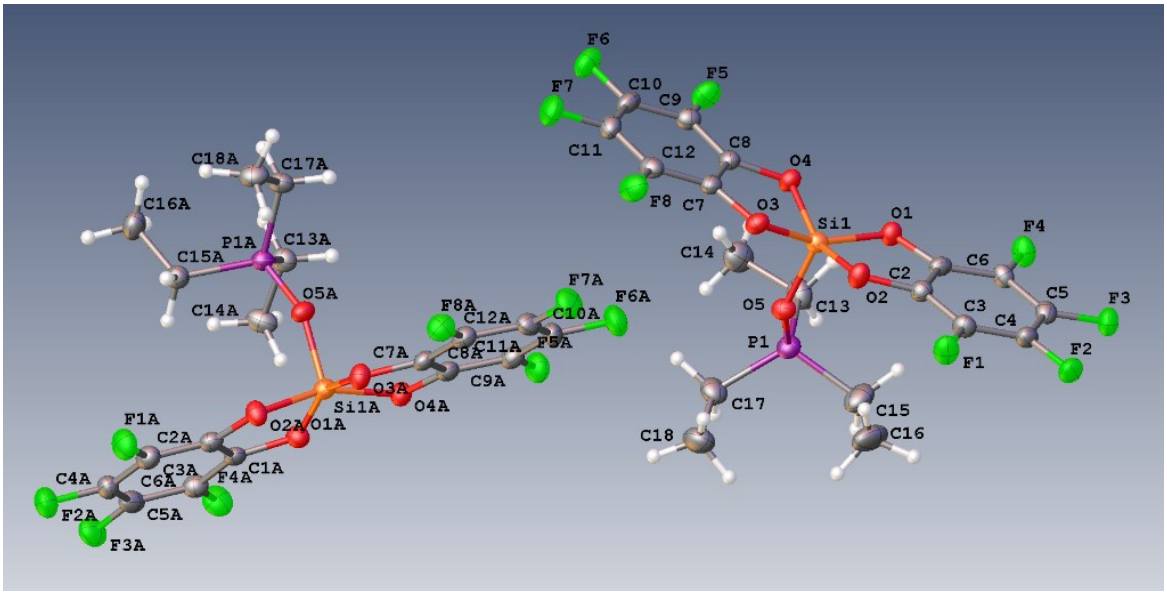

Identification code	ms93_P21
Empirical formula	$C_{18}H_{15}O_5F_8SiP$
Formula weight	522.36
Temperature/K	120
Crystal system	monoclinic
Space group	$P2_1/c$
a/Å	21.898(4)
b/Å	12.467(3)
c/Å	14.654(3)
α/°	90
β/°	91.49(3)
γ/°	90
Volume/Å^3	3999.2(14)
Z	8
ρ_{calc} g/cm^3	1.735
μ/mm^{-1}	0.302
F(000)	2112.0
Crystal size/mm^3	0.5 × 0.5 × 0.4
Radiation	MoK_α (λ = 0.71073)
2Θ range for data collection/°	3.76 to 58
Index ranges	-29 ≤ h ≤ 29, -16 ≤ k ≤ 17, -19 ≤ l ≤ 19
Reflections collected	20488
Independent reflections	10615 [R_{int} = 0.0644, R_{sigma} = 0.0878]
Data/restraints/parameters	10615/0/601
Goodness-of-fit on F^2	0.981
Final R indexes [I>=2σ (I)]	R_1 = 0.0466, wR_2 = 0.0944
Final R indexes [all data]	R_1 = 0.1171, wR_2 = 0.1162

Largest diff. peak/hole / e $Å^{-3}$	0.36/-0.39

Et_3PO-**Si(cat^{Br})$_2$**-$OPEt_3$

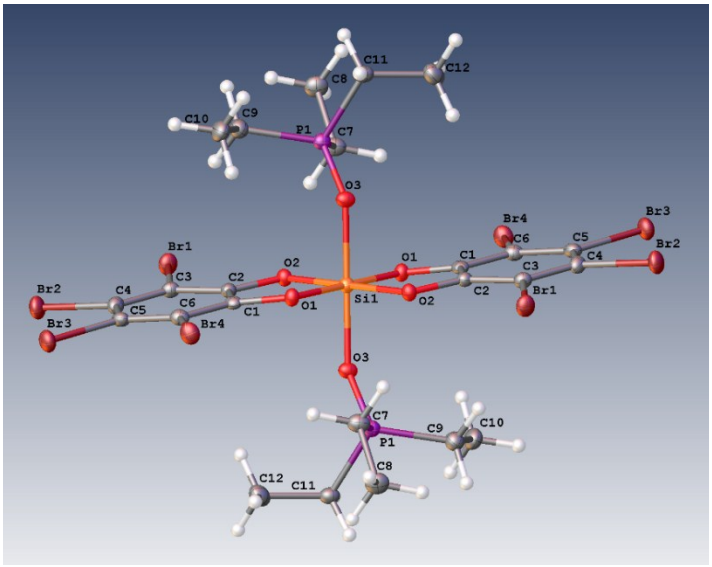

Identification code	lg_ms13
Empirical formula	$C_{24}H_{30}O_6SiP_2Br_8$
Formula weight	1143.79
Temperature/K	120
Crystal system	triclinic
Space group	P-1
a/Å	7.9270(16)
b/Å	9.2410(18)
c/Å	12.596(3)
α/°	69.63(3)
β/°	81.67(3)
γ/°	79.50(3)
Volume/Å^3	847.2(3)
Z	1
ρ_{calc} g/cm^3	2.242
μ/mm^{-1}	9.634
F(000)	546.0
Crystal size/mm^3	0.25 × 0.2 × 0.2
Radiation	MoK_α (λ = 0.71073)
2Θ range for data collection/°	4.75 to 60.072
Index ranges	-11 ≤ h ≤ 11, -12 ≤ k ≤ 13, -17 ≤ l ≤ 17
Reflections collected	8898
Independent reflections	4925 [R_{int} = 0.0295, R_{sigma} = 0.0492]
Data/restraints/parameters	4925/0/190
Goodness-of-fit on F^2	1.013
Final R indexes [I>=2σ (I)]	R_1 = 0.0311, wR_2 = 0.0615
Final R indexes [all data]	R_1 = 0.0484, wR_2 = 0.0670

Largest diff. peak/hole / e Å^{-3} 0.69/-0.71

Multi-scan absorption correction (Bruker Sadabs) was used.

Et_3PO-**Si(cat^H)$_2$**-$OPEt_3$

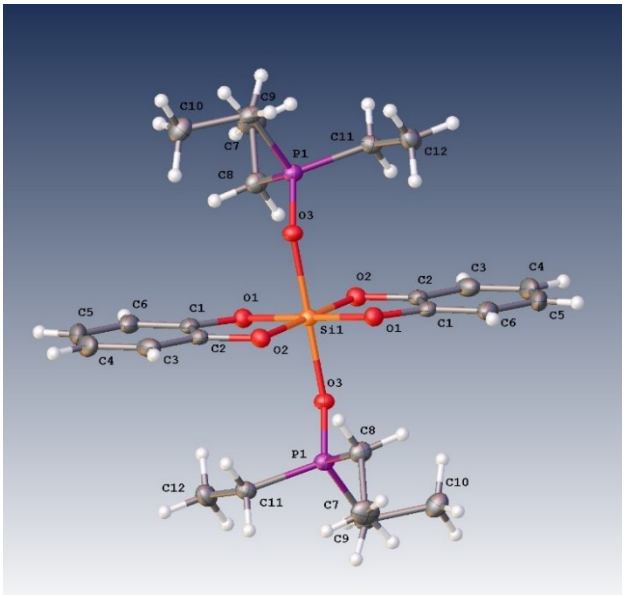

Identification code	ms24d
Empirical formula	$C_{24}H_{38}O_6SiP_2$
Formula weight	512.57
Temperature/K	120
Crystal system	triclinic
Space group	P-1
a/Å	7.8500(16)
b/Å	8.4840(17)
c/Å	10.295(2)
α/°	83.80(3)
β/°	73.07(3)
γ/°	83.17(3)
Volume/Å^3	649.3(3)
Z	1
ρ_{calc} g/cm^3	1.311
μ/mm^{-1}	0.250
F(000)	274.0
Crystal size/mm^3	0.8 × 0.7 × 0.7
Radiation	MoK_α (λ = 0.71073)
2Θ range for data collection/°	4.148 to 57.99
Index ranges	-10 ≤ h ≤ 10, -11 ≤ k ≤ 10, -13 ≤ l ≤ 14
Reflections collected	6011
Independent reflections	3414 [R_{int} = 0.0354, R_{sigma} = 0.0618]
Data/restraints/parameters	3414/0/227
Goodness-of-fit on F^2	1.061

Final R indexes [I>=2σ (I)]	R_1 = 0.0451, wR_2 = 0.1079
Final R indexes [all data]	R_1 = 0.0812, wR_2 = 0.1246
Largest diff. peak/hole / e Å^{-3}	0.65/-0.49

Et_3PO-**Si(cat^F)$_2$**-$OPEt_3$

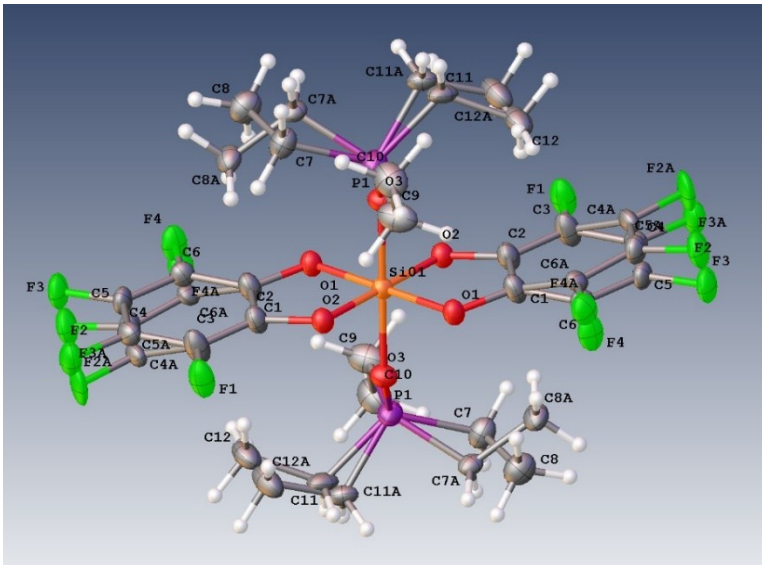

Identification code	ms29c_P2_1
Empirical formula	$C_{24}H_{30}F_8O_6P_2Si$
Formula weight	656.51
Temperature/K	120
Crystal system	monoclinic
Space group	$P2_1/n$
a/Å	10.753(2)
b/Å	11.953(2)
c/Å	11.361(2)
α/°	90
β/°	107.90(3)
γ/°	90
Volume/Å^3	1389.4(5)
Z	2
ρ_{calc} g/cm^3	1.569
μ/mm^{-1}	0.292
F(000)	676.0
Crystal size/mm^3	0.45 × 0.4 × 0.4
Radiation	MoK_α (λ = 0.71073)
2Θ range for data collection/°	4.564 to 60.104
Index ranges	-15 ≤ h ≤ 15, -16 ≤ k ≤ 16, -15 ≤ l ≤ 15
Reflections collected	7789
Independent reflections	4058 [R_{int} = 0.0420, R_{sigma} = 0.0617]
Data/restraints/parameters	4058/22/285

Goodness-of-fit on F^2	1.074
Final R indexes [I>=2σ (I)]	R_1 = 0.0634, wR_2 = 0.1574
Final R indexes [all data]	R_1 = 0.1055, wR_2 = 0.1769
Largest diff. peak/hole / e $Å^{-3}$	0.74/-0.40

Disorder in CH_2 and CH_3 groups and C_6F_4 ring.

[K@18-crown-6]**[F-Si(cat^F)$_2$]**, polymorph A

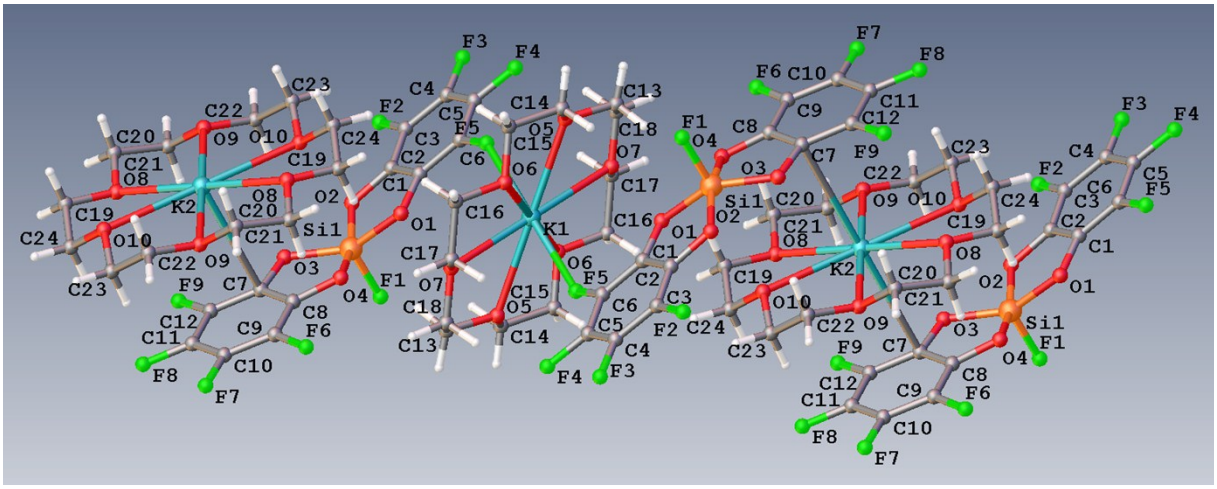

Identification code	ms83_P1
Empirical formula	$C_{24}H_{24}F_9KO_{10}Si$
Formula weight	710.62
Temperature/K	120
Crystal system	triclinic
Space group	P-1
a/Å	9.3030(19)
b/Å	10.781(2)
c/Å	15.544(3)
α/°	77.14(3)
β/°	77.77(3)
γ/°	69.26(3)
Volume/$Å^3$	1406.2(6)
Z	2
ρ_{calc} g/cm^3	1.678
μ/mm^{-1}	0.347
F(000)	724.0
Crystal size/mm^3	0.6 × 0.55 × 0.4
Radiation	MoK_α (λ = 0.71073)
2Θ range for data collection/°	4.094 to 60.246
Index ranges	-13 ≤ h ≤ 13, -14 ≤ k ≤ 15, -21 ≤ l ≤ 21
Reflections collected	14651
Independent reflections	8189 [R_{int} = 0.0254, R_{sigma} = 0.0464]
Data/restraints/parameters	8189/0/409

Goodness-of-fit on F^2	1.024
Final R indexes [I>=2σ (I)]	R_1 = 0.0385, wR_2 = 0.0868
Final R indexes [all data]	R_1 = 0.0680, wR_2 = 0.0994
Largest diff. peak/hole / e $Å^{-3}$	0.39/-0.37

[K@18-crown-6]**[F-Si(cat^F)$_2$]**, polymorph B

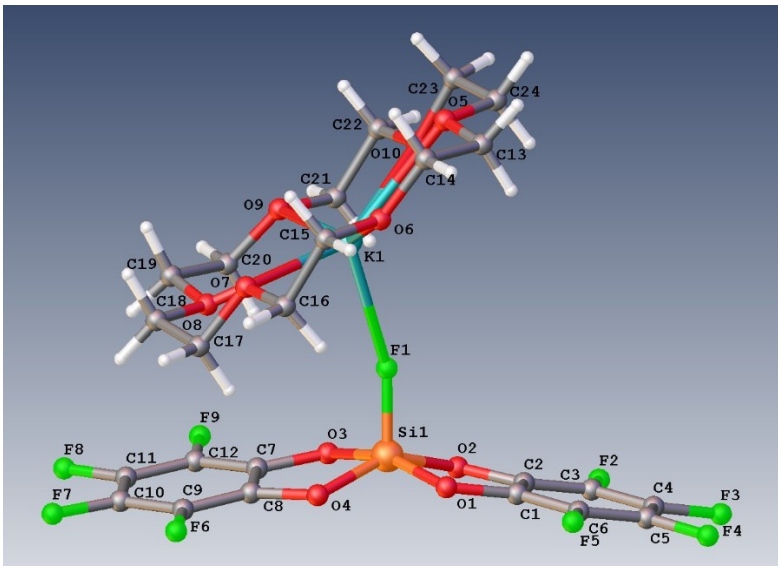

Identification code	ms78_P1
Empirical formula	$C_{24}H_{24}F_9KO_{10}Si$
Formula weight	710.62
Temperature/K	120
Crystal system	triclinic
Space group	P-1
a/Å	11.414(2)
b/Å	11.840(2)
c/Å	11.872(2)
α/°	99.78(3)
β/°	96.63(3)
γ/°	112.37(3)
Volume/Å^3	1433.3(6)
Z	2
ρ_{calc} g/cm^3	1.647
μ/mm^{-1}	0.340
F(000)	724.0
Crystal size/mm^3	0.5 × 0.45 × 0.3
Radiation	MoK_α (λ = 0.71073)
2Θ range for data collection/°	3.552 to 59.962
Index ranges	-16 ≤ h ≤ 15, -16 ≤ k ≤ 16, -16 ≤ l ≤ 16
Reflections collected	14839
Independent reflections	8299 [R_{int} = 0.0597, R_{sigma} = 0.1160]
Data/restraints/parameters	8299/0/406
Goodness-of-fit on F^2	0.964
Final R indexes [I>=2σ (I)]	R_1 = 0.0540, wR_2 = 0.1026
Final R indexes [all data]	R_1 = 0.1533, wR_2 = 0.1340

Largest diff. peak/hole / e Å^{-3} 0.34/-0.43

[K@18-crown-6]**[F-Si(cat^{Br})$_2$]**

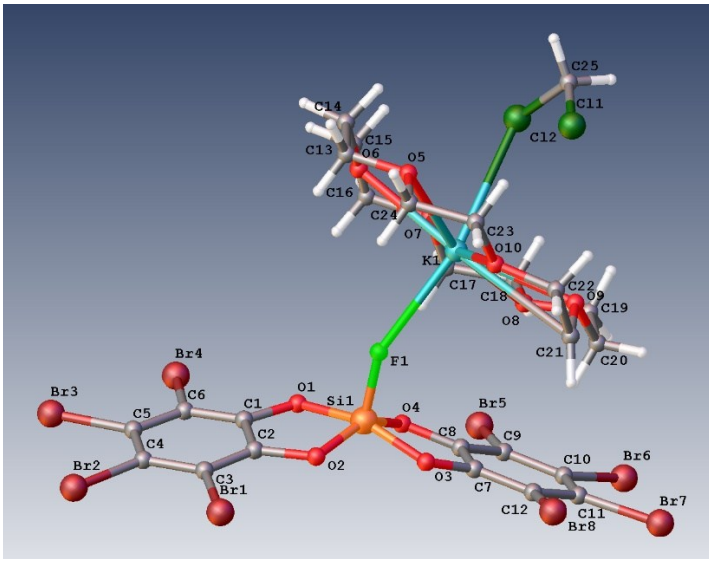

Identification code	ms25_P1
Empirical formula	$C_{25}H_{25}Br_8Cl_2FKO_{10}Si$
Formula weight	1281.82
Temperature/K	120
Crystal system	triclinic
Space group	P-1
a/Å	11.428(2)
b/Å	12.750(3)
c/Å	15.069(3)
α/°	71.12(3)
β/°	71.13(3)
γ/°	69.23(3)
Volume/Å^3	1887.7(9)
Z	2
ρ_{calc} g/cm^3	2.255
μ/mm^{-1}	8.836
F(000)	1222.0
Crystal size/mm^3	0.25 × 0.25 × 0.25
Radiation	MoK_α (λ = 0.71073)
2Θ range for data collection/°	2.94 to 60.058
Index ranges	-15 ≤ h ≤ 16, -17 ≤ k ≤ 17, -21 ≤ l ≤ 20
Reflections collected	19733
Independent reflections	10960 [R_{int} = 0.0459, R_{sigma} = 0.0808]
Data/restraints/parameters	10960/0/433
Goodness-of-fit on F^2	0.999
Final R indexes [I>=2σ (I)]	R_1 = 0.0421, wR_2 = 0.0738

Final R indexes [all data]	R_1 = 0.0911, wR_2 = 0.0855
Largest diff. peak/hole / e Å^{-3}	1.00/-0.78

[PPN]**[Cl-Si(cat^{H})$_2$]**

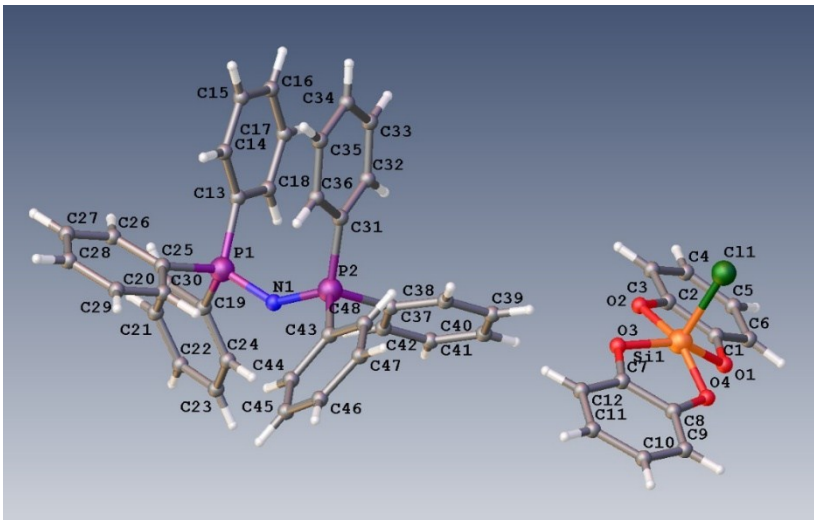

Identification code	ms46P41
Empirical formula	$C_{48}H_{38}ClNO_4P_2Si$
Formula weight	818.27
Temperature/K	120
Crystal system	tetragonal
Space group	$P4_3$
a/Å	10.4250(15)
b/Å	10.4250(15)
c/Å	37.648(8)
α/°	90
β/°	90
γ/°	90
Volume/Å^3	4091.6(14)
Z	4
ρ_{calc} g/cm^3	1.328
μ/mm^{-1}	0.248
F(000)	1704.0
Crystal size/mm^3	0.5 × 0.3 × 0.2
Radiation	MoK_α (λ = 0.71073)
2Θ range for data collection/°	4.054 to 60.094
Index ranges	-14 ≤ h ≤ 14, -14 ≤ k ≤ 14, -52 ≤ l ≤ 52
Reflections collected	84460
Independent reflections	11798 [R_{int} = 0.1705, R_{sigma} = 0.1822]
Data/restraints/parameters	11798/1/514
Goodness-of-fit on F^2	0.989
Final R indexes [I>=2σ (I)]	R_1 = 0.0593, wR_2 = 0.0957

Final R indexes [all data]	R_1 = 0.1843, wR_2 = 0.1262
Largest diff. peak/hole / e Å^{-3}	0.31/-0.36
Flack parameter	-0.09(4)

Multi-scan absorption correction.

[K@18-crown-6]**[F-Si(cat^{F})(cat^{Br})]**

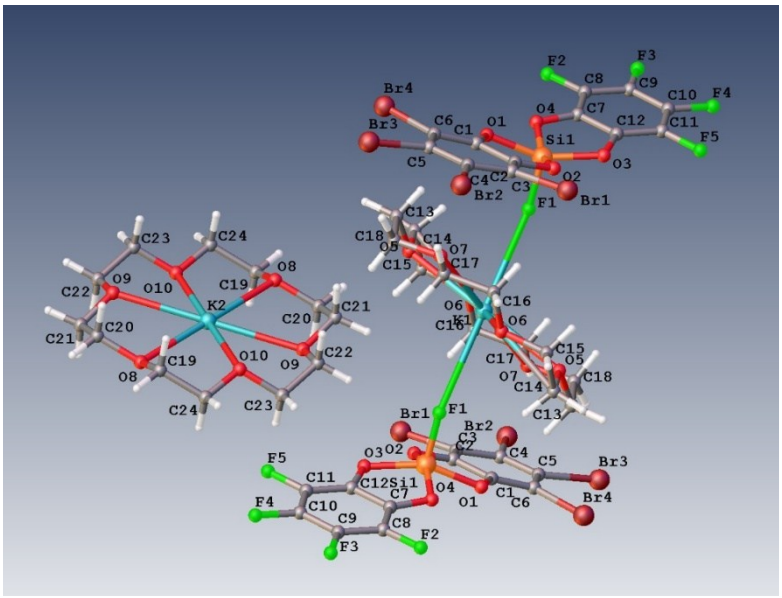

Identification code	ms108_P1
Empirical formula	$C_{24}H_{24}O_{10}F_5SiKBr_4$
Formula weight	954.26
Temperature/K	120
Crystal system	triclinic
Space group	P-1
a/Å	9.6800(19)
b/Å	10.278(2)
c/Å	15.852(3)
α/°	91.94(3)
β/°	92.84(3)
γ/°	92.24(3)
Volume/Å^3	1573.0(6)
Z	2
ρ_{calc} g/cm^3	2.015
μ/mm^{-1}	5.370
F(000)	932.0
Crystal size/mm^3	0.4 × 0.4 × 0.35
Radiation	MoK_α (λ = 0.71073)
2Θ range for data collection/°	2.574 to 58
Index ranges	-13 ≤ h ≤ 13, -14 ≤ k ≤ 14, -21 ≤ l ≤ 21
Reflections collected	14762
Independent reflections	8277 [R_{int} = 0.0831, R_{sigma} = 0.1500]

Data/restraints/parameters	8277/0/409
Goodness-of-fit on F^2	1.007
Final R indexes [I>=2σ (I)]	R_1 = 0.0664, wR_2 = 0.1191
Final R indexes [all data]	R_1 = 0.1758, wR_2 = 0.1485
Largest diff. peak/hole / e $Å^{-3}$	0.95/-0.86

Et_2O-**Si(cat^{Br})$_2$**-OEt_2

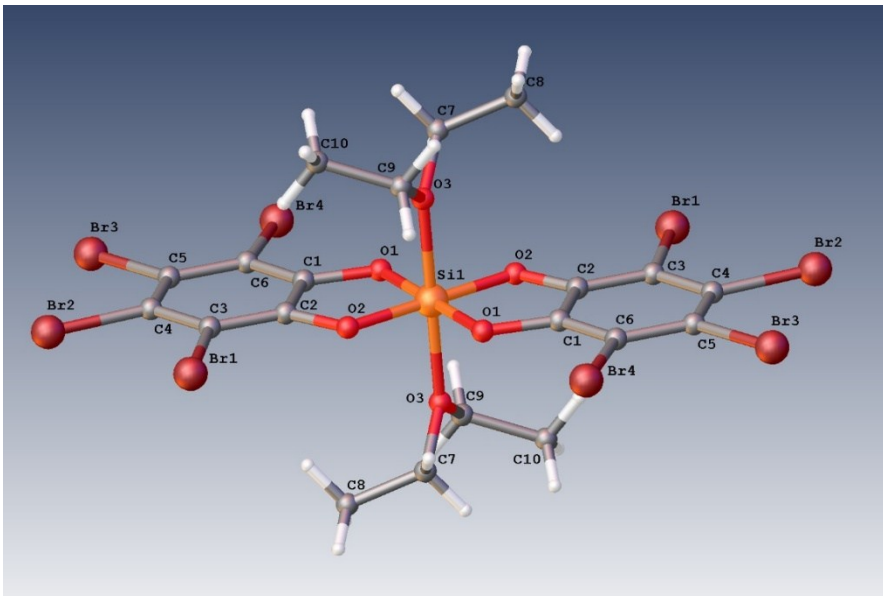

Identification code	ms125a
Empirical formula	$C_{20}H_{20}Br_8O_6Si$
Formula weight	1023.73
Temperature/K	120
Crystal system	Monoclinic
Space group	P21/c
a/Å	8.6390(17)
b/Å	9.5980(19)
c/Å	17.384(4)
α/°	90
β/°	93.00(3)
γ/°	90
Volume/$Å^3$	1439.5(5)
Z	2
ρ_{calc} g/cm^3	2.362
μ/mm^{-1}	11.219
F(000)	964.0
Crystal size/mm^3	0.45 × 0.45 × 0.4
Radiation	MoK_α (λ = 0.71073)
2Θ range for data collection/°	4.692 to 56
Index ranges	-9 ≤ h ≤ 11, -11 ≤ k ≤ 12, -22 ≤ l ≤ 22
Reflections collected	11000
Independent reflections	3415 [R_{int} = 0.0635, R_{sigma} = 0.0861]

Data/restraints/parameters	3415/0/162
Goodness-of-fit on F^2	0.993
Final R indexes [I>=2σ (I)]	R_1 = 0.0404, wR_2 = 0.0618
Final R indexes [all data]	R_1 = 0.0814, wR_2 = 0.0709
Largest diff. peak/hole / e $Å^{-3}$	0.79/-0.89

5. NMR Spectra

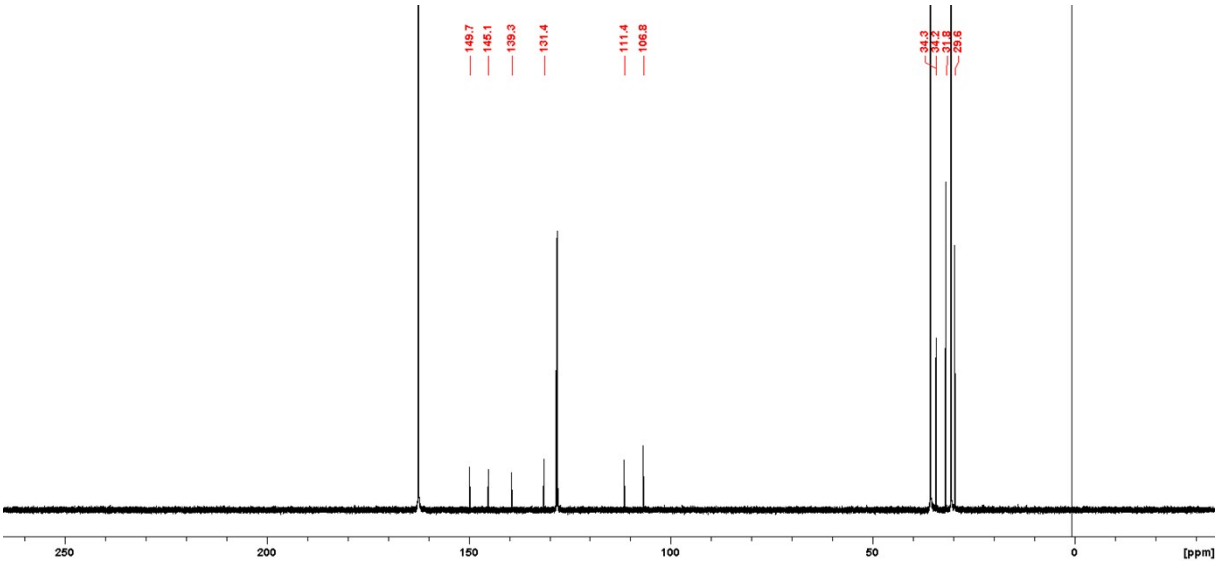

^{13}C-NMR (100 MHz, DMF) of Si(cat^{tBu})$_2$(DMF).

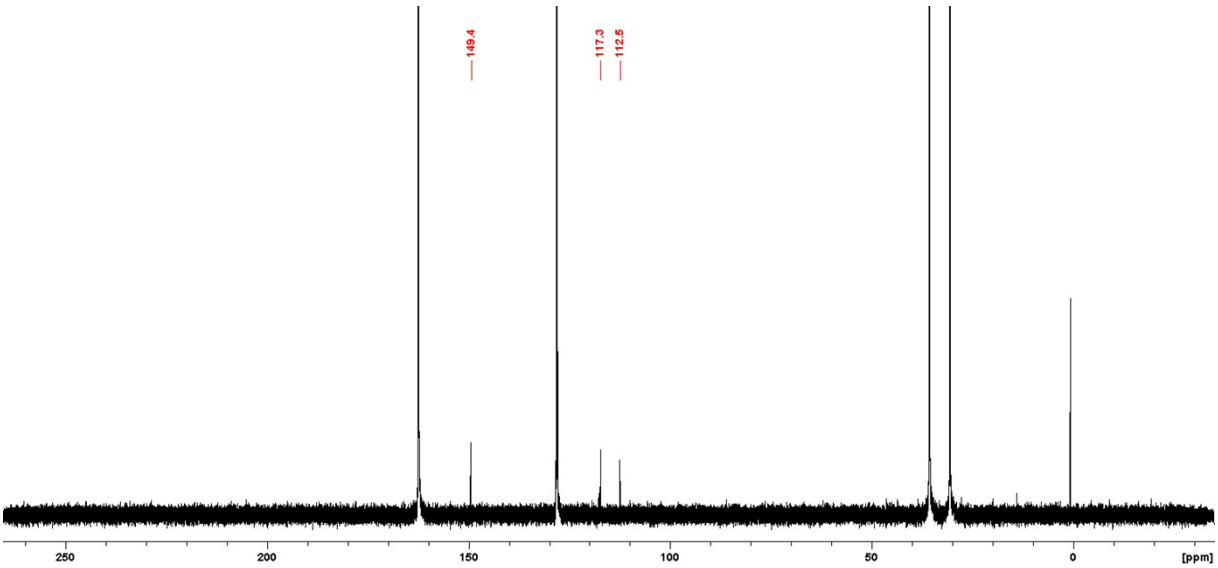

^{13}C-NMR (100 MHz, DMF) of Si(cat^{Cl})$_2$(DMF).

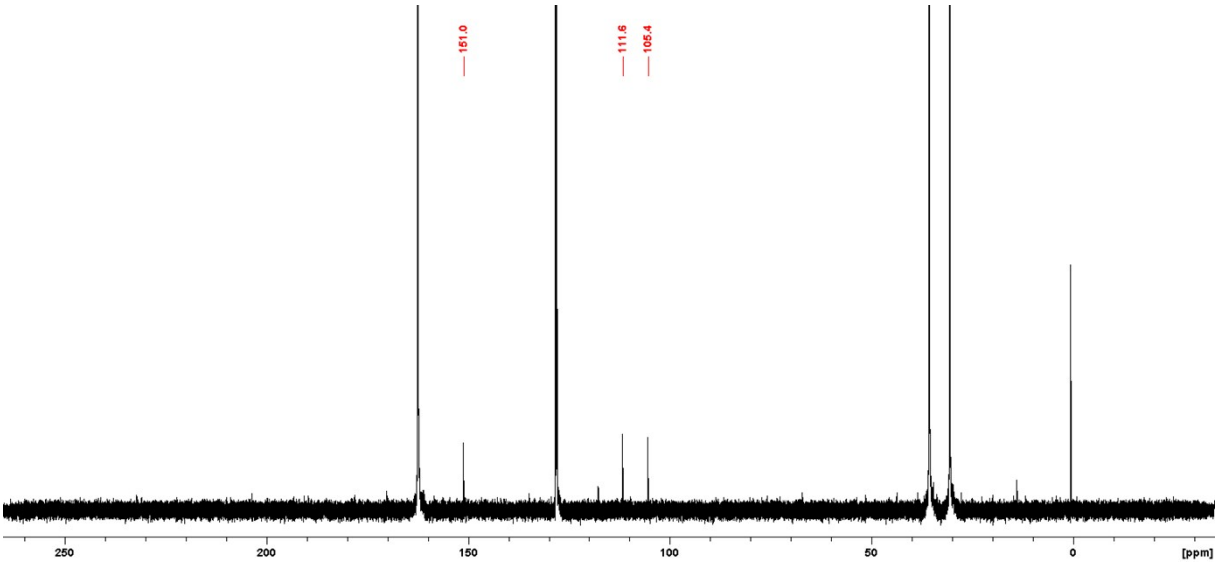

^{13}C-NMR (100 MHz, DMF) of Si(cat^{Br})$_2$(DMF).

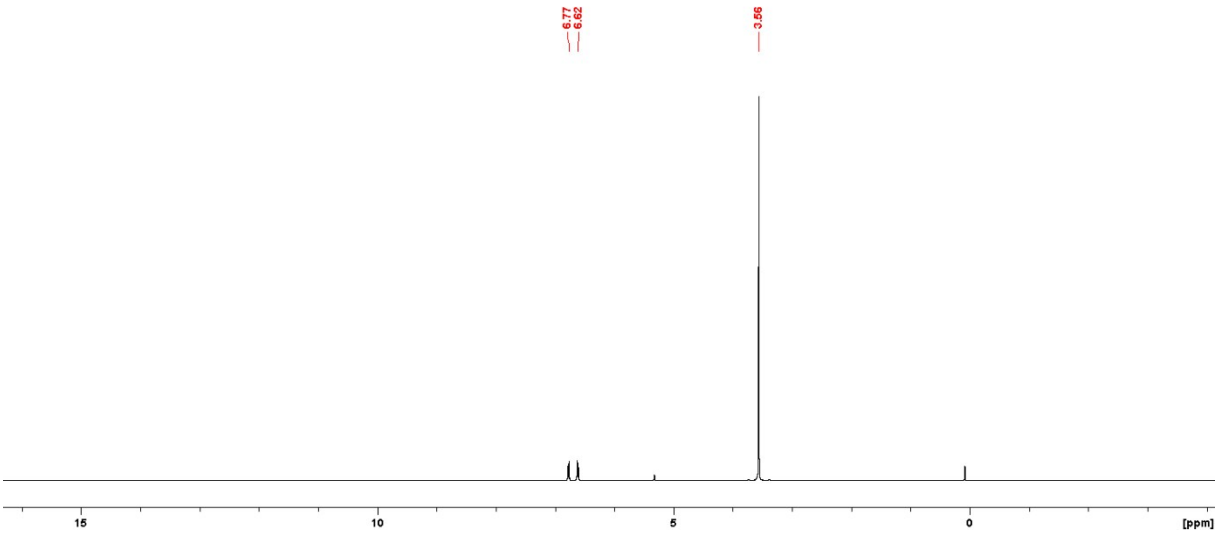

^{1}H-NMR (400 MHz, CD_2Cl_2) of [K@18-crown-6][F-Si(cat^{H})$_2$].

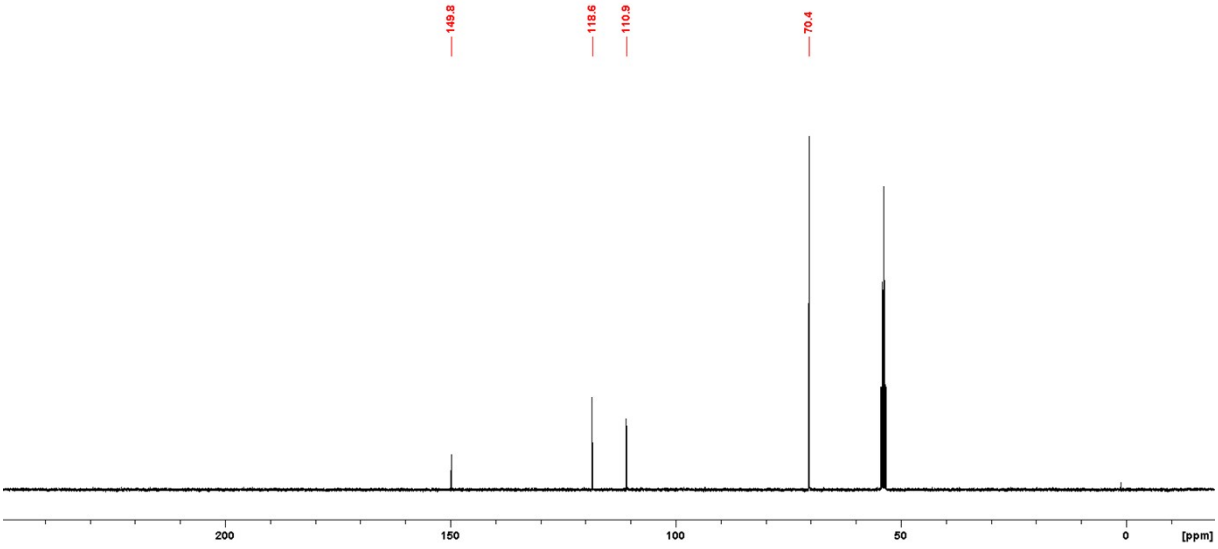

^{13}C-NMR (100 MHz, CD_2Cl_2) of [K@18-crown-6][F-Si(cat^{H})$_2$].

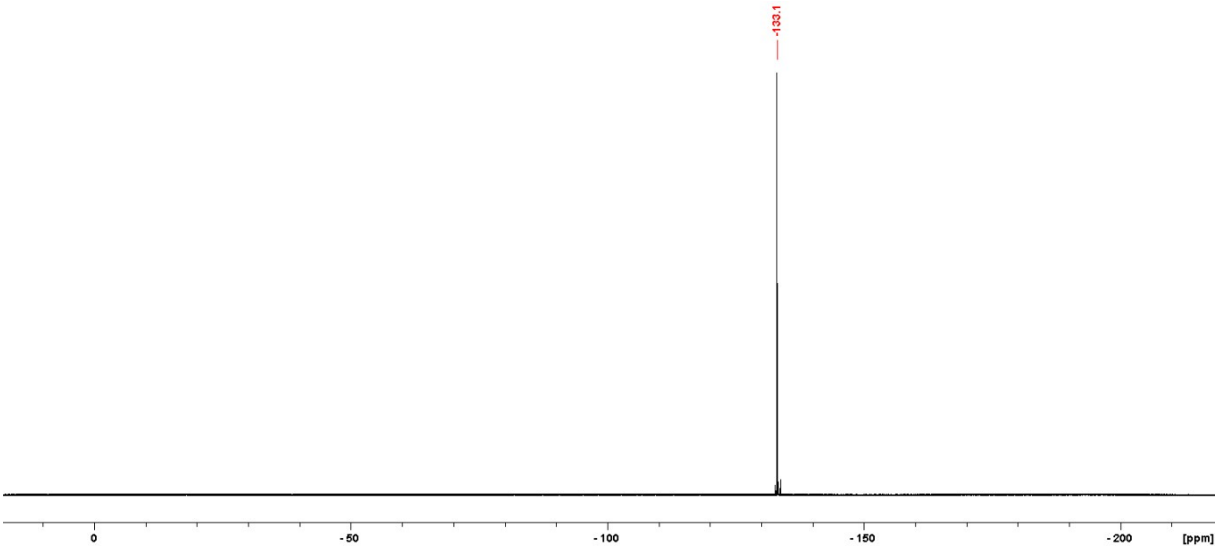

^{19}F-NMR (376 MHz, CD_2Cl_2) of [K@18-crown-6][F-Si(cat^{H})$_2$].

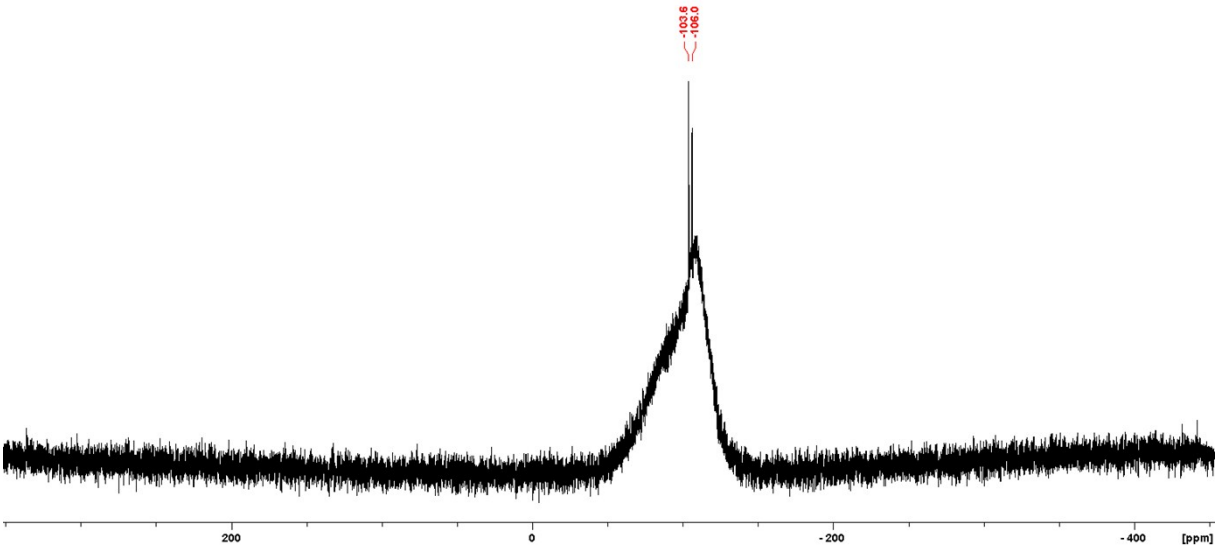

^{29}Si-NMR (79 MHz, CD_2Cl_2) of [K@18-crown-6][F-Si(cat^{H})$_2$].

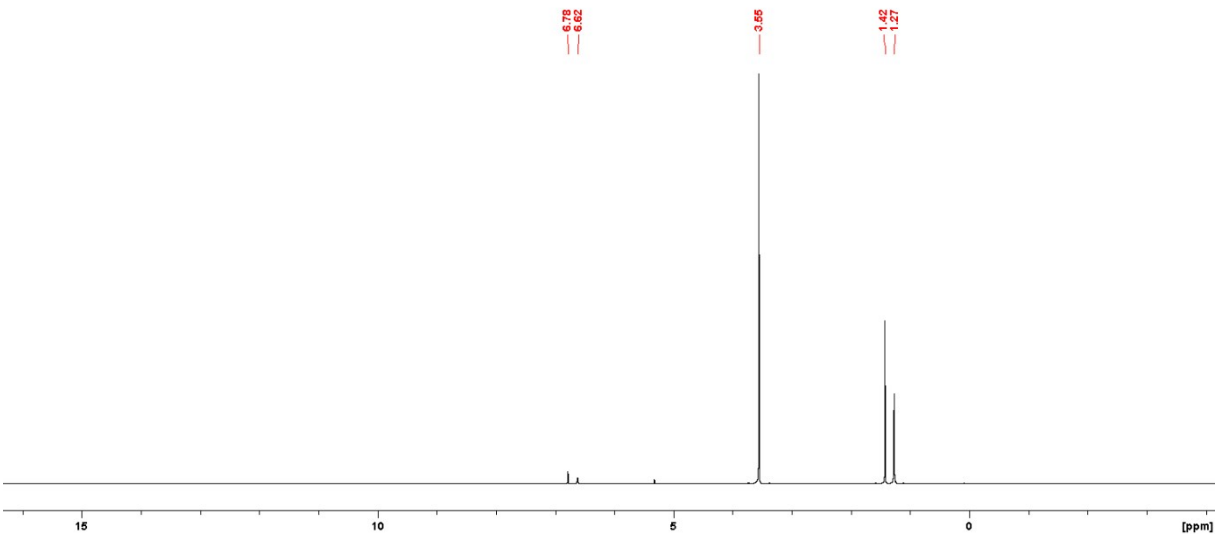

^{1}H-NMR (400 MHz, CD_2Cl_2) of [K@18-crown-6][F-Si(cat^{tBu})$_2$].

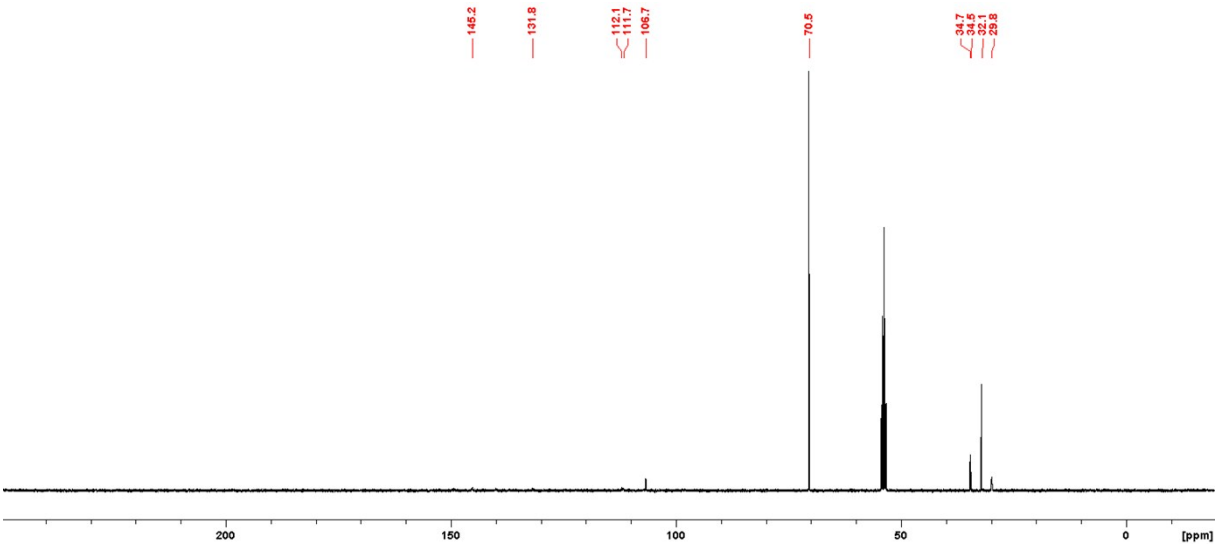

^{13}C-NMR (100 MHz, CD_2Cl_2) of [K@18-crown-6][F-Si(cat^{tBu})$_2$]. Due to dynamic effects between different stereoisomers of the preferred tbp-confirmation (see Figure S5), severe signal broadening occurred, hampering peak identification.

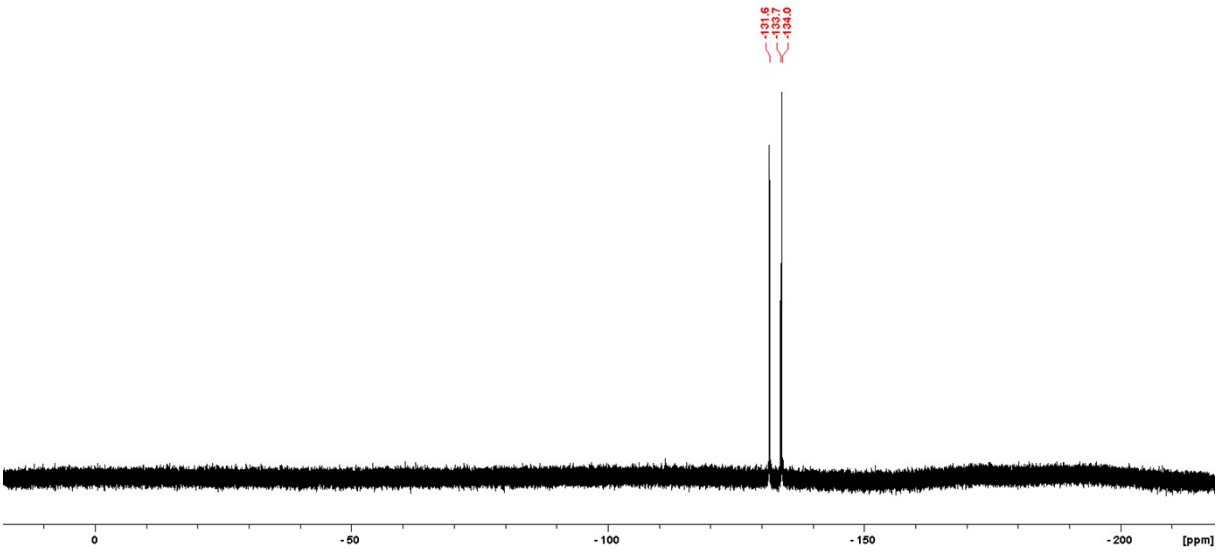

^{19}F-NMR (376 MHz, CD_2Cl_2) of [K@18-crown-6][F-Si(cat^{tBu})$_2$].

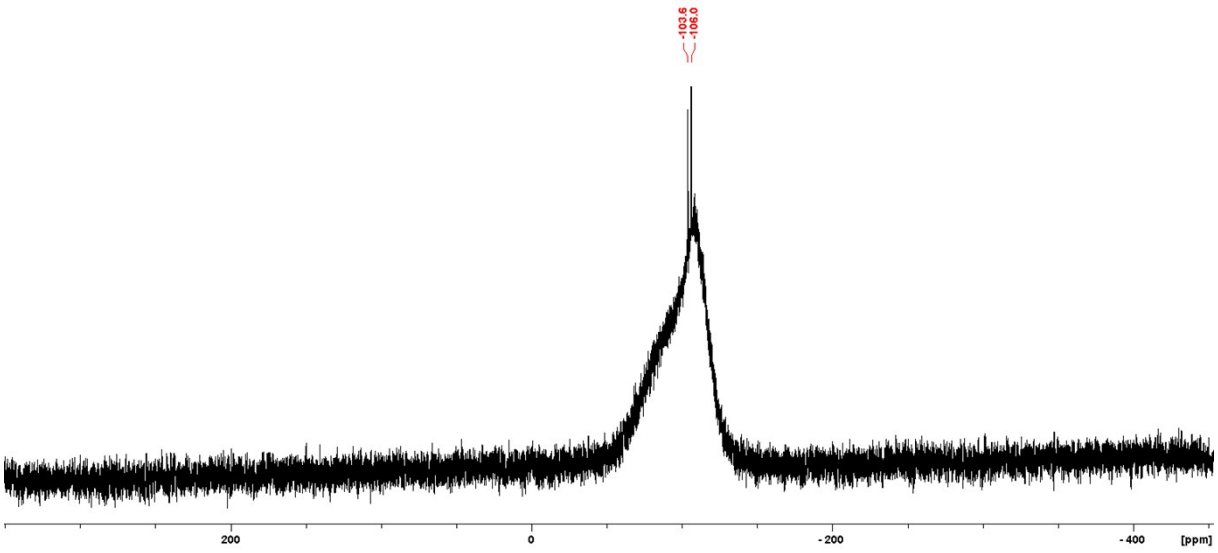

^{29}Si-NMR (79 MHz, CD_2Cl_2) of [K@18-crown-6][F-Si(cat^{tBu})$_2$].

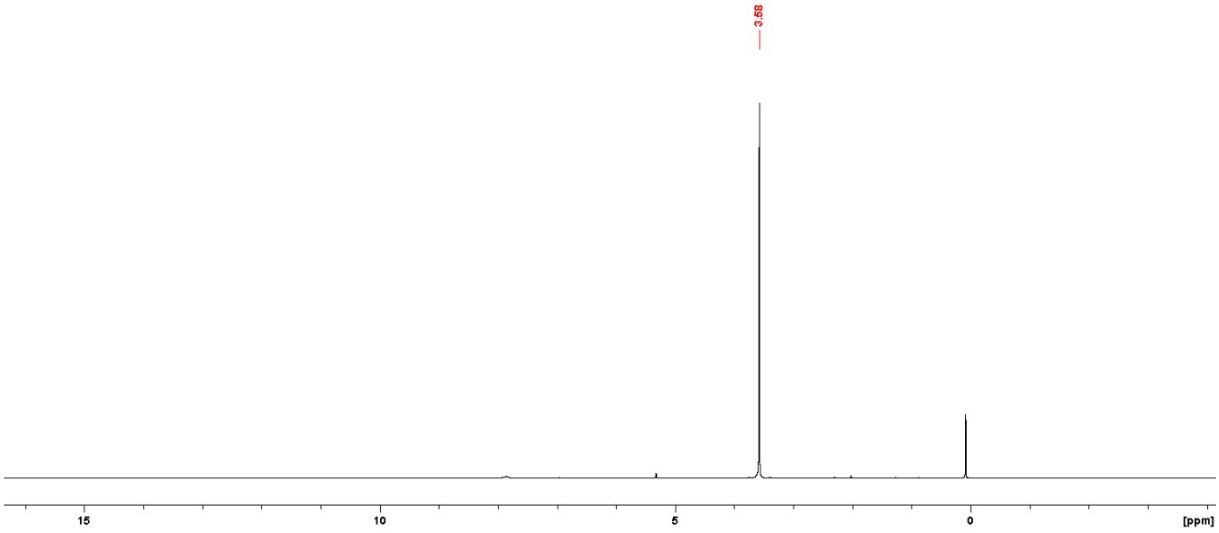

^{1}H-NMR (400 MHz, CD_2Cl_2) of [K@18-crown-6][F-Si(cat^{F})$_2$].

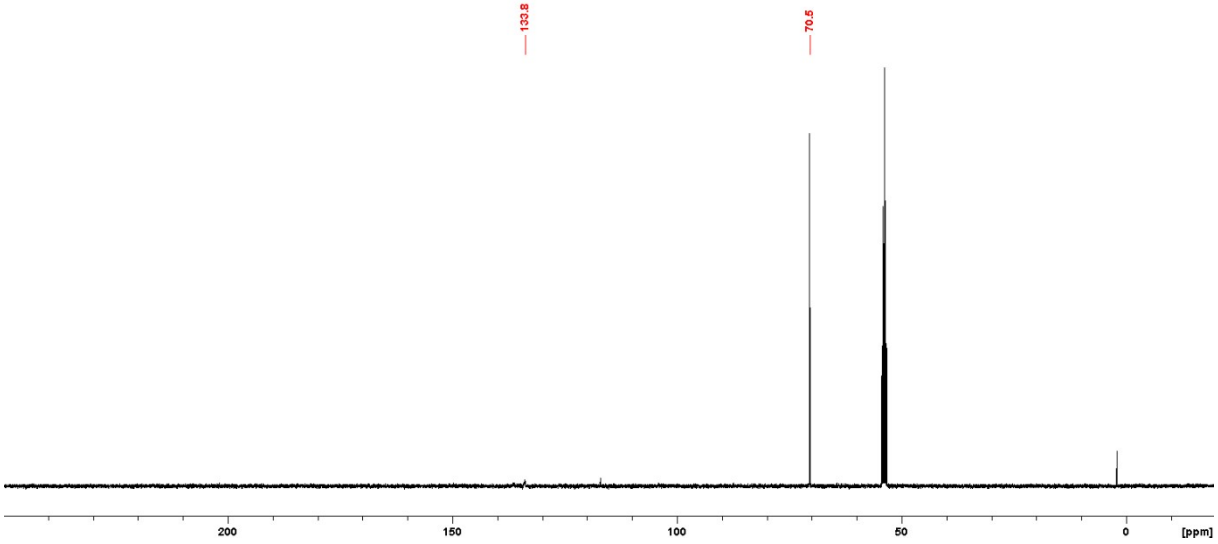

^{13}C-NMR (100 MHz, CD_2Cl_2) of [K@18-crown-6][F-Si(cat^{F})$_2$].

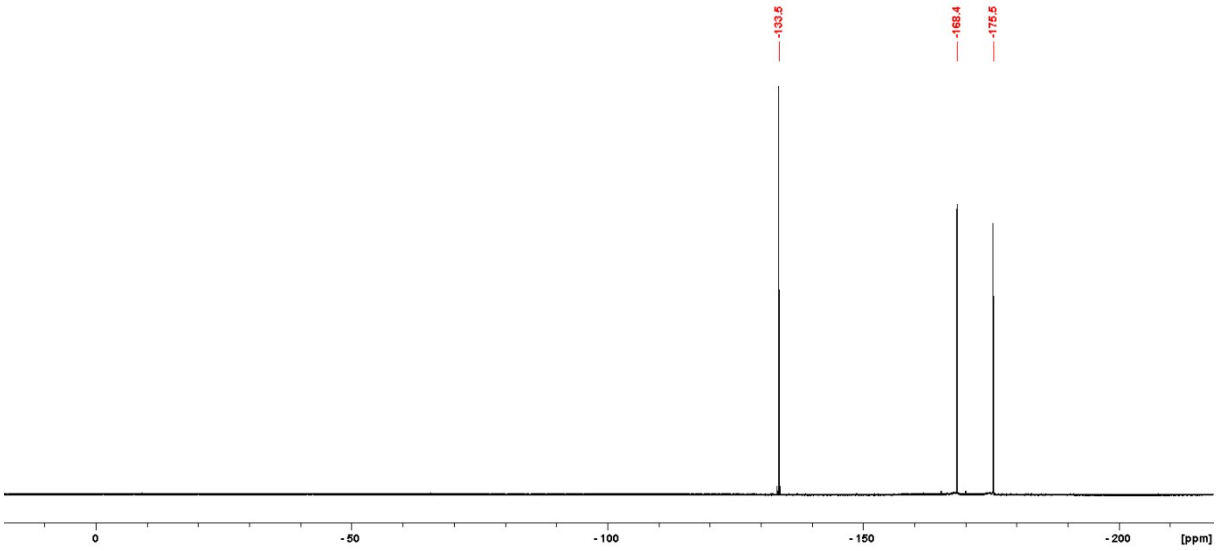

^{19}F-NMR (376 MHz, CD_2Cl_2) of [K@18-crown-6][F-Si(cat^{F})$_2$].

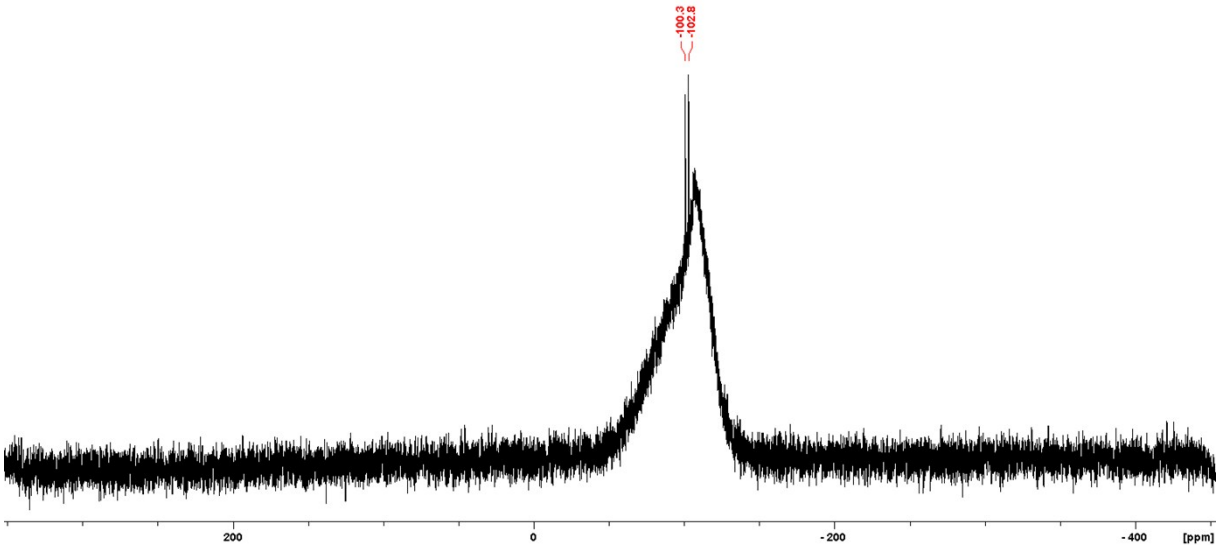

^{29}Si-NMR (79 MHz, CD_2Cl_2) of [K@18-crown-6][F-Si(cat^{F})$_2$].

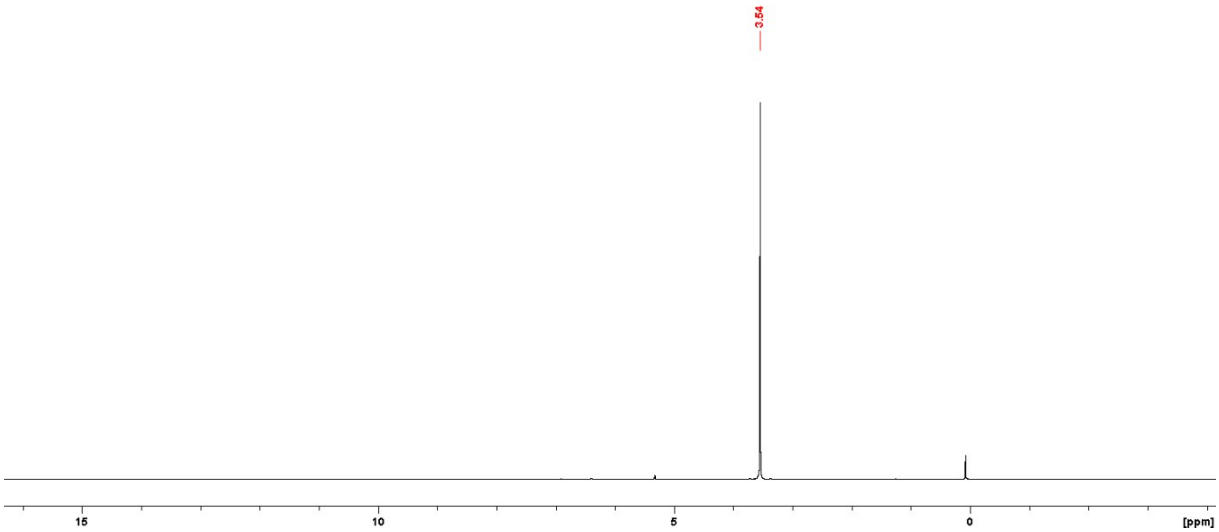

^{1}H-NMR (400 MHz, CD_2Cl_2) of [K@18-crown-6][F-Si(cat^{Cl})$_2$].

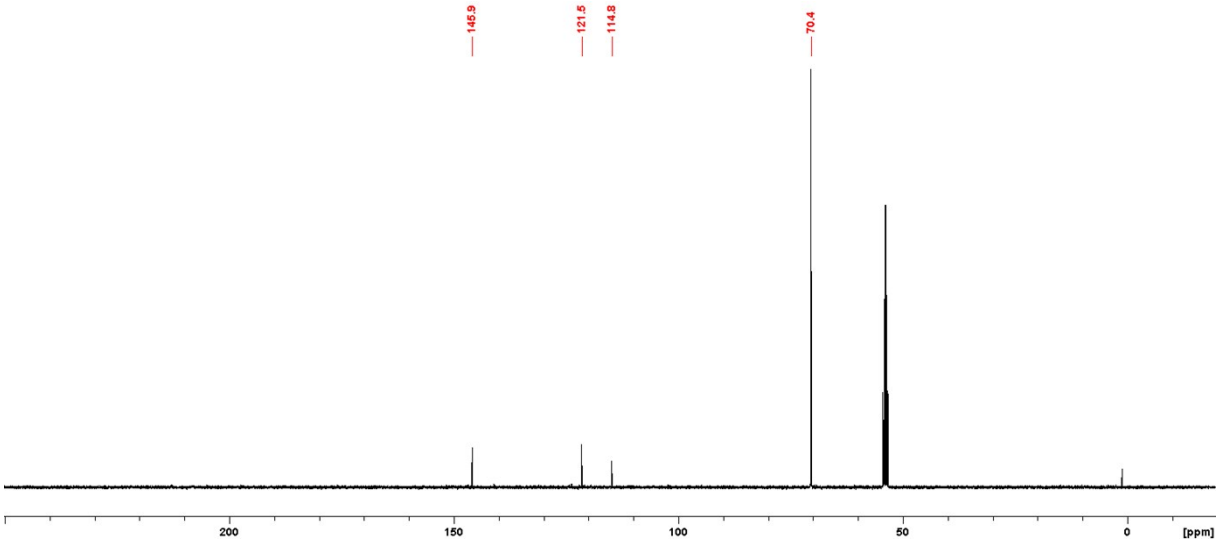

^{13}C-NMR (100 MHz, CD_2Cl_2) of [K@18-crown-6][F-Si(cat^{Cl})$_2$].

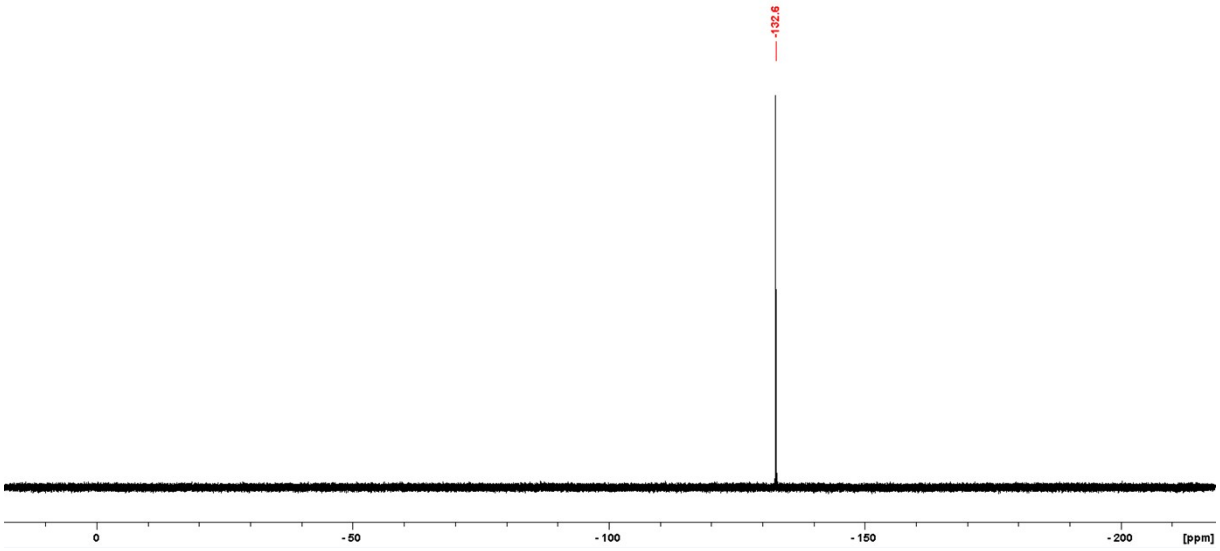

^{19}F-NMR (376 MHz, CD_2Cl_2) of [K@18-crown-6][F-Si(cat^{Cl})$_2$].

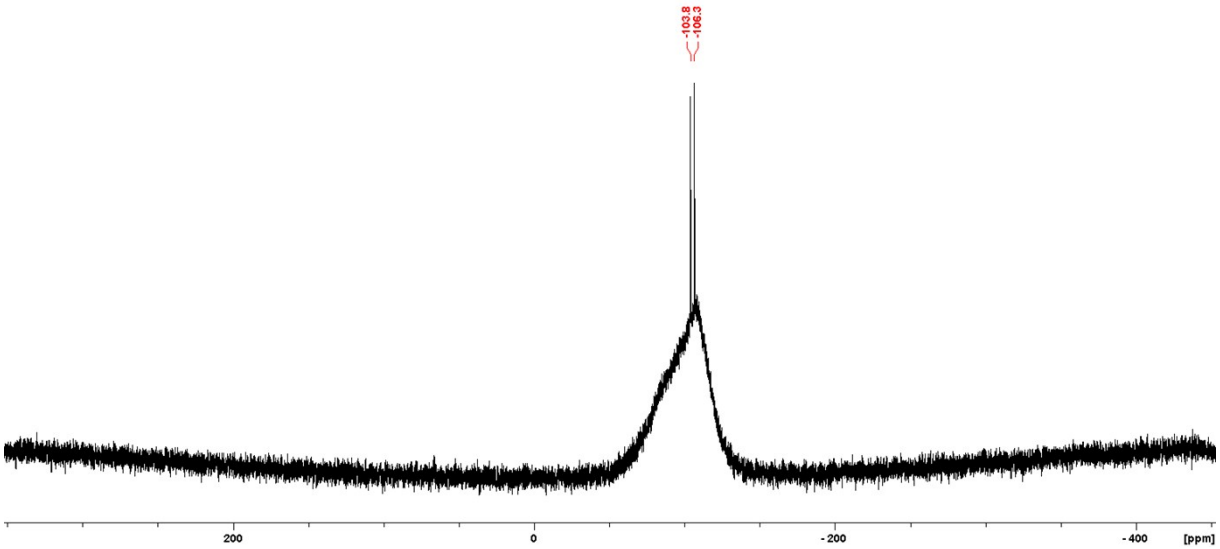

^{29}Si-NMR (79 MHz, CD_2Cl_2) of [K@18-crown-6][F-Si(cat^{Cl})$_2$].

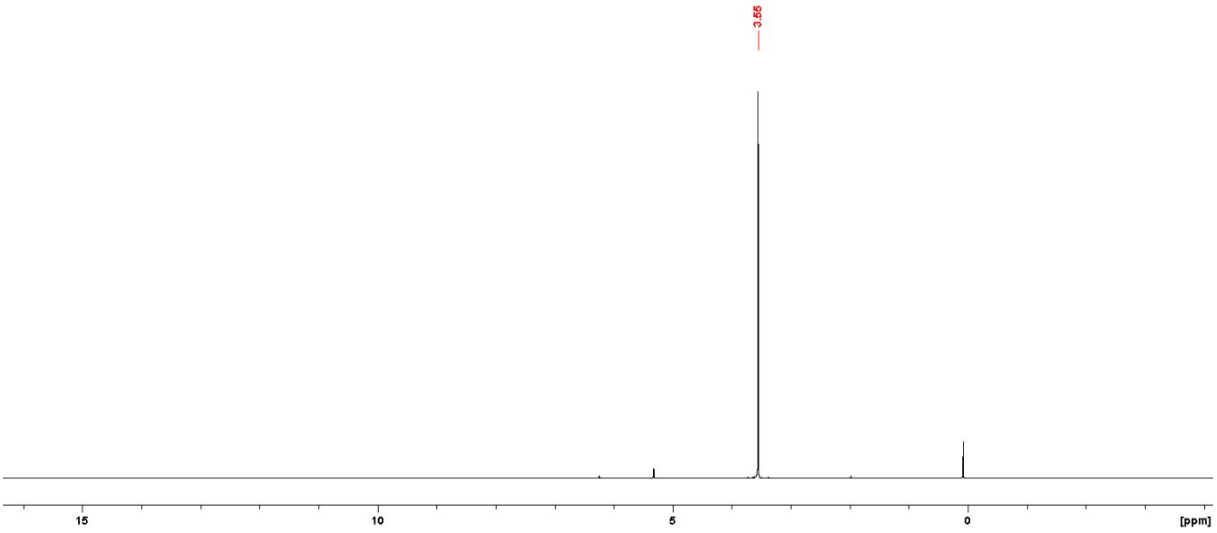

^{1}H-NMR (400 MHz, CD_2Cl_2) of [K@18-crown-6][F-Si(cat^{Br})$_2$].

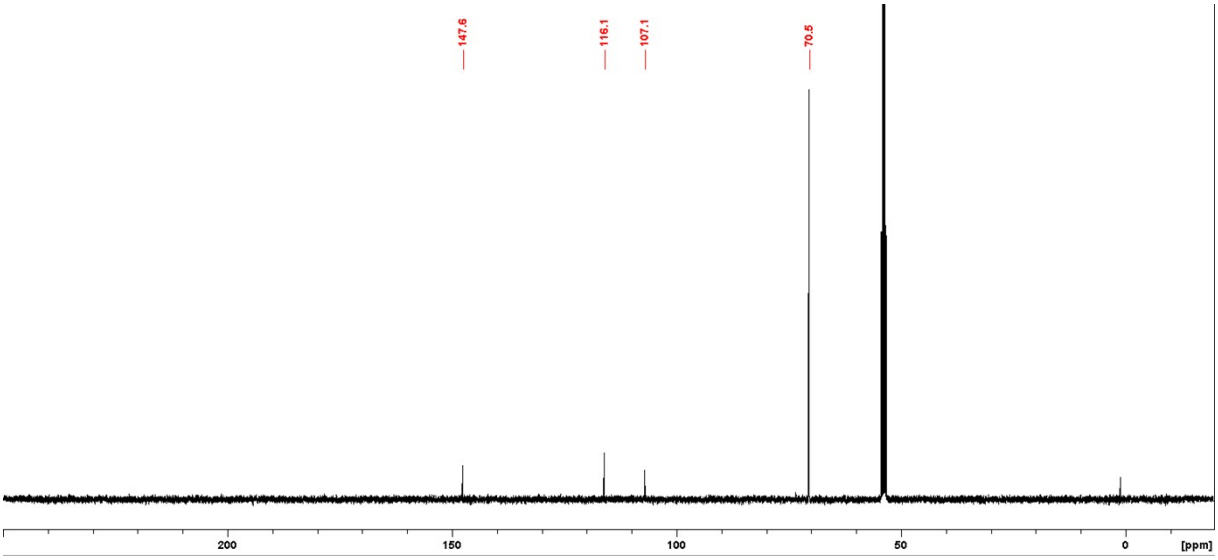

^{13}C-NMR (100 MHz, CD_2Cl_2) of [K@18-crown-6][F-Si(cat^{Br})$_2$].

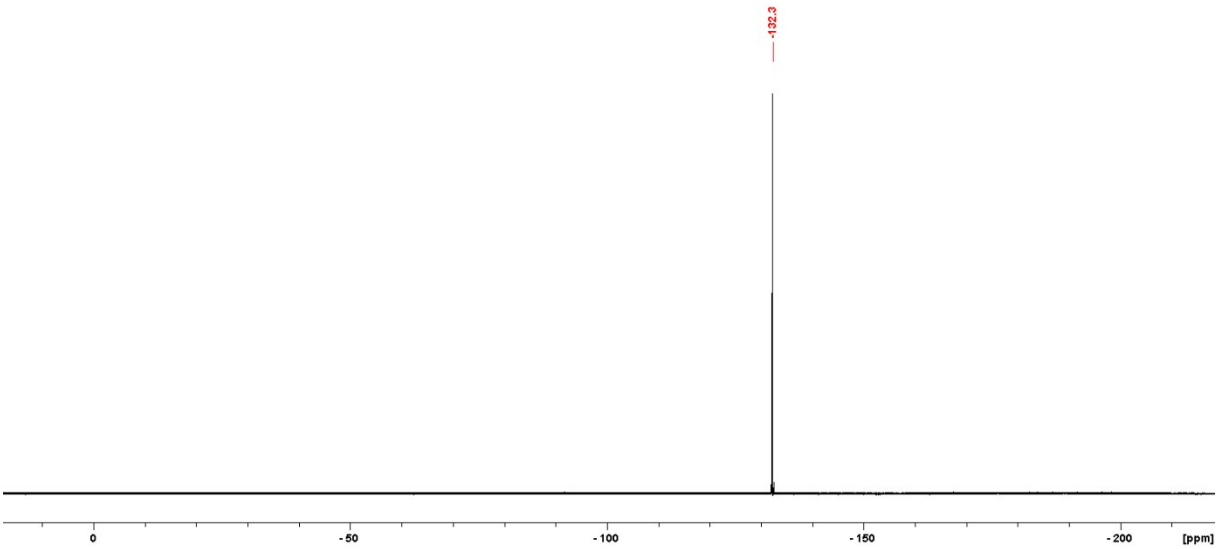

^{19}F-NMR (376 MHz, CD_2Cl_2) of [K@18-crown-6][F-Si(cat^{Br})$_2$].

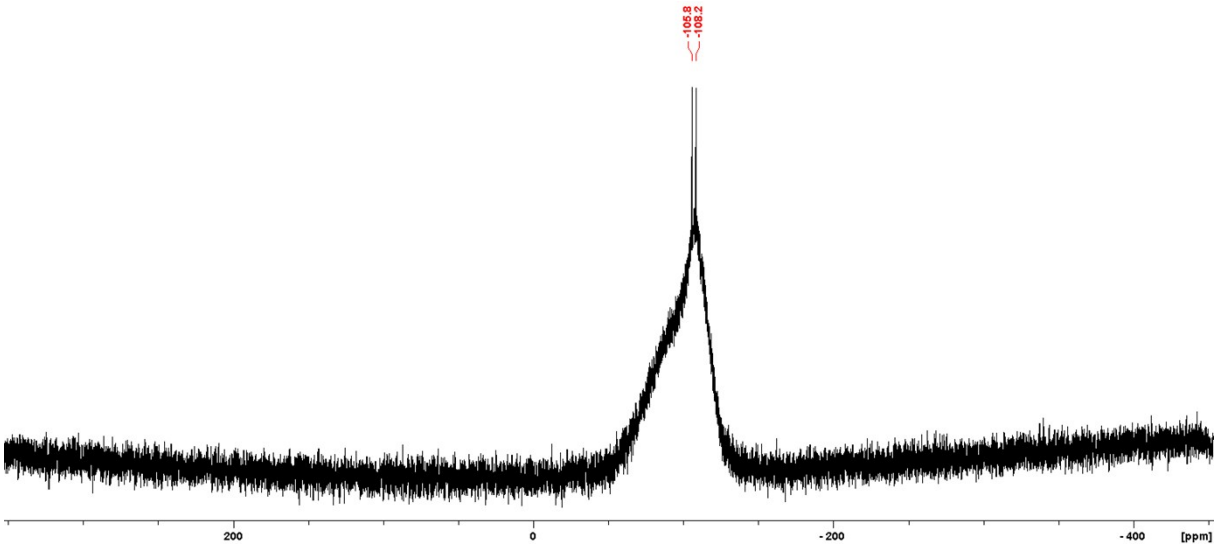

^{29}Si-NMR (79 MHz, CD_2Cl_2) of [K@18-crown-6][F-Si(cat^{Br})$_2$].

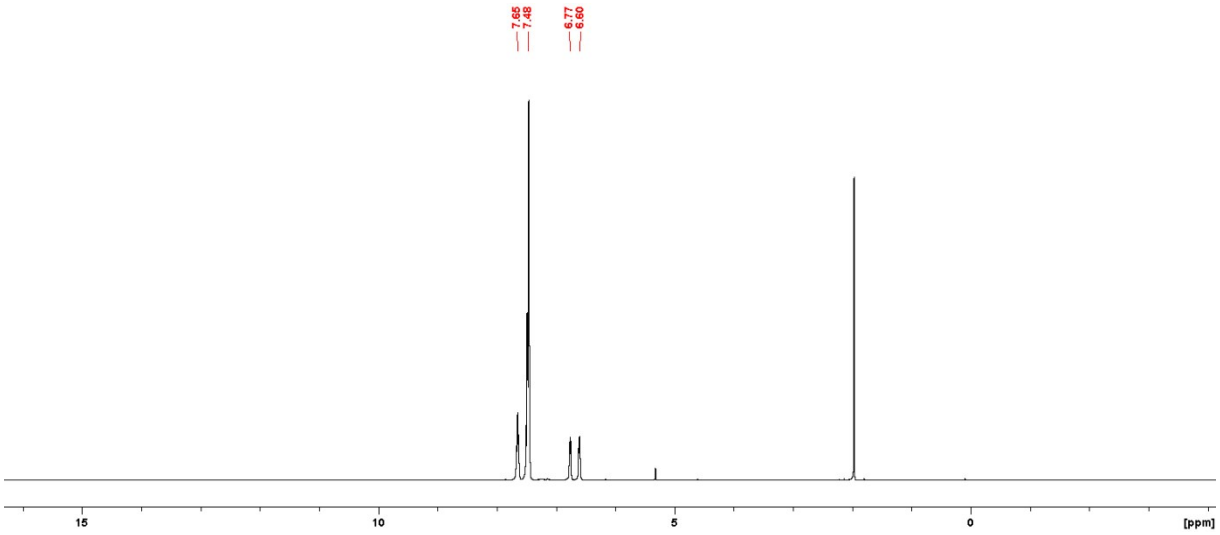

^{1}H-NMR (400 MHz, CD_2Cl_2) of [PPN][Cl-Si(cat^{H})$_2$].

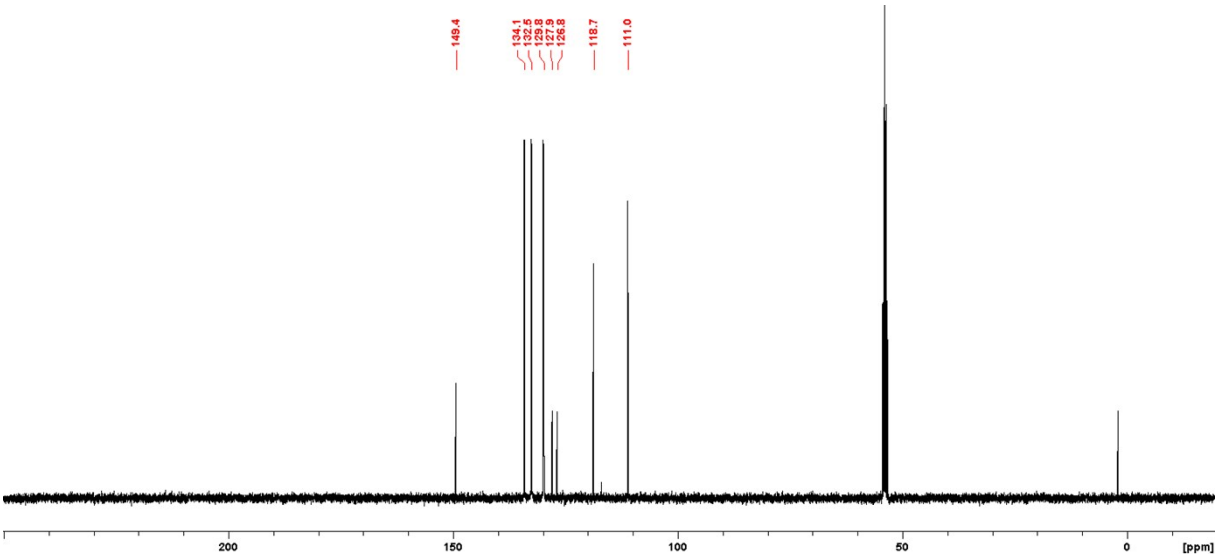

^{13}C-NMR (100 MHz, CD_2Cl_2) of [PPN][Cl-Si(cat^H)$_2$].

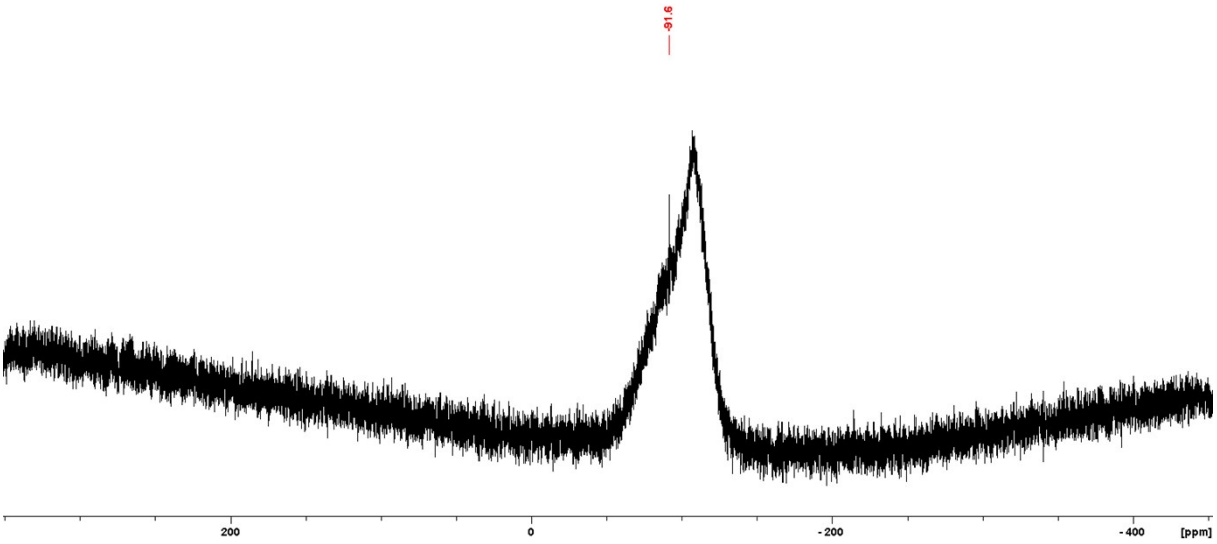

^{29}Si-NMR (79 MHz, CD_2Cl_2) of [PPN][Cl-Si(cat^H)$_2$].

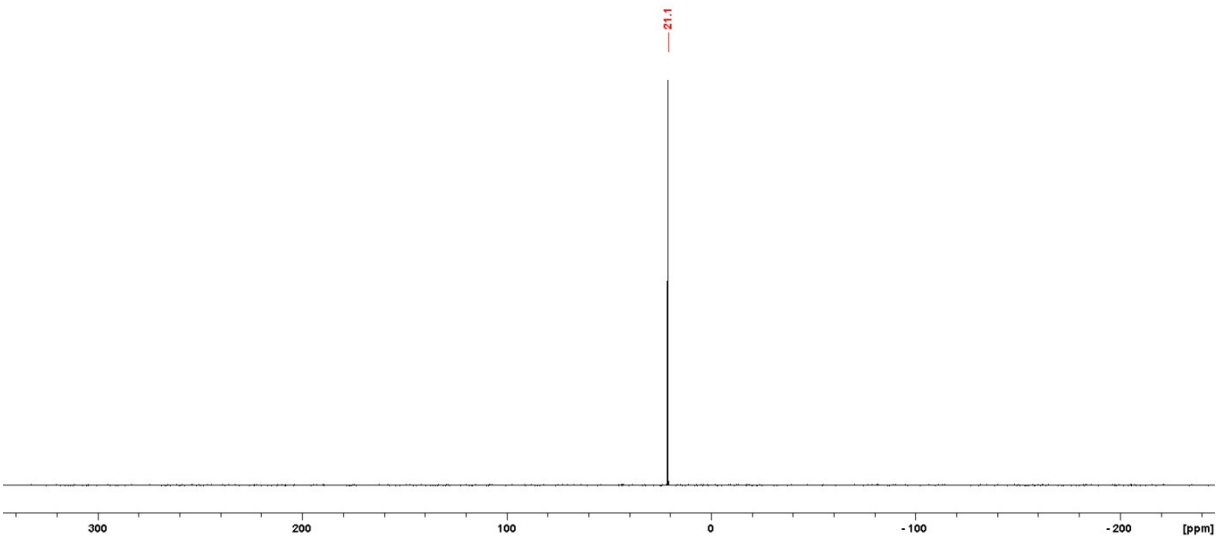

^{31}P-NMR (162 MHz, CD_2Cl_2) of [PPN][Cl-Si(cat^H)$_2$].

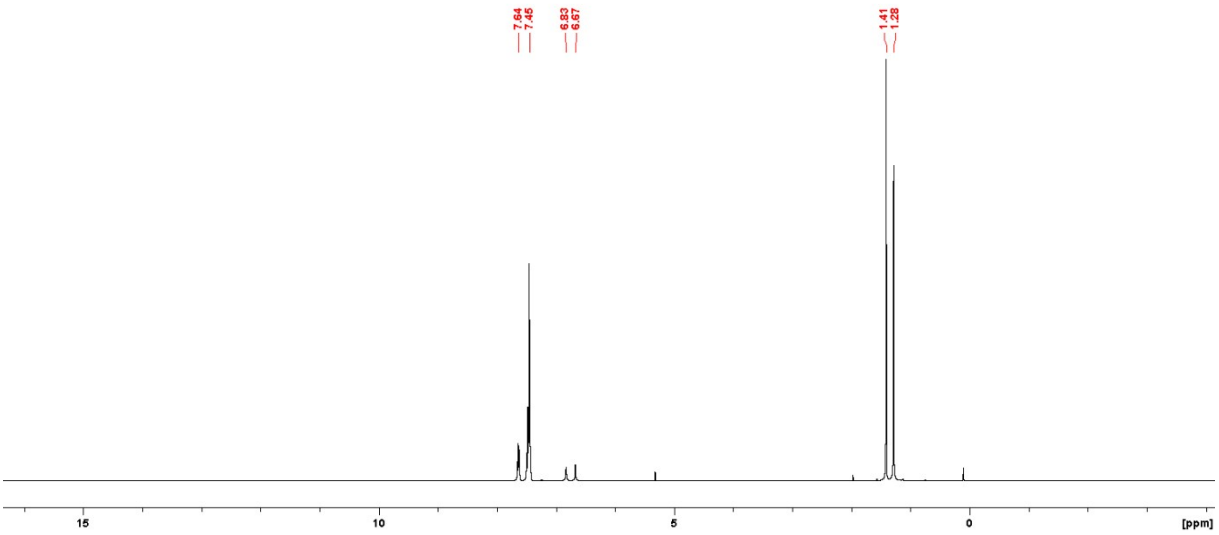

^{1}H-NMR (400 MHz, CD_2Cl_2) of [PPN][Cl-Si(cat$^{t\mathrm{Bu}}$)$_2$].

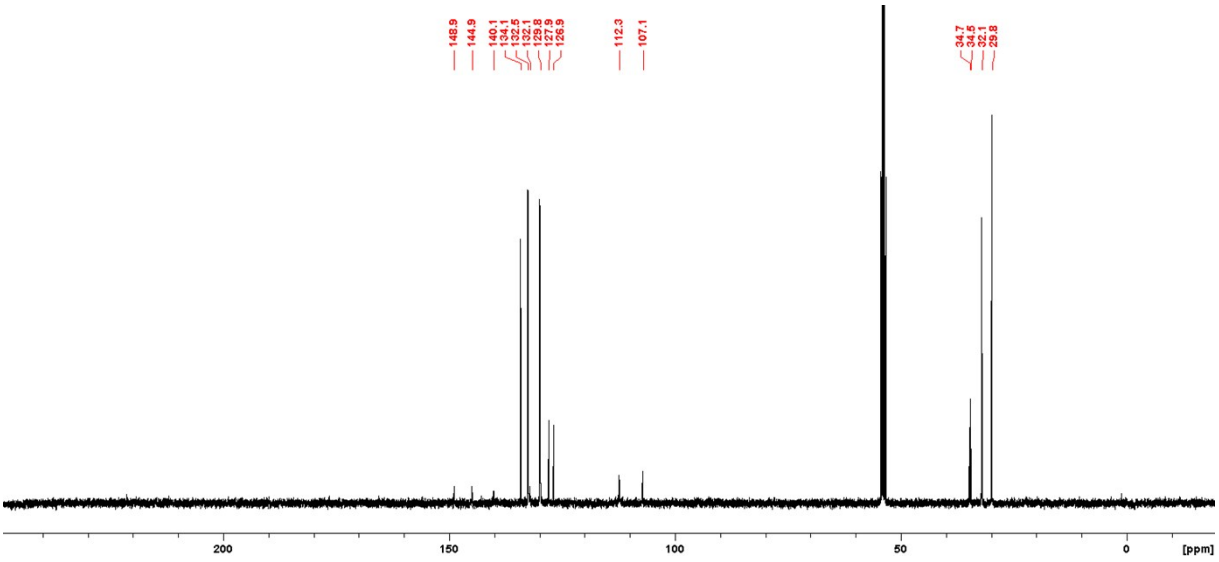

^{13}C-NMR (100 MHz, CD_2Cl_2) of [PPN][Cl-Si(cat$^{t\mathrm{Bu}}$)$_2$].

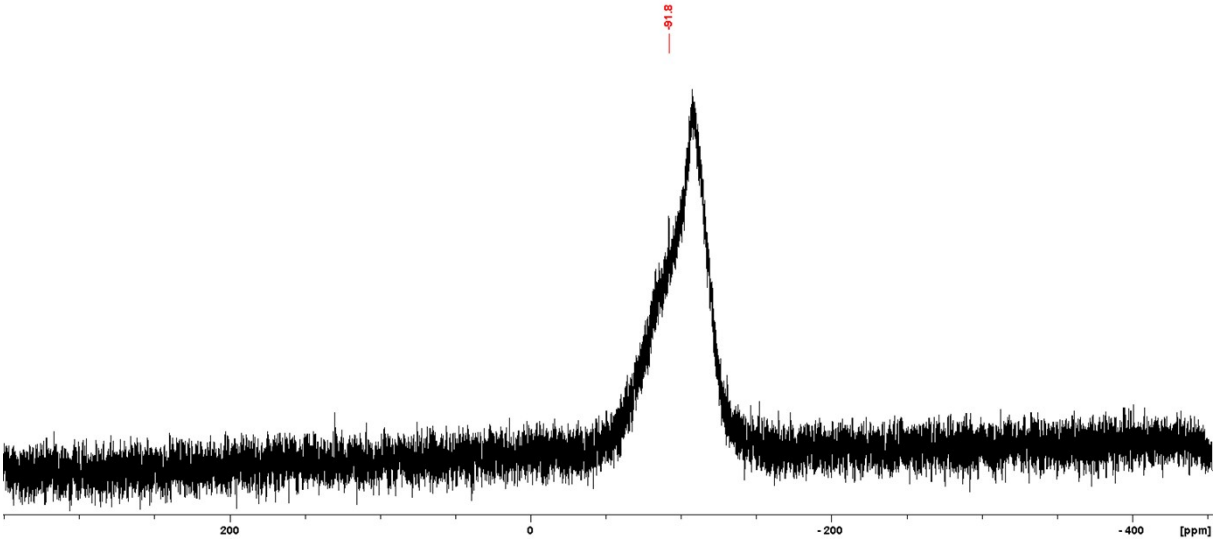

^{29}Si-NMR (79 MHz, CD_2Cl_2) of [PPN][Cl-Si(cat$^{t\mathrm{Bu}}$)$_2$].

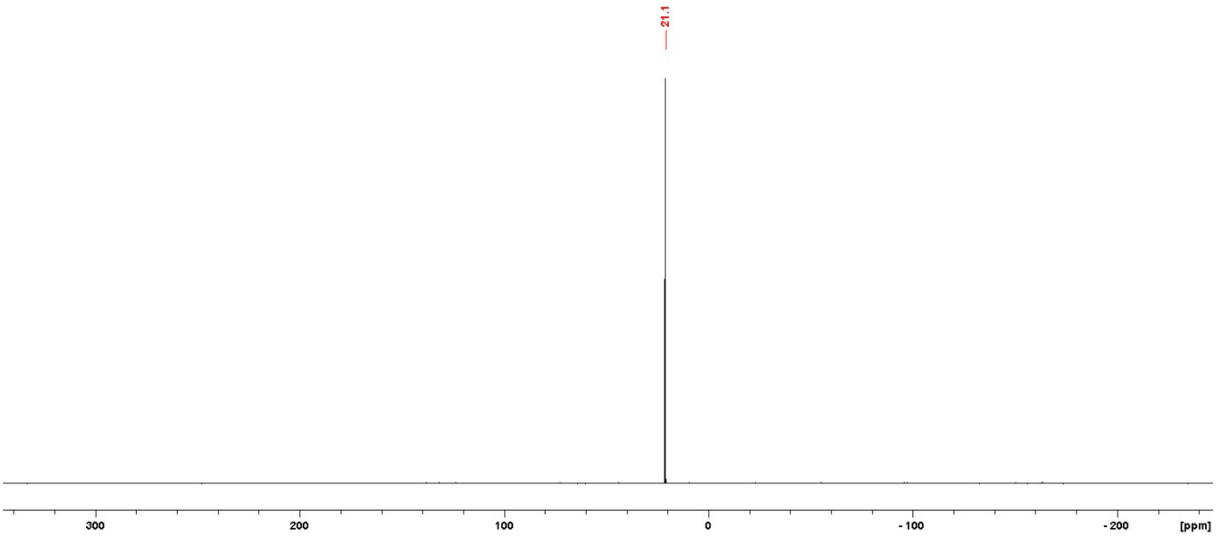

^{31}P-NMR (162 MHz, CD_2Cl_2) of [PPN][Cl-Si(cat^{tBu})$_2$].

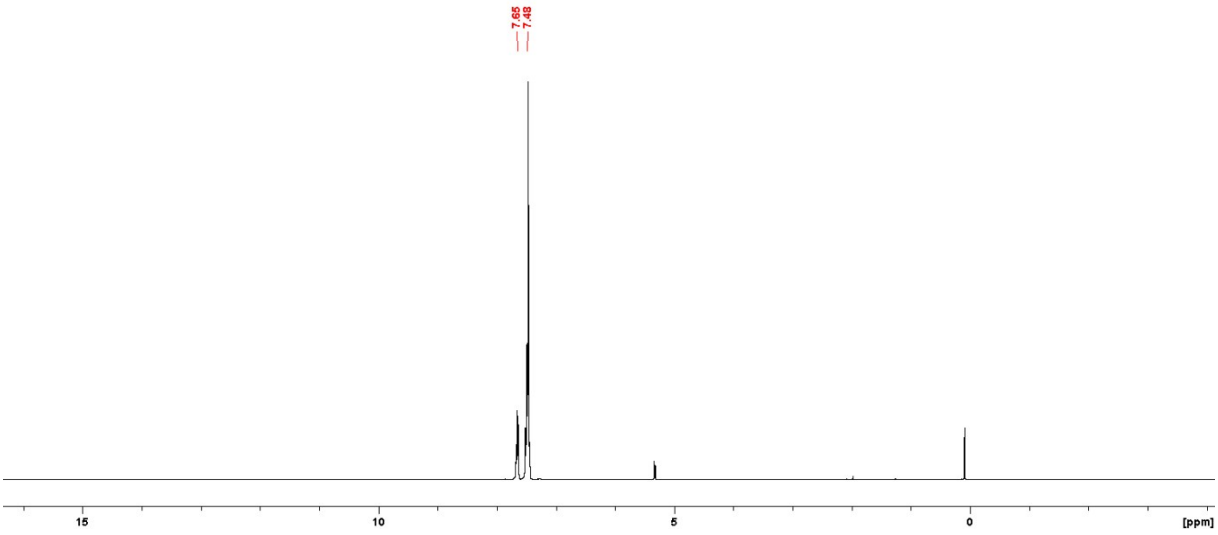

^{1}H-NMR (400 MHz, CD_2Cl_2) of [PPN][Cl-Si(cat^{F})$_2$].

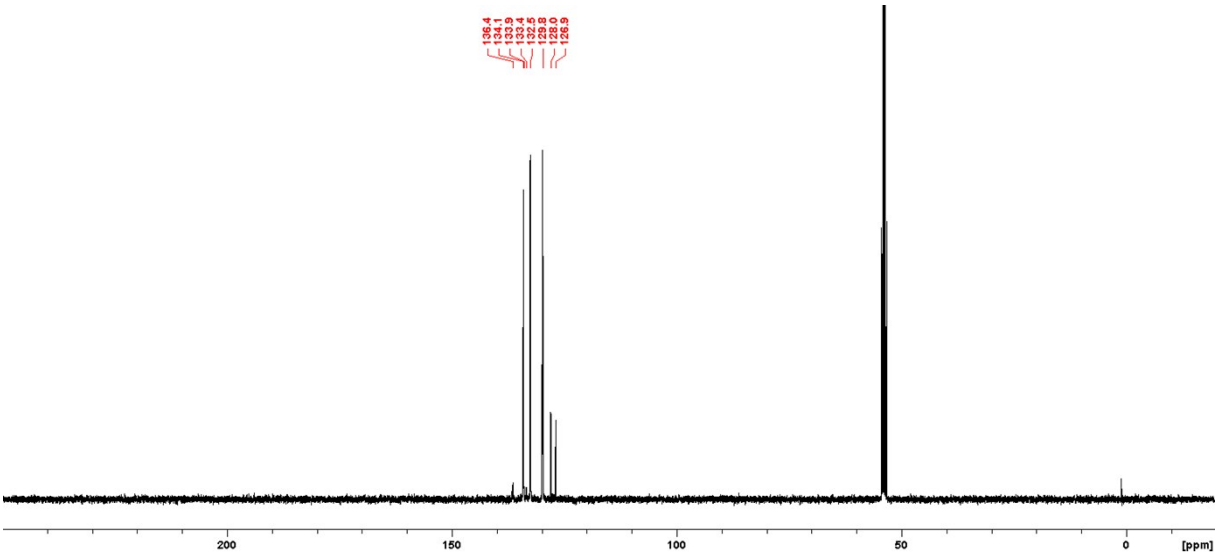

^{13}C-NMR (100 MHz, CD_2Cl_2) of [PPN][Cl-Si(cat^F)$_2$]. Assignement of cat-signals was not possible due to the higher order multiplets of carbon caused by fluorine coupling

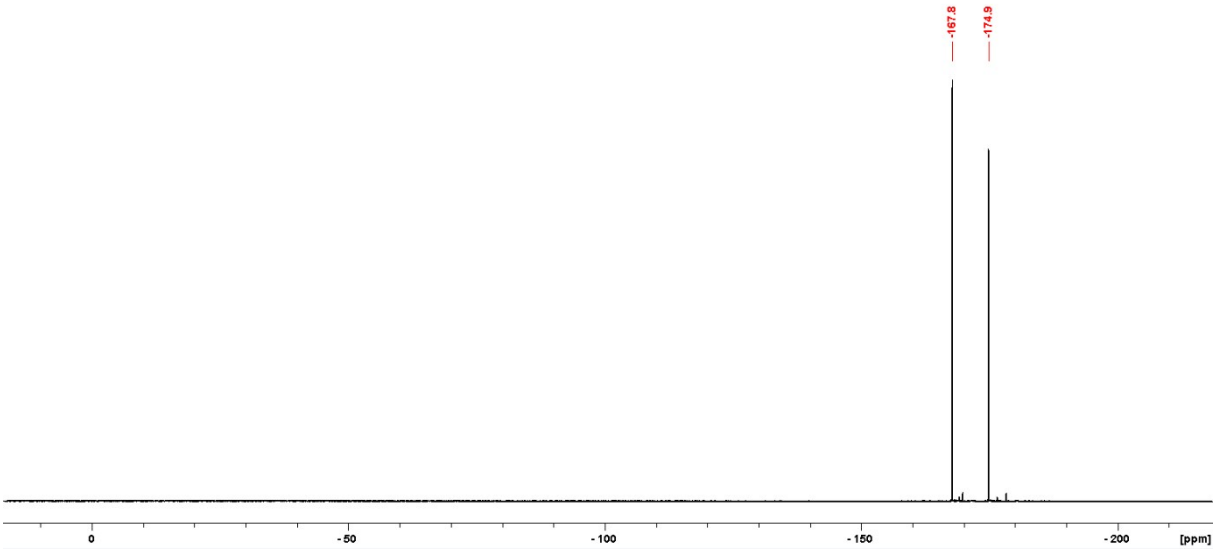

^{19}F-NMR (376 MHz, CD_2Cl_2) of [PPN][Cl-Si(cat^F)$_2$].

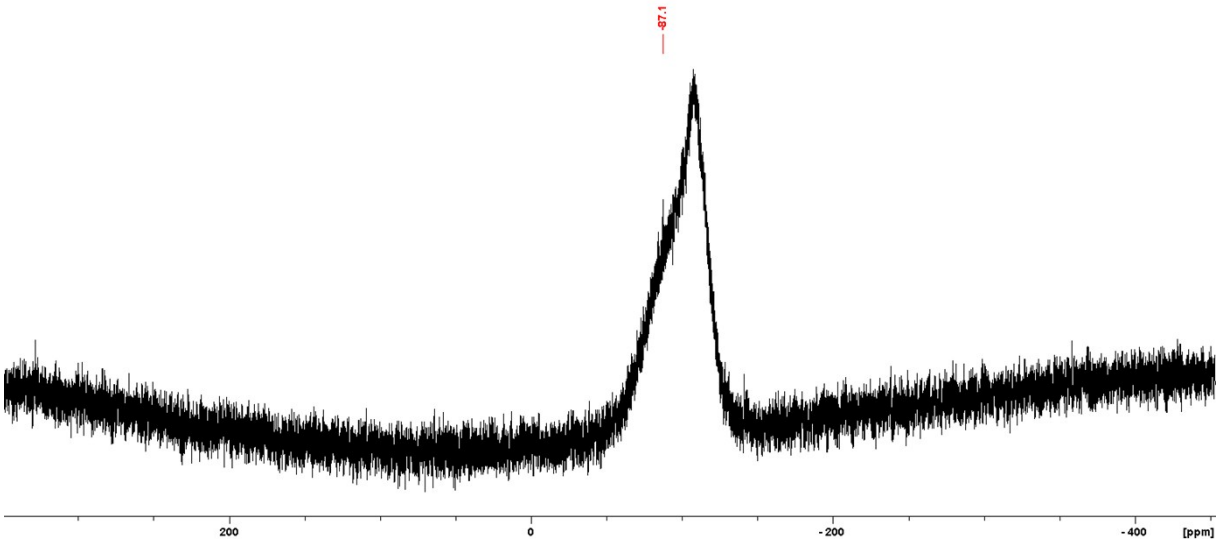

^{29}Si-NMR (79 MHz, CD_2Cl_2) of [PPN][Cl-Si(cat^F)$_2$].

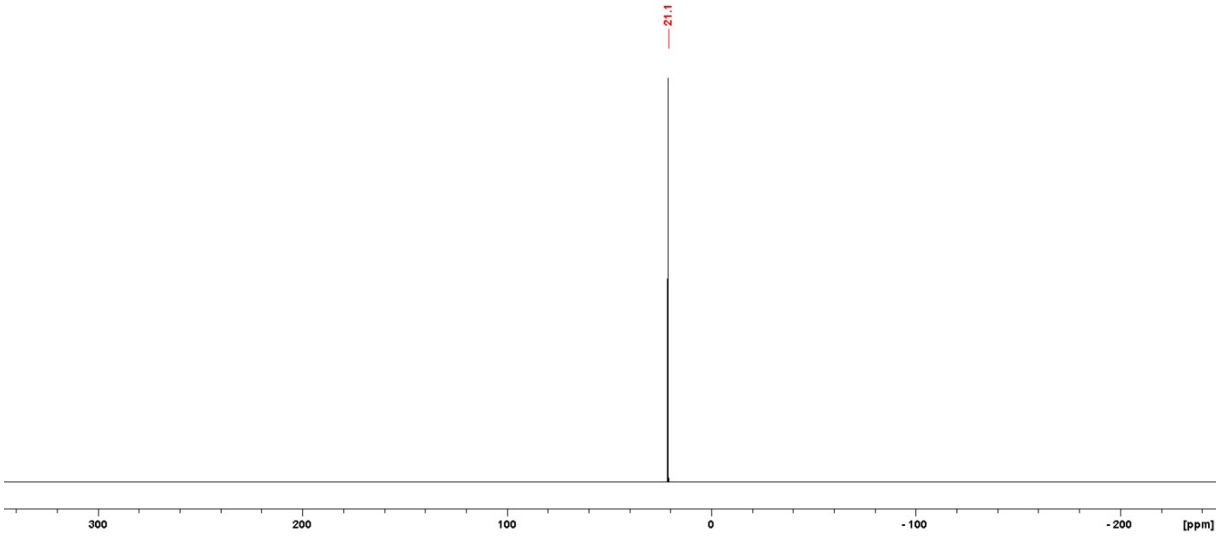

^{31}P-NMR (162 MHz, CD_2Cl_2) of [PPN][Cl-Si(cat^F)$_2$].

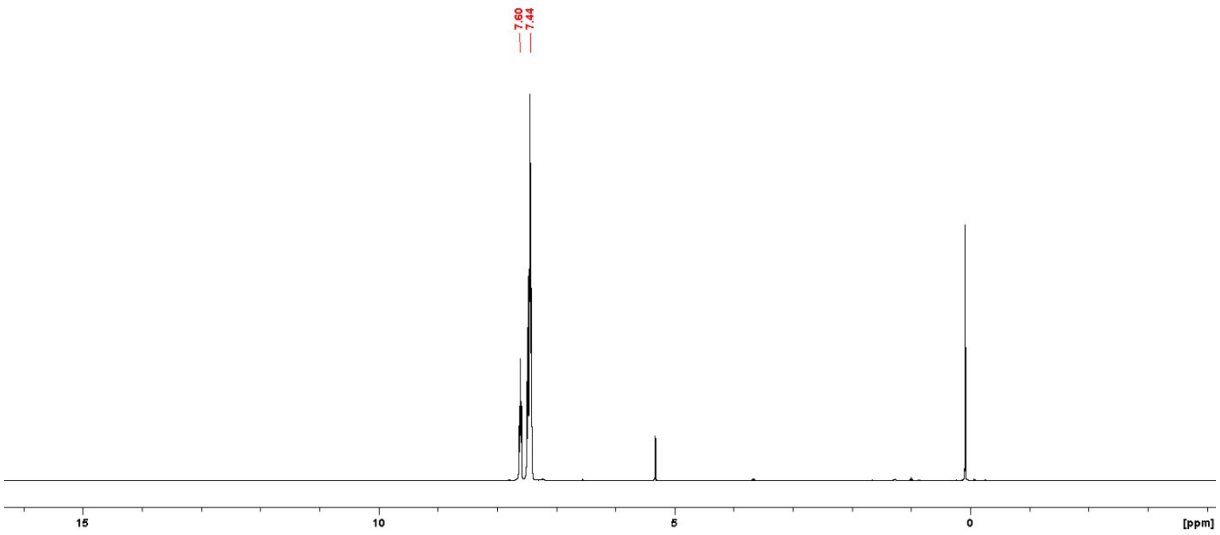

^{1}H-NMR (400 MHz, CD_2Cl_2) of [PPN][Cl-Si(cat^{Cl})$_2$].

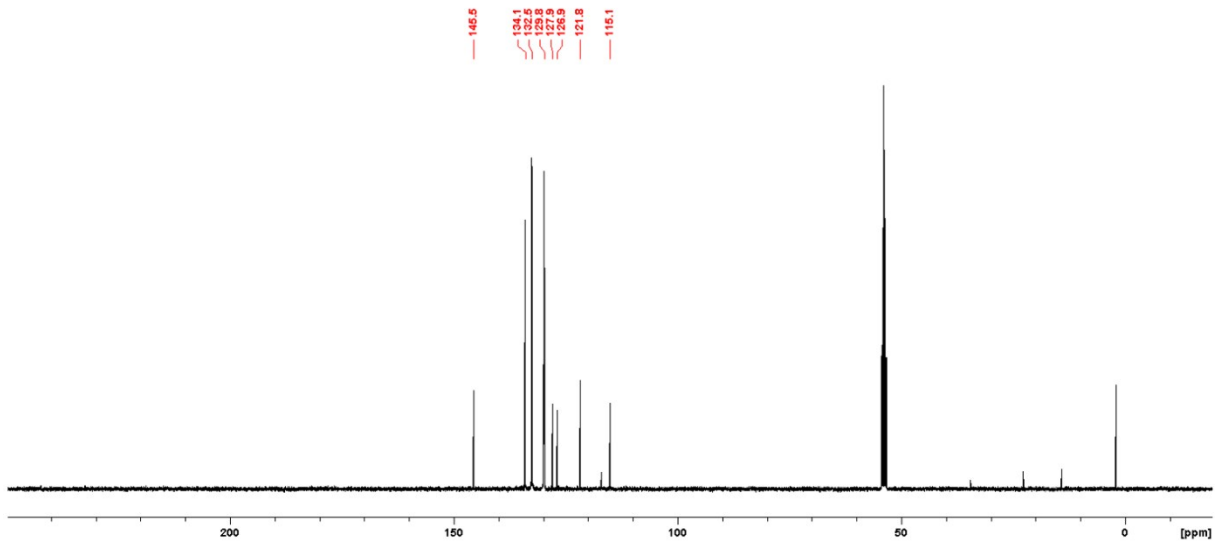

^{13}C-NMR (100 MHz, CD_2Cl_2) of [PPN][Cl-Si(cat^{Cl})$_2$].

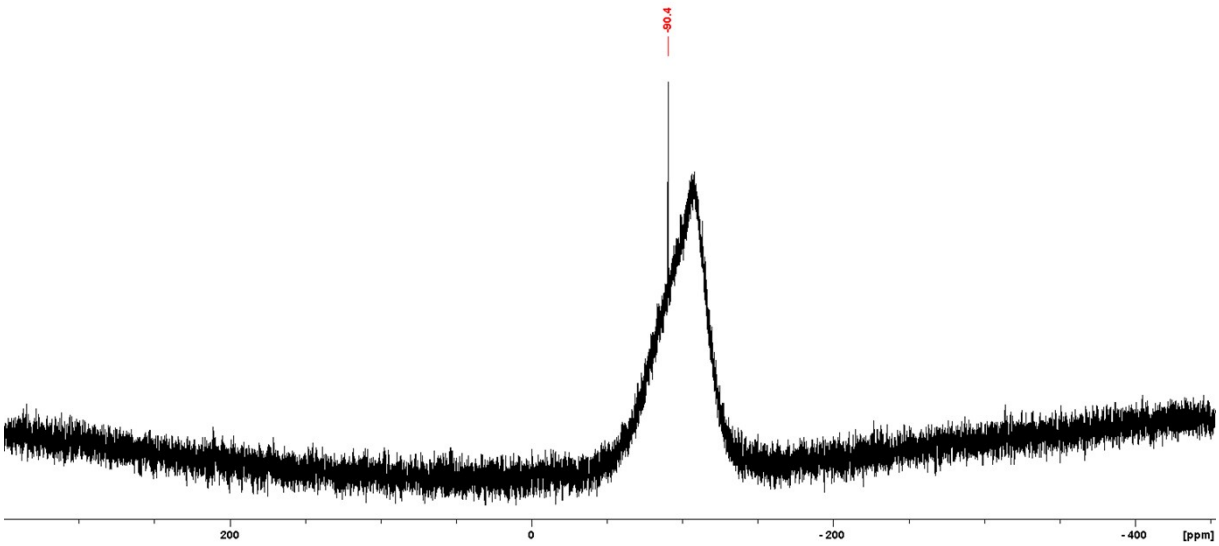

^{29}Si-NMR (79 MHz, CD_2Cl_2) of [PPN][Cl-Si(cat^{Cl})$_2$].

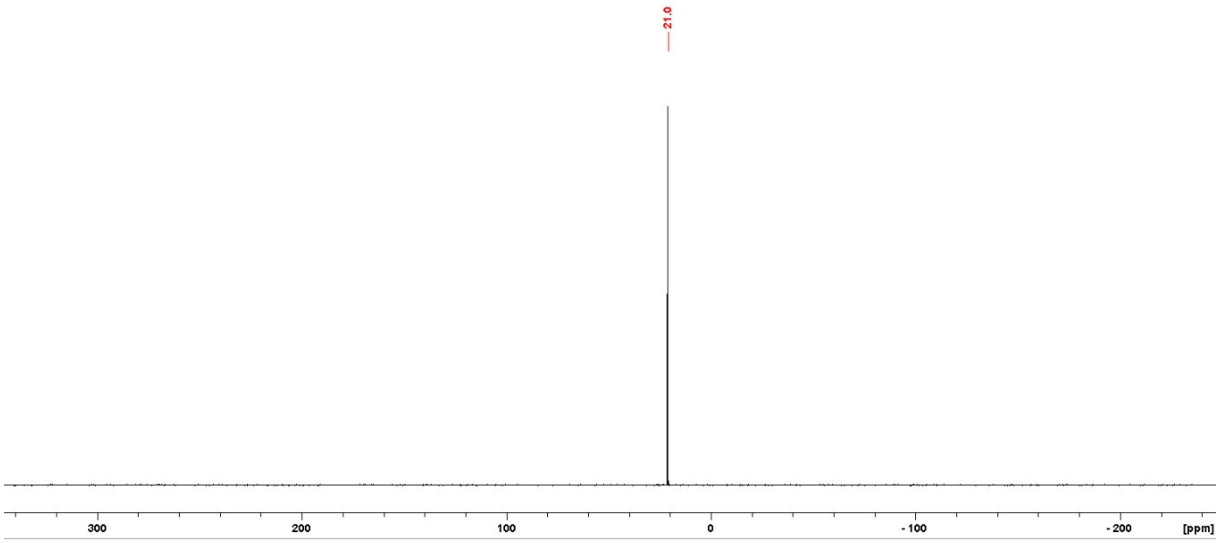

^{31}P-NMR (162 MHz, CD_2Cl_2) of [PPN][Cl-Si(cat^{Cl})$_2$].

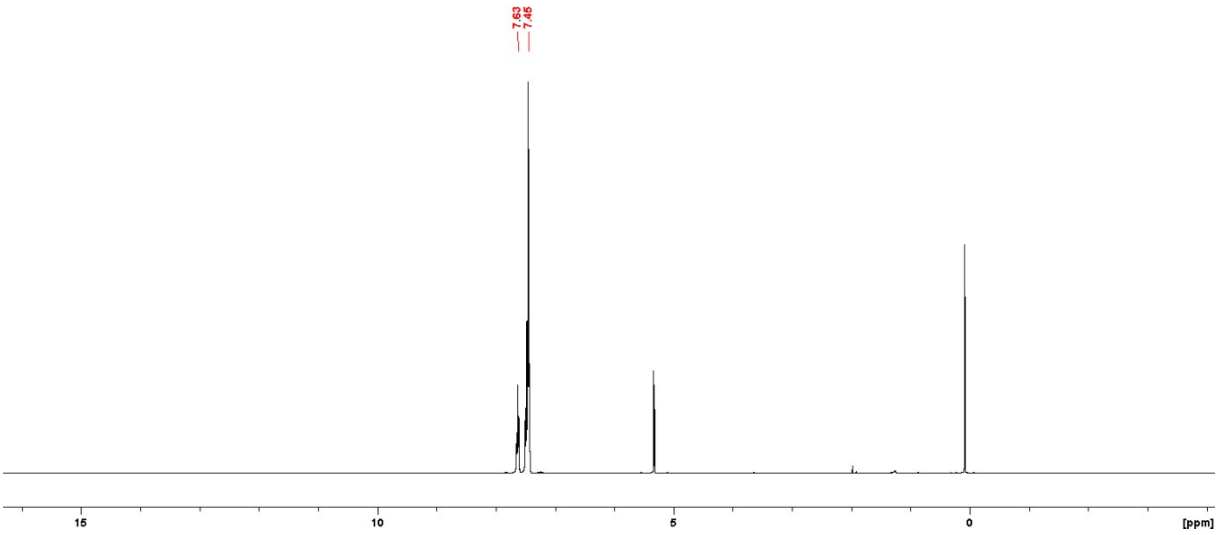

^{1}H-NMR (400 MHz, CD_2Cl_2) of [PPN][Cl-Si(cat^{Br})$_2$].

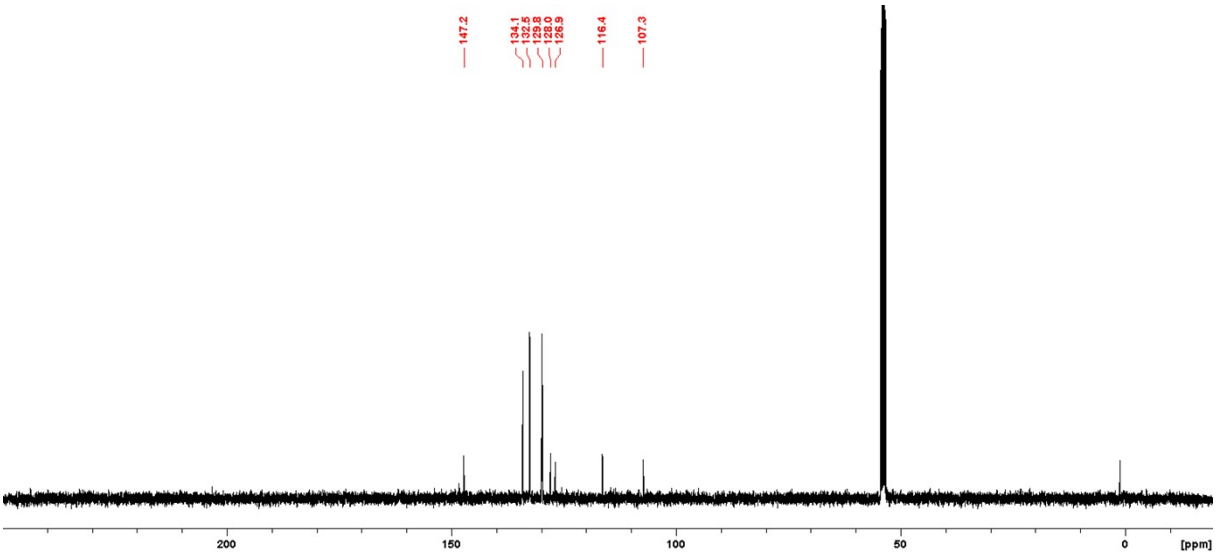

^{13}C-NMR (100 MHz, CD_2Cl_2) of [PPN][Cl-Si(cat^{Br})$_2$].

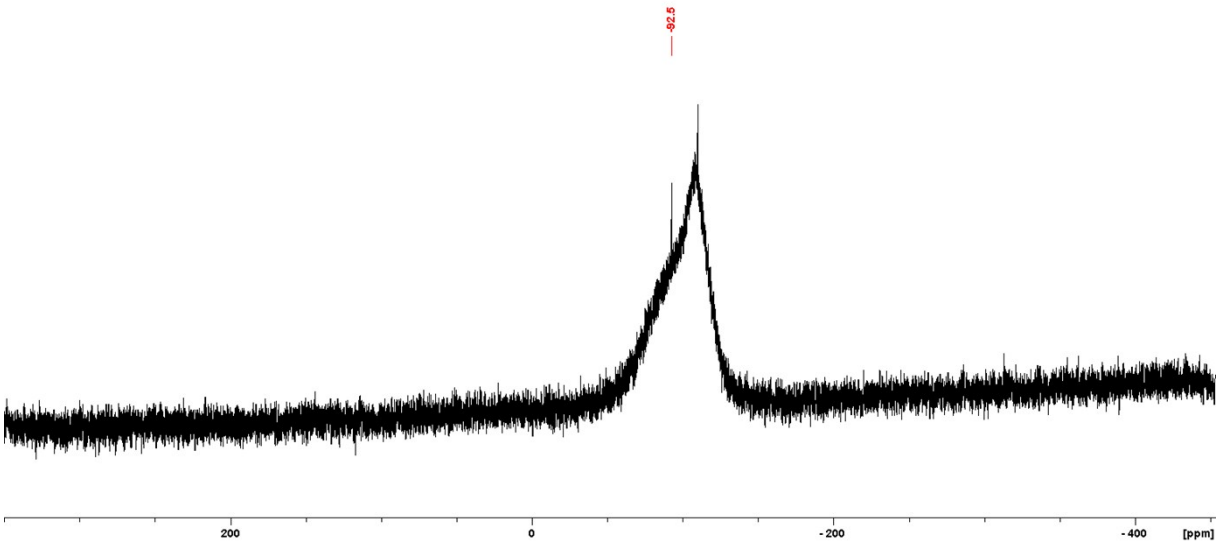

^{29}Si-NMR (79 MHz, CD_2Cl_2) of [PPN][Cl-Si(cat^{Br})$_2$]. The signal at –109.9 ppm belongs to a so far unidentified second species, in which another donor coordinates at the [Cl-Si(cat^{Br})$_2$]$^-$ moiety.

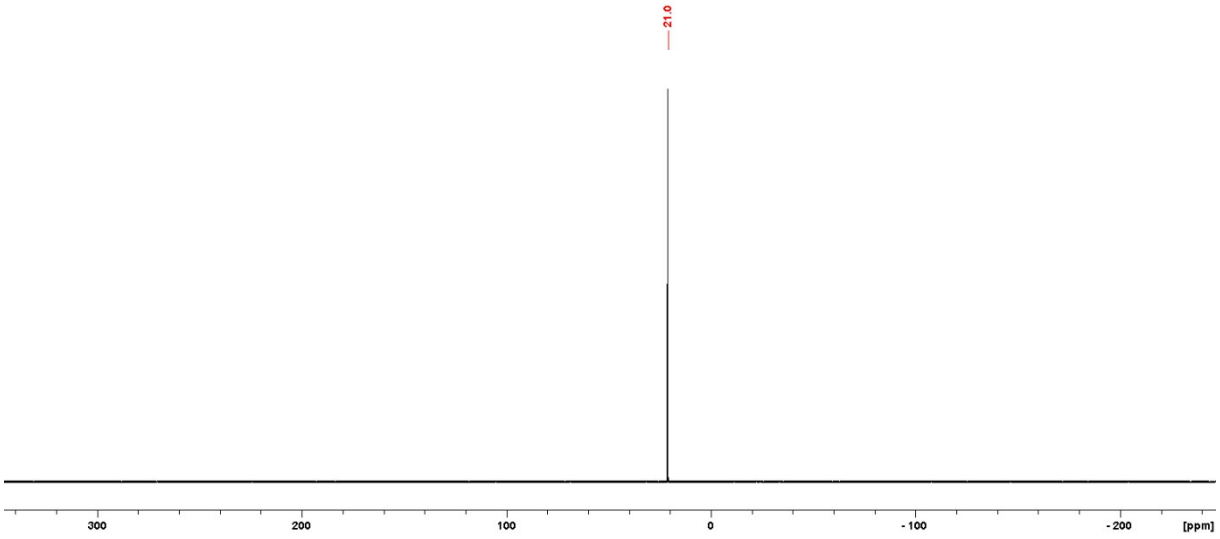

^{31}P-NMR (162 MHz, CD_2Cl_2) of [PPN][Cl-Si(cat^{Br})$_2$].

References

[1] a) H. R. Allcock, T. A. Nugent, L. A. Smeltz, *Synthesis and Reactivity in Inorganic and Metal-Organic Chemistry* **1972**, *2*, 97-104; b) A. K. Chekalov, A. I. Prokof'ev, N. N. Bubnov, S. P. Solodovnikov, A. A. Zhdanov, M. I. Kabachnik, *Bull. Acad. Sci. USSR, Div. Chem. Sci.* **1981**, *30*, 2064-2071; c) E. Hey-Hawkins, U. Dettlaff-Weglikowska, D. Thiery, H. G. von Schnering, *Polyhedron* **1992**, *11*, 1789-1794; d) A. L. Liberman-Martin, R. G. Bergman, T. D. Tilley, *J. Am. Chem. Soc.* **2015**, *137*, 5328-5331.

[2] E. L. Myers, C. P. Butts, V. K. Aggarwal, *Chem. Comm.* **2006**, 4434-4436.

[3] E. P. A. Couzijn, J. C. Slootweg, A. W. Ehlers, K. Lammertsma, *J. Am. Chem. Soc.* **2010**, *132*, 18127-18140.

[4] a) F. Neese, *Wiley Interdisc. Rev: Comp. Mol. Sci.* **2012**, *2*, 73-78; b) F. Neese, *Wiley Interdisciplinary Reviews: Computational Molecular Science* **2017**, e1327-n/a.

[5] K. Eichkorn, O. Treutler, H. Öhm, M. Häser, R. Ahlrichs, *Chem. Phys. Lett.* **1995**, *240*, 283-290.

[6] K. Eichkorn, F. Weigend, O. Treutler, R. Ahlrichs, *Theor. Chem. Acc.* **1997**, *97*, 119-124.

[7] Y. Zhao, D. G. Truhlar, *J. Phys. Chem. A* **2005**, *109*, 5656-5667.

[8] S. Grimme, J. Antony, S. Ehrlich, H. Krieg, *J. Chem. Phys.* **2010**, *132*, 154104.

[9] a) S. Grimme, S. Ehrlich, L. Goerigk, *J. Comput. Chem.* **2011**, *32*, 1456-1465; b) A. D. Becke, E. R. Johnson, *J. Chem. Phys.* **2005**, *122*, 154104; c) E. R. Johnson, A. D. Becke, *J. Chem. Phys.* **2005**, *123*, 024101.

[10] a) A. Schäfer, C. Huber, R. Ahlrichs, *J. Chem. Phys.* **1994**, *100*, 5829-5835; b) F. Weigend, R. Ahlrichs, *Phys. Chem. Chem. Phys.* **2005**, *7*, 3297-3305.

[11] S. Grimme, *Chem. Eur. J.* **2012**, *18*, 9955-9964.

[12] a) F. Neese, A. Hansen, D. G. Liakos, *J. Chem. Phys.* **2009**, *131*, 064103; b) C. Riplinger, F. Neese, *J. Chem. Phys.* **2013**, *138*, 034106; c) C. Riplinger, B. Sandhoefer, A. Hansen, F. Neese, *J. Chem. Phys.* **2013**, *139*, 134101.

[13] E. Paulechka, A. Kazakov, *J. Phys. Chem. A* **2017**, *121*, 4379-4387.

[14] G. Bistoni, A. A. Auer, F. Neese, *Chem. Eur. J.* **2017**, *23*, 865-873.

[15] a) L. O. Müller, D. Himmel, J. Stauffer, G. Steinfeld, J. Slattery, G. Santiso-Quiñones, V. Brecht, I. Krossing, *Angew. Chem. Int. Ed.* **2008**, *47*, 7659-7663; b) H. Böhrer, N. Trapp, D. Himmel, M. Schleep, I. Krossing, *Dalton. Trans.* **2015**, *44*, 7489-7499.

[16] a) A. Klamt, *J. Phys. Chem.* **1995**, *99*, 2224-2235; b) F. Eckert, A. Klamt, *AlChE J.* **2002**, *48*, 369-385; c) A. Klamt, B. Mennucci, J. Tomasi, V. Barone, C. Curutchet, M. Orozco, F. J. Luque, *Acc. Chem. Res.* **2009**, *42*, 489-492.

[17] E. J. Baerends, T. Ziegler, A. J. Atkins, J. Autschbach, D. Bashford, O. Baseggio, A. Brces, F. M. Bickelhaupt, C. Bo, P. M. Boerritger, L. Cavallo, C. Daul, D. P. Chong, D. V. Chulhai, L. Deng, R. M. Dickson, J. M. Dieterich, D. E. Ellis, M. van Faassen, A. Ghysels, A. Giammona, S. J. A. van Gisbergen, A. Goez, A. W. Gtz, S. Gusarov, F. E. Harris, P. van den Hoek, Z. Hu, C. R. Jacob, H. Jacobsen, L. Jensen, L. Joubert, J. W. Kaminski, G. van Kessel, C. Knig, F. Kootstra, A. Kovalenko, M. Krykunov, E. van Lenthe, D. A. McCormack, A. Michalak, M. Mitoraj, S. M. Morton, J. Neugebauer, V. P. Nicu, L. Noodleman, V. P. Osinga, S. Patchkovskii, M. Pavanello, C. A. Peeples, P. H. T. Philipsen, D. Post, C. C. Pye, H. Ramanantoanina, P. Ramos, W. Ravenek, J. I. Rodrguez, P. Ros, R. Rger, P. R. T. Schipper, D. Schlns, H. van Schoot, G. Schreckenbach, J. S. Seldenthuis, M. Seth, J. G. Snijders, Sol.

[18] E. Van Lenthe, E. J. Baerends, *J. Comput. Chem.* **2003**, *24*, 1142-1156.

[19] a) G. Schreckenbach, T. Ziegler, *J. Phys. Chem.* **1995**, *99*, 606-611; b) M. Krykunov, T. Ziegler, E. v. Lenthe, *Int. J. Quantum Chem* **2009**, *109*, 1676-1683.

[20] C. Adamo, V. Barone, *J. Chem. Phys.* **1999**, *110*, 6158-6170.

[21] a) E. v. Lenthe, E. J. Baerends, J. G. Snijders, *J. Chem. Phys.* **1993**, *99*, 4597-4610; b) E. van Lenthe, E. J. Baerends, J. G. Snijders, *J. Chem. Phys.* **1994**, *101*, 9783-9792; c) E. van Lenthe, J.

G. Snijders, E. J. Baerends, *J. Chem. Phys.* **1996**, *105*, 6505-6516; d) S. K. Wolff, T. Ziegler, E. van Lenthe, E. J. Baerends, *J. Chem. Phys.* **1999**, *110*, 7689-7698.
[22] A. Klamt, G. Schuurmann, *J. Chem. Soc., Perkin Trans. 2* **1993**, 799-805.
[23] C. C. Pye, T. Ziegler, *Theor. Chem. Acc.* **1999**, *101*, 396-408.
[24] J. NBO 7.0. E. D. Glendening, K. Badenhoop, A. E. Reed, J. E. Carpenter, J. A. Bohmann, C. M. Morales, C. R. Landis, and F. Weinhold, Theoretical Chemistry Institute, University of Wisconsin, Madison (2018).
[25] T. A. K. AIMAll (Version 17.01.25), TK Gristmill Software, Overland Park KS, USA, 2017 (aim.tkgristmill.com).
[26] a) R. F. W. Bader, H. Essén, *J. Chem. Phys.* **1984**, *80*, 1943-1960; b) R. F. W. Bader, *Chem. Rev.* **1991**, *91*, 893-928; c) F. Cortés-Guzmán, R. F. W. Bader, *Coord. Chem. Rev.* **2005**, *249*, 633-662; d) D. Stalke *Chem. Eur. J.* **2011**, *17*, 9264-9278.
[27] a) R. G. Parr, L. v. Szentpály, S. Liu, *J. Am. Chem. Soc.* **1999**, *121*, 1922-1924; b) A. R. Jupp, T. C. Johnstone, D. W. Stephan, *Dalton Trans* **2018**, *47*, 7029-7035; c) A. R. Jupp, T. C. Johnstone, D. W. Stephan, *Inorg. Chem.* **2018**, *57*, 14764-14771.
[28] O. V. Dolomanov, L. J. Bourhis, R. J. Gildea, J. A. K. Howard, H. Puschmann, *J. Appl. Crystallogr.* **2009**, *42*, 339-341.
[29] G. M. S. U. o. G. G. Sheldrick, Germany.